

MOLECULES TO MARINESCAPES: THE CHARACTERIZATION OF MICROBIAL
LIFE IN THE ARCTIC OCEAN

By

Brandon T. Hassett

RECOMMENDED:



Dr. J. Andrés López



Dr. Jenifer McBeath



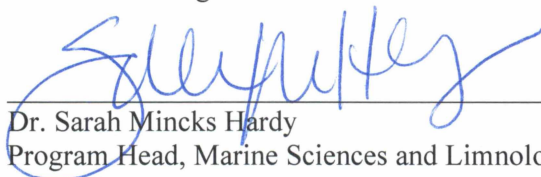
Dr. Mary Beth Leigh



Dr. R. Eric Collins

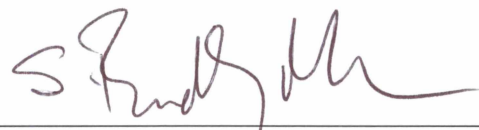


Dr. Rolf Gradinger

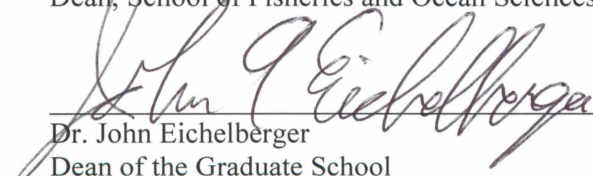


Dr. Sarah Mincks Hardy
Program Head, Marine Sciences and Limnology

APPROVED:



Dr. S. Bradley Moran
Dean, School of Fisheries and Ocean Sciences



Dr. John Eichelberger
Dean of the Graduate School

4/5/2016

Date

MOLECULES TO MARINESCAPES: THE CHARACTERIZATION OF MICROBIAL
LIFE IN THE ARCTIC OCEAN

A
DISSERTATION

Presented to the Faculty
of the University of Alaska Fairbanks
in Partial Fulfillment of the Requirements
for the Degree of

DOCTOR OF PHILOSOPHY

By

Brandon T. Hassett, B.S., M.S.

Fairbanks, AK

May 2016

Abstract

Microbes are the base of all marine food webs and comprise >90% of all living biomass in the world's oceans. Microbial life and functioning in high-latitude seas is characterized by the predominance of unknown species that encode uncharacterized genes, replenish nutrients, and modulate ecosystem health by interfacing with disease processes. This research elucidates eukaryotic microbial diversity and functionality in Arctic and sub-Arctic marine environments by describing the culturable and genetic diversity of eukaryotic microbes and the life histories of marine fungi belonging to the Chytridiomycota. This work includes the description of two new mesomycetozoean species, the assembled and annotated genome of *Sphaeroforma sirikka*, the first description of a cryptic carbon cycle (the mycoloop) mediated by fungi from any marine environment, and the description of large-scale eukaryotic microbial diversity patterns driven by temperature and latitude in the eastern Bering Sea. These results help establish a valuable baseline of microbial diversity in high latitude seas.

Dedication

This work is dedicated to a woman who spoke of boundless grandeur and nourished my spirit with unconditional love and more beauty than Alaska holds. To my mother.

Table of Contents

	Page
Signature Page	i
Title Page	iii
Abstract	v
Dedication	vii
Table of Contents	ix
List of Figures	xi
List of Tables	xiii
Acknowledgements	xv
Introduction	1
References	4
Chapter 1: Two New Species of Marine Saprotrophic Sphaeroformids in the Mesomycetozoea Isolated From the Sub-Arctic Bering Sea	9
Introduction	10
Results	10
Light Microscopy and Ultrastructure	11
Ultrastructure	13
Taxonomic summary	14
Discussion	16
Conclusions	18
Methods	18
Isolation and culture	18
DNA extraction, amplification, and sequencing	19
Phylogenetic analysis	19
Morphology and substrate utilization	20
TEM	20
Acknowledgements	21
Works Cited	29
Supplemental Materials	31
Chapter 2: Draft Genome Sequence of <i>Sphaeroforma sirkka</i> B5	33
Genome Announcement	34
Chapter 3: Chytrids Dominate Arctic Marine Fungal Communities	35

Introduction.....	36
Results.....	37
Discussion.....	39
Materials and Methods.....	41
Acknowledgments.....	43
References.....	47
Supplemental Materials	53
Chapter 4: Eukaryotic Microbial Richness Increases with Latitude and Decreasing Temperature in the Pacific Arctic Domain in Late Winter.	59
Introduction.....	60
Materials and Methods.....	61
Results.....	62
Discussion.....	64
Acknowledgements.....	67
Works Cited	74
Supplemental Materials	79
General Conclusions.....	89
References.....	92

List of Figures

	Page
Figure 1.0. Maximum likelihood tree	22
Figure 1.1. Light microscopy-observed morphology of <i>Sphaeroforma sirkka</i>	23
Figure 1.2. Light microscopy-observed morphology of <i>Sphaeroforma napiecek</i>	24
Figure 1.3. Life cycle of <i>Sphaeroforma sirkka</i> and <i>S. napiecek</i>	25
Figure 1.4. Electron micrographs of <i>S. napiecek</i> and <i>S. sirkka</i>	26
Figure 1.5. <i>S. napiecek</i> and <i>S. sirkka</i> cells containing crescent shaped structures.....	27
Supplemental Figure 1.0. Cross section of a plasmodial <i>S. napiecek</i> cell	31
Figure 3.0. Chytridiomycota from Barrow, AK (May 2013).....	44
Figure 3.1. Seasonal patterns of the Chytridiomycota	45
Figure 3.2. Snow depth helps regulates parasitic activity of the Chytridiomycota.....	46
Supplemental Figure 3.0. Dense algae growing at the bottom of ice cores	53
Supplemental Figure 3.1. Neighbor joining, bootstrap consensus tree	54
Supplemental Figure 3.2. <i>Pleurosigma sp.</i> filled with chytrid-like organisms from Barrow Sediment	55
Supplemental Figure 3.3. Normalized abundance of chytrid sequences.....	56
Figure 4.0. Study area in the eastern Bering Sea during an expedition on the in March 2015	68
Figure 4.1. Relative abundance of eukaryotic supergroups illustrating general community structure	69
Figure 4.2. MDS plots of eukaryotic microbial community structure	70
Supplemental Figure 4.0. Sampling rarefaction curves	79
Supplemental Figure 4.1. Shared OTU map	80
Figure 5.0. KEGG-classified gene products	93
Figure 5.1. KEGG-classified metabolic pathways.....	94

List of Tables

	Page
Table 1.0. Sequence database classification with NCBI accession numbers, isolates, and targeted rRNA locus used for phylogenetic analysis and generation of trees	28
Supplemental Table 3.0. List of 18S rRNA taxa and accession numbers used in phylogenetic analysis ..	57
Table 4.0. Sampling locations, date, depth of chlorophyll <i>a</i> maximum, temperature (T) and salinity (S) .	71
Table 4.1. Site diversity and attributes of vetted datasets	72
Table 4.2. Comparative analysis between terminal sites representing the number of shared OTUs	73
Supplemental Table 4.0. Inorganic nutrient data (μM)	81
Supplemental Table 4.1. Condensed taxonomy of detected organisms in the Bering Sea region	82

Acknowledgements

Above all, I wish to thank God for affording me a sporting chance to be the first to understand a miniscule of his divinely provident plan.

Secondly, I would like to acknowledge my PI, Dr. Rolf Gradinger for his support. I am grateful for his scientific insight, lab space, and time reviewing manuscripts. Additionally, I would like to thank my committee members, Eric Collins, Mary Beth Leigh, Jenifer McBeath and Andrés López for their critical reviews of my research.

Next, I would like to acknowledge and thank my sister, Ms. Erin Hassett for her skillful sketches of the *Sphaeroforma* lifecycle. It is a comforting thought to know that no matter how far a fellow roams, the front lights of home will always be glowing bright. For this, I am deeply thankful to my family.

Braving the tempestuous sea of graduate school alone is a tall order. I am thankful for everyone who has shared this journey with me and contributed to its successes.

Introduction

The Arctic Ocean remains one of the least studied oceanographic regions in the world (Gradinger, 2009) and is changing at an unprecedented rate (Arrigo and van Dijken, 2011; Nelson *et al.*, 2014).

Exemplifying these changes are decreases in summer sea ice extent and thickness (Holland *et al.*, 2010; Stroeve *et al.*, 2007), increases in water temperatures (Steele *et al.*, 2008), and alterations in primary productivity (Arrigo *et al.*, 2012). These physical changes are yielding observed and predicted changes in biotic diversity and ecosystem processes (e.g. Bluhm and Gradinger, 2008; Gradinger, 1995; Boyd *et al.*, 2014; Howes *et al.*, 2015; Laidre *et al.*, 2015). While changes in Arctic terrestrial systems are well documented (e.g. Forbes *et al.*, 2010), relatively little information is available from the Arctic marine environment, which includes three major realms: sea ice, water column and sea floor (Wassmann *et al.*, 2011; Gradinger *et al.*, 2010).

Although substantial progress has been made towards characterizing marine biodiversity (e.g. Comeau *et al.*, 2013; Poulin, 2004; Doney *et al.*, 2012; Pernice *et al.*, 2015), thousands of species remain undescribed (Pedrós-Alió, 2006; Sogin *et al.*, 2006), especially in the microbial realm. Microbes comprise 90% of all living biomass in oceans (Suttle, 2007), yet their diversity and functionality are largely unknown, especially in the Arctic Ocean. Historically, microbial research has employed culture-based assessments of diversity, coupled with microscopy to elucidate the community composition and functioning of microbes; however, these methods are severely limiting, as less than 1% of microbes are culturable (Staley and Konopka, 1985) and morphological diagnostics lead to incorrect taxonomic assignments (Gleason *et al.*, 2008). To address these limitations, microbial ecologists are employing culture-independent methods to assess diversity, such as next-generation sequencing (NGS). Driven by this advancement in technology, research on Arctic prokaryotes has drastically increased in the last decade (e.g. Mason *et al.*, 2009; Ladau *et al.*, 2013; Galand *et al.*, 2009); however, these technology-driven research advancements have yet to be fully developed and extended to the eukaryotic research community, as many databases (e.g. SILVA) are still actively being curated to create a reliable consensus taxonomy.

As NGS continues to revolutionize the field of microbial ecology, global microbial diversity is being found to exceed prior estimates (Schuster, 2008), driven by the dominance of cryptic microbial life, especially in the Arctic. Molecular-based studies in Greenland, Norway and the Barents Sea found that 42% of all eukaryotic sequences were less than 98% similar to any sequences in GenBank and that 15% of total sequences were less than 95% similar to any sequences previously recovered (Lovejoy *et al.*, 2006). This cryptic life and its biological processes challenge ecologists' understanding of food web

dynamics and community structures (e.g. Hollowed *et al.*, 2013; Comeau *et al.*, 2011; Boetius *et al.*, 2013).

To adequately assess microbial responses to climate change, baseline research is first needed to inventory microbes, supplemented by organismal research that assesses ecological roles, especially within the eukaryotic domain. These baseline studies are imperative for predicting and assessing future changes. Unequivocally, fungi are the most cryptic among the eukaryotic kingdoms within the marine system and are widely understudied in the Arctic (Jones, 2011). Assessments of Arctic eukaryotic diversity have explicitly omitted fungi in diversity studies (Comeau *et al.*, 2011). Despite this, fungi are as important in aquatic nutrient cycling as they are in terrestrial soil systems (Barlocher, 2007), and possess the ability to change primary production patterns through parasitism (Gleason *et al.*, 2008). Members of the fungal phylum Chytridiomycota (chytrids) are distinct from other fungi in that they require water to disseminate flagellated infection propagules called zoospores. In addition to many aquatic ecosystems, chytrids can dominate fungal biodiversity in cold habitats, such as water-saturated glacial soils (Freeman *et al.*, 2009) and snow fields (Naff *et al.*, 2013). Chytrids have been reported from the Arctic (Horner and Schrader, 1982; Terrado *et al.*, 2011); yet, their diversity and functional role remains unknown. Ecologically, chytrids can reshape ecosystems through intense parasitism of primary producers. This parasitic pressure can alter food web structures, collapse phytoplankton communities (Jones, 2011), alter phytoplankton succession (Lepère *et al.*, 2008) and delay the timing of maximum algal density (Ibelings *et al.*, 2004; Lepère *et al.*, 2008) by colonizing up to 90% of a given phytoplankton species (Powell, 1993). If Arctic marine chytrids follow a similar life-history strategy then chytrids would constitute a major missing link in Arctic Ocean marine ecology.

The distinct connection between microbial diversity, abiotic environmental drivers, and food web structure has remained a key question in marine science (Worm *et al.*, 2002). To accurately predict microbial responses to climate change, research is needed to elucidate the current abiotic drivers of eukaryotic community structure. One of the major changes predicted in future Arctic climate scenarios is a shift in precipitation and sea ice coverage duration, potentially leading to reduced snow cover (Hezel *et al.*, 2013; Webster *et al.*, 2014) and increased influxes of light. Shifts in nutrient regimes associated with larger oceanographic processes can stress or favor the growth of phototrophic eukaryotes (Manes and Gradinger, 2009). Understanding the abiotic structuring components of microbial communities is essential for explaining the current spatial diversity patterns of microbes.

Understanding abiotic drivers of microbial diversity patterns is important, but these analyses fail to incorporate biological-mediate mechanisms (e.g. nutrient cycling) and interactions into spatial diversity

assessments. Arctic marine environments contain a vast reserve of polysaccharides, lignins and proteins (Goñi *et al.*, 2000) that are susceptible to microbial metabolism. Metabolizing or modifying these compounds for biogenic processes is predicated on the local gene assemblages encoded by microbes. In the marine system, the eukaryotes encode an array of enzymes that are responsible for the molecular modification and uptake of dissolved organic nitrogen (DON), dissolved inorganic nitrogen (DIN) and DOC. Fungal amino acid permease, nitrate reductase (Gorfer *et al.*, 2011), monooxygenases, phenol oxidase, cellobiohydrolases, chitobiohydrolases (Žifčáková and Baldrian, 2012), esterases, pectinases, and amylase (list not comprehensive) (van Den Brink and De Vries, 2011) facilitate catabolic modifications and uptake of organic material and DIN. The presence/absence of genes that encode catalytic enzymes can serve as a biological marker and proxy for ecosystem function. The rate at which these compounds are metabolized govern overall biogeochemical cycling and structure of marine ecosystems (Amon *et al.*, 2001). Ultimately, as select organisms degrade available molecules, microbial community structure, diversity, and abundance changes in favor of organisms that can metabolize remaining substrates.

Characterizing current microbial diversity and identifying the drivers of community structure are complex tasks that require a suite of scientific tools. The objective of this research was to blend current state-of-the-art technologies with traditional microbiological methods to assess diversity and abiotic drivers of microbial community structure, including, functional roles of certain community members, with a focus on marine fungi and fungal-like organisms. The Pacific Arctic Domain is of particular interest in understanding changing Arctic marine ecosystem functioning and diversity and for assessing the impacts of changing oceanographic conditions on them (Grebmeier *et al.*, 2010). This research established baseline information on the seasonality of microbial eukaryotes in Barrow, Alaska, by employing culture-based assessments of diversity and culturing-independent NextGen sequencing. To build off these seasonal data, I assessed the abiotic drivers and spatial diversity of eukaryotic microbes across several locations in the Arctic and sub-Arctic. Lastly, to predict the functioning of select eukaryotes, this research studied the genetic potential by assembling and annotating the genome of a novel eukaryote, *Sphaeroforma sirikka*.

References

- Amon RMW, Fitznar HP, Benner R. (2001). Linkages among the bioreactivity, chemical composition, and diagenetic state of marine dissolved organic matter. *Limnol Oceanogr* **46**:287–297.
- Arrigo KR, van Dijken GL. (2011). Secular trends in Arctic Ocean net primary production. *J Geophys Res* **116**:1–15.
- Arrigo KR, Perovich DK, Pickart RS, Brown ZW, Dijken GL Van, Lowry KE, *et al.* (2012). Massive phytoplankton blooms under Arctic sea ice. *Science* **336**:1408.
- Barlocher F. (2007). Decomposition and fungal community structure in aquatic environments. In: *Manual of Environmental Microbiology*, Hurst C, Crawford R, Garland J, Lipson D, Mills A, & Stetzenbach L (eds), ASM Press: Washington D.C., pp. 469–478.
- Bluhm B, Gradinger R. (2008). Regional variability in food availability for Arctic marine mammals. *Ecol Appl* **18**:S77–S96.
- Boetius A, Albrecht S, Bakker K, Bienhold C, Felden J, Fernández-Méndez M, *et al.* (2013). Export of algal biomass from the melting Arctic sea ice. *Science* **339**:1430–2.
- Boyd PW, Lennartz ST, Glover DM, Doney SC. (2014). Biological ramifications of climate-change-mediated oceanic multi-stressors. *Nat Clim Chang* **5**:71–79.
- Comeau AM, Li WKW, Tremblay JÉ, Carmack EC, Lovejoy C. (2011). Arctic ocean microbial community structure before and after the 2007 record sea ice minimum. *PLoS One* **6**, doi:10.1371/journal.pone.0027492.
- Comeau AM, Philippe B, Thaler M, Gosselin M, Poulin M, Lovejoy C. (2013). Protists in Arctic drift and land-fast sea ice. *J Phycol* **49**:229–240.
- Doney S, Ruckelshaus M, Duffy E, Barry J, Chan F, English C, *et al.* (2012). Climate change impacts on marine ecosystems. *Ann Rev Mar Sci* **4**:11–37.
- Forbes BC, Fauria MM, Zetterberg P. (2010). Russian Arctic warming and ‘greening’ are closely tracked by tundra shrub willows. *Glob Chang Biol* **16**:1542–1554.
- Freeman KR, Martin AP, Karki D, Lynch RC, Mitter MS, Meyer a F, *et al.* (2009). Evidence that chytrids dominate fungal communities in high-elevation soils. *Proc Natl Acad Sci U S A* **106**:18315–18320.
- Galand PE, Casamayor EO, Kirchman DL, Potvin M, Lovejoy C. (2009). Unique archaeal assemblages in the Arctic Ocean unveiled by massively parallel tag sequencing. *ISME J* **3**:860–869.
- Gleason FH, Kagami M, Lefevre E, Sime-Ngando T. (2008). The ecology of chytrids in aquatic ecosystems: roles in food web dynamics. *Fungal Biol Rev* **22**:17–25.
- Goñi MA, Yunker MB, MacDonald RW, Eglinton TI. (2000). Distribution and sources of organic biomarkers in Arctic sediments from the Mackenzie River and Beaufort Shelf. *Mar Chem* **71**:23–51.

- Gorfer M, Blumhoff M, Klaubauf S, Urban A, Inselsbacher E, Bandian D, *et al.* (2011). Community profiling and gene expression of fungal assimilatory nitrate reductases in agricultural soil. *ISME J* **5**:1771–1783.
- Gradinger R. (1995). Climate change and biological oceanography of the Arctic Ocean. *Philos Trans R Soc A Math Phys Eng Sci* **352**:277–286.
- Gradinger R. (2009). The Changing Arctic sea Ice Landscape. In: *The biology of polar seas*, Hempel, G & Hempel, I (eds), *Wirtschaftsverlag*: Bonn, pp. 239–246.
- Gradinger R, Bluhm B, Hopcroft R, Gebruk A, Kosobokova A, Sirenka B, *et al.* (2010). Marine life in the Arctic. In: *Life in the world's oceans: diversity, distribution and abundance*, MacIntyre, A (ed), Wiley-Blackwell, pp. 183–202.
- Grebmeier JM, Moore SE, Overland JE, Frey KE, Gradinger R. (2010). Biological response to recent pacific Arctic sea ice retreats. *Eos* **91**:161–162.
- Hezel PJ, Zhang X, Bitz CM, Kelly BP, Massonnet F. (2013). Projected decline in spring snow depth on Arctic sea ice caused by progressively later autumn open ocean freeze-up this century. *Geophys Res Lett* **39**:6–11.
- Holland MM, Serreze MC, Stroeve J. (2010). The sea ice mass budget of the Arctic and its future change as simulated by coupled climate models. *Clim Dyn* **34**:185–200.
- Hollowed AB, Planque B, Loeng H. (2013). Potential movement of fish and shellfish stocks from the sub-Arctic to the Arctic Ocean. *Fish Oceanogr* **22**:355–370.
- Horner R, Schrader GC. (1982). Relative contributions of ice algae, phytoplankton, and benthic microalgae to primary production in nearshore regions of the Beaufort Sea. *Arctic* **35**:485–503.
- Howes EL, Joos F, Eakin CM, Gattuso JP. (2015). An updated synthesis of the observed and projected impacts of climate change on the chemical, physical and biological processes in the oceans. *Front Mar Sci* **2**:1–27.
- Ibelings BW, De Bruin A, Kagami M, Rijkeboer M, Brehm M, Donk E Van. (2004). Host parasite interactions between freshwater phytoplankton and chytrid fungi (Chytridiomycota). *J Phycol* **40**:437–453.
- Jones EB. (2011). Fifty years of marine mycology. *Fungal Divers* **50**:73–112.
- Ladau J, Sharpton TJ, Finucane MM, Jospin G, Kembel SW, O'Dwyer J, *et al.* (2013). Global marine bacterial diversity peaks at high latitudes in winter. *ISME J* **7**:1669–77.
- Laidre KL, Stern H, Kovacs KM, Lowry L, Moore SE, Regehr E V, *et al.* (2015). Arctic marine mammal population status, sea ice habitat loss, and conservation recommendations for the 21st century. *Conserv Biol* **00**:1–14.
- Lepère C, Domaizon I, Debroas D. (2008). Unexpected importance of potential parasites in the composition of the freshwater small-eukaryote community. *Appl Environ Microbiol* **74**:2940–2949.

- Lovejoy C, Massana R, Pedro C. (2006). Diversity and distribution of marine microbial eukaryotes in the Arctic Ocean and adjacent seas. *Appl Environ Microbiol* **72**:3085–3095.
- Manes SS, Gradinger R. (2009). Small scale vertical gradients of Arctic ice algal photophysiological properties. *Photosynth Res* 1–14.
- Mason OU, Di Meo-Savoie C a, Van Nostrand JD, Zhou J, Fisk MR, Giovannoni SJ. (2009). Prokaryotic diversity, distribution, and insights into their role in biogeochemical cycling in marine basalts. *ISME J* **3**:231–242.
- Naff CS, Darcy JL, Schmidt SK. (2013). Phylogeny and biogeography of an uncultured clade of snow chytrids. *Environ Microbiol* **15**:2672–2680.
- Nelson J, Ashjian C, Bluhm B, Conlan K, Gradinger R, Grebmeier J, *et al.* (2014). Biodiversity and biogeography of the lower trophic taxa of the Pacific Arctic Region: sensitivities to climate change. In: *The Pacific Arctic Region: ecosystem status and trends in a rapidly changing environment*, pp. 269–336.
- Pedrós-Alió C. (2006). Marine microbial diversity: can it be determined? *Trends Microbiol* **14**:257–263.
- Pernice MC, Giner CR, Logares R, Perera-Bel J, Acinas SG, Duarte CM, *et al.* (2015). Large variability of bathypelagic microbial eukaryotic communities across the world's oceans. *ISME J* 1–14.
- Poulin R. (2004). Parasite species richness in New Zealand fishes: a grossly underestimated component of biodiversity? *Divers Distrib* **10**:31–37.
- Powell MJ. (1993). Looking at mycology with a Janus face: a glimpse at Chytridiomycetes active in the environment. *Mycologia* **85**:1–20.
- Schuster SC. (2008). Next-generation sequencing transforms today's biology. *Nat Methods* **5**:16–18.
- Sogin ML, Morrison HG, Huber JA, Welch DM, Huse SM, Neal PR, *et al.* (2006). Microbial diversity in the deep sea and the underexplored 'rare biosphere'. *Proc Natl Acad Sci* **103**:12115–12120.
- Staley FT, Konopka A. (1985). Microorganisms in aquatic and terrestrial habitats. *Annu Rev Microbiol* **39**:321–346.
- Steele M, Ermold W, Zhang J. (2008). Arctic Ocean surface warming trends over the past 100 years. *Geophys Res Lett* **35**:1–6.
- Stroeve J, Holland MM, Meier W, Scambos T, Serreze M. (2007). Arctic sea ice decline: Faster than forecast. *Geophys Res Lett* **34**:1–5.
- Suttle CA. (2007). Marine viruses--major players in the global ecosystem. *Nat Rev Microbiol* **5**:801–812.
- Terrado R, Medrinal E, Dasilva C, Thaler M, Vincent WF, Lovejoy C. (2011). Protist community composition during spring in an Arctic flaw lead polynya. *Polar Biol* **34**:1901–1914.

van Den Brink J, De Vries RP. (2011). Fungal enzyme sets for plant polysaccharide degradation. *Appl Microbiol Biotechnol* **91**:1477–1492.

Wassmann P, Duarte CM, Agustí S, Sejr MK. (2011). Footprints of climate change in the Arctic marine ecosystem. *Glob Chang Biol* **17**:1235–1249.

Webster MA, Rigor IG, Nghiem S V., Kurtz NT, Farrell SL, Perovich DK, *et al.* (2014). Interdecadal changes in snow depth on Arctic sea ice. *J Geophys Res Ocean* **119**:5395–5406.

Worm B, Lotze HK, Hillebrand H, Sommer U. (2002). Consumer versus resource control of species diversity and ecosystem functioning. *Nature* **417**:848–851.

Žifčáková L, Baldrian P. (2012). Fungal polysaccharide monooxygenases: new players in the decomposition of cellulose. *Fungal Ecol* **5**:481–489.

Chapter 1: Two New Species of Marine Saprotrrophic Sphaeroformids in the Mesomycetozoea Isolated
From the Sub-Arctic Bering Sea¹

Abstract

The genus *Sphaeroforma* previously encompassed organisms isolated exclusively from animal symbionts in marine systems. The first saprotrophic sphaeroformids (Mesomycetozoea) isolated from non-animal hosts are described here. *Sphaeroforma sirkka* and *S. napiecek* are also the first species in the genus possessing endogenous DNA-containing motile propagules and central vacuoles, traits that have previously guided morphological differentiation of sphaeroformids from the genus *Creolimax*. Phylogenetic analysis of DNA sequences from the 18S rRNA and the ITS1-5.8S--ITS2 loci firmly place *S. sirkka* and *S. napiecek* within *Sphaeroforma*, extending the number of known species to six within this genus. The discovery of these species increases the geographical range, cellular variation and life history complexity of the sphaeroformids.

¹Hassett BT, Lopez AJ, Gradinger R (2015) Two new species of marine saprophytic sphaeroformids in the Mesomycetozoea isolated from the sub-Arctic Bering Sea. Protist, 166: 310-322.

Introduction

Osmotrophic protists of the Mesomycetozoea (Ichthyosporia) are ecological commensals, mutualists, and parasites in marine, freshwater and terrestrial habitats that have been isolated exclusively from animal symbionts (Glockling et al. 2013). The lack of obvious morphological diagnostic features of the Mesomycetozoea (Marshall and Berbee 2013) hinder the application of morphological characteristics to delineate species boundaries. To circumvent this barrier, DNA sequences of the nuclear ribosomal RNA operon coding region have been used as the basis for the detection and diagnosis of novel species (Jøstensen et al., 2002 and Marshall and Berbee, 2011), the circumscription of novel clades, and the reclassification of previously described species within the Mesomycetozoea (Lohr et al., 2010 and Marshall and Berbee, 2013). Currently, there are over 40 taxa described in the Mesomycetozoea, about half of these are phylotypes (Glockling et al. 2013).

The Mesomycetozoea currently includes two 18S-SSU rRNA monophyletic subgroups: the dermocystida and ichthyophonida (Marshall and Berbee 2011) that branch near the animal-fungal divergence within the eukaryotic supergroup Opisthokonta (Paps et al. 2013). Taxonomy within ichthyophonida has recently been revised to include the placement of *Pseudoperkinsia tapetis* in the genus *Sphaeroforma*, as well as by the addition of two new species: *S. gastrica* and *S. nootkatensis* (Marshall and Berbee 2013). At present, *Sphaeroforma* comprises four species (Marshall and Berbee 2013), which are proposed as a monophyletic assemblage among mesomycetozoean lineages based on molecular evidence.

We investigated the presence and diversity of free-living mesomycetozoeans for the first time in a sub-Arctic water sample, collected from a nearshore estuarine environment in the Bering Sea, close to Nome, Alaska. Culturing and DNA sequence screening revealed two phylogenetically divergent clades of mesomycetozoeans saprobic on pollen. Molecular analysis of concatenated partial small subunit nuclear rRNA (18S) and ITS1-5.8S-ITS2 (ITS) sequences from six isolates places these Bering Sea isolates into the genus *Sphaeroforma*. Additionally, life history characteristics of these isolates differ from those of previously described life histories. We describe these as two new species based on molecular data and life history information.

Results

After editing, alignment and removing incompletely overlapping homologous sequences, the finished multiple sequence alignments (MSAs) consisted of 30 ITS1-5.8S-ITS2 sequences, 24 18S sequences and 21 concatenated sequences (Table 1), where both ITS and 18S reads were available for a specific isolate. Because *Sphaeroforma Arctica* 18S (Jøstensen et al. 2002) and ITS sequences (Marshall and Berbee

2013) are only available from single, distinct isolates, we chose to include a chimeric 18S and ITS concatenation of the two sequences in the concatenated MSA. After end trimming, the aligned sequences spanned 998 basepairs and 656 basepairs for 18S and ITS1-5.8S-ITS2, respectively. No DNA regions were excluded in the alignment procedure or removed from the finished MSAs. A preliminary screening of isolated organisms was conducted using sequences from a fragment of the 28S gene. A BLAST query of sequenced 28S amplicons from B1 and B2 isolates yielded a closest match (89% identity) with a sequence reported from *Amoebidium parasiticum* (GENBANK Accession #EU011932.1). Additional BLAST queries, using 18S rRNA and ITS1-5.8-ITS2 sequences from all isolates examined here, revealed a close similarity (96% and 99% identity for ITS and 18S, respectively) to sequences from isolates of *Sphaeroforma nootkatensis*.

Maximum likelihood (ML) and maximum parsimony analyses of concatenated MSAs, including sequences from the six Nome isolates, all other known members of *Sphaeroforma*, and two *Creolimax fragrantissima* isolates, consistently support two distinct clades, corresponding to two new unique phylotypes nested within *Sphaeroforma*: *S. napiecek* forming a clade with *S. nootkatensis* and *S. sirkka* as the sister group of the *S. nootkatensis/S. napiecek* clade (Fig. 1.0). ML and maximum parsimony trees produced near identical tree topologies with bootstrap values greater than 98% supporting the uniqueness of these phylotypes.

Light Microscopy and Ultrastructure

Once pollen was plated onto PmTG agar media, sphaeroformids were identified by conglomerations of raised circular cells. When subcultured and streaked on tryptone, peptonized milk, and PmTG with variable salt concentration-containing media, *S. sirkka* and *S. napiecek* produced two unique colony types: colonies with a consistent opaque unraised matrix of cells with low adhesion properties that were more likely to smear across a plate than fix to a probing object and easily harvestable, discretely raised large colonies. All isolates of both *S. napiecek* and *S. sirkka* were capable of growing on 9, 18, 26 and 35 salinity-amended peptonized milk agar.

Sphaeroforma sirkka

Following 20 days of incubation and observation, *S. sirkka* isolate B1 failed to release endospores at 4 °C in PmTG broth. In the first 48-hours, cells grew steadily and displayed active organization of cytoplasmic material. Within 48-hours of observation, small (<1 µm) hyaline motile propagules (MPs) were observed entering the field of view, suggesting an alternative method of reproduction than endospore release. Examination of isolate B1 at 1000x magnification revealed the presence of numerous sphaeroformid cells

containing exclusive vacuole-localized and complete cell-associated MPs (Supplemental Material: Video 1) of a similar size class. All isolates of *S. sirrka* produced these small MPs; while these MP-containing sphaeroformid cells were regularly observed, this cell variety constituted <1% of all cells. The quantity of vacuole-localized MPs varied from several small dark granular MPs (Fig. 1.1I) to innumerable larger dark and hyaline MPs (Supplemental Material: Video 1). Complete sphaeroformid cell-associated endogenous swarming MPs were also observed (Supplemental Material: Video 1), but less frequently than the vacuole-localized variety. When small endogenous MP swarms were observed, the cell vacuole was noticed to be absent or to have lost structural integrity, appearing collapsed in nature. DAPI staining of MPs indicate the presence of DNA within these MPs (Supplemental Material: Video 2). Partial release of swarming propagules through a small operculate-like opening in the cell wall was observed twice; however, MPs were not observed to be amoeboid in nature and were too small to detect the presence of flagella through light microscopy. Upon release, hyaline MPs remained motile for over a minute, while those propagules that did not escape and were retained within the cell wall remained motile indefinitely. Motile propagules were produced by three predominant cell types: those with a granular endogenous matrix (Fig. 1.1B), spherical cells with a visible vacuole (Fig. 1.1I), and cells with seemingly no intercellular structures beyond swarming MPs (Supplemental Material: Video 1).

At 1000x magnification, granular cells were observed in a variety of sizes, from newly released spherical endospores (Fig. 1.1J) 3 -10 μm diameter, to large undifferentiated cells over 50- μm in diameter (Fig. 1.1C). Large undifferentiated granular cells were observed to undergo equatorial splitting and release of cell content (Fig. 1.1K), including some motile propagules that became quiescent immediately after release. Small granular cells likewise possessed the ability to produce pseudopod-like projections (Fig. 1.1F) and to differentiate into lobed cells. Contrary to granular cells, lobed cells were not observed developing into the granular variety.

Lobed cells were frequently observed containing a variety of cleaved and uncleaved endospores, ranging from 2 to over 10 lobes (Fig. 1.1H, J, L). After 20-days of monitored growth, massive endospore release was induced by warming colonies to room temperature. Equatorial splitting and release of endospores was observed upon warming, leaving wall castings, many curling at the ends. Likewise, release of endospores through a small terminal opening occurred in mounted specimens. Some cells with smaller vacuole-associated endospores also produced vacuole-localized MPs (Fig. 1.1I). Granular plasmodial cells were frequently observed; however, MPs were not observed associated with granular plasmodial cells. Life history is illustrated in Figure 1.3. The development of MPs and endospores into mature cells is inferred.

Sphaeroforma napiecek

S. napiecek was identified, isolated and cultured in the same manner as *S. sirkka*. Like *S. sirkka*, *S. napiecek* formed plasmodial (Fig. 1.2E), multilobed (Fig. 1.2A, B, C), and granular cells with the same observable life history, including the production of pseudopod-like projections (Fig. 1.2F) and motile propagules. Specifically, vacuole-localized motile propagules were observed in newly released endospores (Fig. 1.2G), as well as in complete-cell swarms (Fig. 1.2D). Consistent with *S. sirkka*, swarms were only observed in cells with collapsed (Fig. 1.2D) or absent (Fig. 1.2I, Supplemental Material: Video 1) vacuoles. Likewise, small motile propagule release was observed through a terminal operculate-like opening in cells (Fig. 1.2I).

Ultrastructure

S. napiecek and *S. sirkka* share many morphological features with other sphaeroformids, including: the presence of cell walls during vegetative growth, multinucleation, presence of cell wall pores and a calyx (Fig. 1.4A, G). Nuclei contain peripheral nucleoli (Fig. 1.4B) and are associated with a single Golgi body with stacked cisternae (when present) (Fig. 1.4A, D). Nuclei of both taxa display swollen perinuclear spaces (Fig. 1.4E). Mitochondria contain flatted plate-like cristae and vary in size; oftentimes, a single mitochondria comprises the majority of cytoplasmic content (Fig. 1.4C).

Cell walls are similar for both taxa and contain a gelatinous calyx exterior to an electron-dense outer and inner layer cell wall. Cell walls vary in thickness, displaying thicker cell walls at polar ends and cell wall blebs (Fig. 1.4H), frequently perforated with pores (Fig. 1.4G). Cell membranes of both taxa are wavy and generally appear to be unassociated with the cell wall.

S. sirkka produces invaginations of the cell membrane that are surrounded by unknown membrane-bound, crescent-shaped structures (CSS) (Fig. 1.5A, B, C, F). CSSs contained numerous folding membranes that were sometimes contiguous with the nuclear and mitochondrial membranes and in association with lipid droplets (Supplemental Figure 1.0B). CSSs form in association with mitochondria, sometimes appearing to share a single membrane (Supplemental Figure 1.0B). CSSs contain electron-dense inclusions (Fig. 1.5A) and remnants of what appear to be mitochondria inside their membranes (Fig. 1.5F). Thick electron-dense strands occur frequently at the base of invaginations (Fig. 1.5B, C, E).

Frequently, the existence of invaginations coincides with membrane-decorated vesicles. These vesicles seem to derive from cell membrane invaginations. (Fig. 1.5A, B, E, F). We were unable to determine the function of CSSs, but they appear related to the formation of invaginations and production of membrane-

decorated vesicles. Some CSSs contain inclusions of a similar nature as membrane-decorated vesicles (Fig. 1.5F), namely: spherical bodies $\sim 0.5 \mu\text{m}$ in diameter accompanied by a short appendage (Fig. 1.5E, F). Dark granular vesicles with short flagellum-like strands were observed outside the cell membrane (Fig. 1.5D).

Cytoplasmic material contains central vacuoles (Fig. 1.5D), inclusions of varied content and lipids. Membrane-bound vacuoles (Fig. 1.4F) differed in number and location in cells. Vacuoles were sometimes associated with the nucleus and capable of absorbing cell content (Fig. 1.4A). Dense lipid droplets were observed in a number of cells, sometimes associated with contiguous nucleus-mitochondria membranes, though not consistently.

Taxonomic summary

Sphaeroforma sirkka

Usually spherically shaped cells $\sim 10 \mu\text{m}$ in diameter, but capable of forming inconsistently shaped plasmodial cells, pseudopodia-like projections and large granular cells greater than $50\text{-}\mu\text{m}$ in diameter. Mitochondria with plate-like cristae, Golgi bodies with stacked cisternae, lipid droplets in cytoplasm, Cell wall composed of a lucent calyx with an electron-dense inner and outer cell wall, perforated by pores. Produces cell membrane invaginations that pinch to form membrane-bound vesicles. Endospore release occurs both through a terminally-located cell wall rupture, as well as through equatorial splitting that leaves empty cell wall castings, capable of curling at the ends. Large granular cells ($>50 \mu\text{m}$) undergo equatorial splitting and release of cell content, in addition to small motile propagules that become quiescent several seconds after release. A number of *S. sirkka* cells possess a central vacuole that contains small ($<1 \mu\text{m}$) swarming motile propagules. This central vacuole appears to collapse or become absent, emptying these small endogenous motile propagules into the main body of the cell. Later, the cell membrane ruptures, releasing these small DNA-containing motile propagules exogenously that stay motile indefinitely. Capable of growing on a variety of media and in the presence of variable salt concentrations on peptonized milk medium ranging in salinity from 9-35. Most closely related to the genus *Creolimax* based on previous phylogenetic studies and morphologically distinguished by the absence of spore release through multiple pore openings. Distinguished from *S. nootkatensis* and *S. Arctica* by the variable presence of plasmodial cells, a central vacuole, the production motile cells $<1 \mu\text{m}$ and phylogenetic inference. Distinguished from *S. tapetis* by the lack of cell wall amoeboid squeezing, a central vacuole, and phylogenetic inference. Distinguished from *S. gastrica* by the absence of pore-associated endospore release, a central vacuole, production of motile propagules, and phylogenetic inference. Distinguished from *S. napiecek* by phylogenetic inference.

Range: Found in association with *Ulva* sp. in estuarine environments in the Bering Sea region of Alaska.

Type: isolate B5, accession #: 18S: KJ736747, ITS: KJ736753

Type locality: subcultured on PmTG medium from sweet gum pollen in conjunction with the macroalgae *Ulva* sp. from a near-shore estuarine system at the Safety Cove Bridge, Nome, Alaska, United States of America. August 2013.

Sphaeroforma napiecek

Usually spherically shaped cells ~10 µm in diameter, but capable of forming inconsistently shaped plasmodial cells, pseudopodia-like projections and large granular cells greater than 50 µm in diameter. Mitochondria with plate-like cristae, Golgi bodies with stacked cisternae, lipid droplets in cytoplasm, Cell wall composed of a lucent calyx with an electron-dense inner and outer cell wall, perforated by pores. Endospore release occurs both through a terminally-located cell wall rupture, as well as through equatorial splitting that leaves empty cell wall castings, capable of curling at the ends. A number of *S. napiecek* cells possess a central vacuole that contains small (<1 µm) swimming motile propagules. This central vacuole appears to collapse or become absent, emptying these small endogenous motile propagules into the main body of the cell. Later, the cell membrane ruptures, releasing these small DNA-containing motile propagules exogenously that stay motile indefinitely. Capable of growing on a variety of media and in the presence of variable salt concentrations on peptonized milk medium ranging from 9-35. Most closely related to the genus *Creolimax* based on previous phylogenetic studies and morphologically distinguished by the absence of spore release through multiple pore openings. Distinguished from *S. nootkatensis* and *S. Arctica* by the variable presence of plasmodial cells, a central vacuole, the production of long-lived motile cells <1 µm and phylogenetic inference. Distinguished from *S. tapetis* by the lack of cell wall amoeboid squeezing, a central vacuole, and phylogenetic inference. Distinguished from *S. gastrica* by the absence of pore-associated endospore release, a central vacuole, production of motile propagules, and phylogenetic inference. Distinguished from *S. sirkka* by phylogenetic inference.

Range: isolated from *Ulva* sp. in an estuarine system of the Bering Sea region, Alaska.

Type: isolate B4, accession #18S: KJ736749; ITS: KJ736755

Type locality: subcultured on PmTG medium from sweet gum pollen in conjunction with the macroalgae *Ulva* from a near-shore estuarine system at the Safety Cove Bridge, Nome, Alaska, United States of America. August 2013.

Discussion

Baiting environmental samples with pollen is an effective method to reduce culturing contaminants and increase cell inoculum prior to plating. This method is high-throughput in that it selects for organisms saprobic on pollen. The limitation to pollen baiting is that, without repeat sampling efforts, it is impossible to determine if cells were free-floating in the environment or associated with a substrate. In this study, a water sample with *Ulva* was collected and buoyant pollen was added. Following several days, large quantities of sphaeroformids were observed on baited pollen. To this end, the estuarine Bering Sea contained a substantial free-floating inoculum load or sphaeroformids migrated to pollen from *Ulva*. In our broth culture analysis, suspended sphaeroformids settled to the bottom of well plates, suggesting that these organisms are not buoyant. Subsequently, we surmise these organisms likely migrated to pollen. Light microscopy observations of motility support this conclusion. Ultimately, the nature of the association of Bering Sea sphaeroformids with *Ulva* is unknown.

Morphologically, *S. sirkka* and *S. napiecek* are unique among the sphaeroformids by having a central vacuole, endogenous motile cells that swarm intercellularly, lipid inclusions and invaginating membranes. Motile stages are not uncommon within the Mesomycetozoa, but do differ between the dermocystida and ichthyophonida, corresponding to a posterior flagellum and amoeboid stages, respectively (Marshall and Berbee 2011). The rapid directional movement observed by the MPs is inconsistent with amoeboid-like motility, suggesting a deviation from the current dogma of motility within the ichthyophonida. TEM analysis revealed hyaline membrane-decorated vesicles with short flagellum-like strands that appear to originate from CSSs. These vesicles are of a similar size class to MPs and occur in areas without cellular material (Fig. 1.5D, E, F), consistent with video and light microscopy observation of MPs. Likewise, dark granular vesicles observed with light microscopy were observed in TEM. These dark granular vesicles had short flagellum-like strands, similar to hyaline vesicles. Extensive TEM was unsuccessful in identifying a 9+2 microtubule arrangement. To this end, the nature of these flagellum-like appendages remains uncharacterized. We hypothesize these vesicles are indeed MPs.

The function of *S. sirkka* and *S. napiecek*'s DNA-containing motile propagules is assumed to be a method of reproduction, though it has not been confirmed. Marshall and Berbee (2010) suggested that *Sphaeroforma tapetis* might be undergoing a cryptic sexual cycle. We did not observe direct evidence for sexual mating (e.g. anastomosis or cell wall fusions); however, it is possible that plasmodial (Supplemental Figure 1.0A) or large granular cells may be a product of cell fusion and the possibility of sex in *S. sirkka* and *S. napiecek* cannot be discounted.

Invaginating membranes are a unique structure among the sphaeroformids, but have been observed in other genera within the Ichthyosporea (Marshall and Berbee 2011). The need for a large cell membrane surface area to produce invaginations could explain the gap/disassociation between cell wall and membrane. The function of CSS is cryptic, but appears intimately associated with formation of invaginations, endoplasmic reticulum and even more so with mitochondria. Endoplasmic reticulum-mitochondrial interactions are a known phenomenon in all Eukarya, responsible for lipid metabolism, calcium cycling and intercellular signaling (Raturi and Simmen 2013); subsequently, observed lipid droplets in association with endoplasmic reticulum-mitochondria complexes (Supplemental Figure 1.0B) support the function of mitochondrial-associated membranes in lipid metabolism in sphaeroformids. Despite this, further research is needed to determine if mitochondria-associated-membranes are involved in reproduction, invagination formation, or CSSs.

Recently *Sphaeroforma* taxa have been distinguished from those in the closely related genus *Creolimax* by the absence of a central vacuole and non-swarming colonies (Marshall and Berbee 2013). The novel morphology of *S. sirkka* and *S. napiecek* eliminates the usefulness of this morphological delineation between the two genera, further limiting the application of morphological-based diagnostics. The life history of sphaeroformids has largely been defined by equatorial splitting and subsequent endospore release, based on *S. Arctica* (Jøstensen et al. 2002), *S. nootkatensis* and *S. gastric* (Marshall and Berbee 2013). The central understanding of *Sphaeroforma* reproduction became increasingly more complex with the reclassification of *Pseudoperkesis tapetis* to *S. tapetis*; in addition to cell wall splitting, *S. tapetis* also produces short-lived motile amoeboid cells (Marshall and Berbee 2013). With the addition of *S. sirkka* and *S. napiecek*, the life history complexity within the genus *Sphaeroforma* increases further. In addition to endospore release through terminal ruptures and equatorial splitting, *S. sirkka* and *S. napiecek* produce motile cells in a central vacuole that release into the cell cavity, before exogenous dissemination, eventually becoming capable of rapidly swimming across several fields of view (>1-mm). *S. sirkka* and *S. napiecek* are also unique among the sphaeroformids in the production of large granular cells (~50-µm) that may release substantial cell content, contributing to the consistent opaque unraised matrix of cells with low adhesion properties, observed in agar media growth. The nature by which large granular cells, plasmodial cell, and MP-containing cells develop is unknown. The complex life cycle of these novel sphaeroformids and the interpretation of the observed cell types and structures offer fascinating opportunities for future work. Based on the current knowledge we propose a general life cycle combining our TEM, and various light microscopical observations. It appears that *S. sirkka* and *S.*

napiecek share similar life histories and morphologies and are distinguished solely by phylogenetic inference.

Both sympatric and allopatric modes of speciation are plausible mechanisms underlying the genetic divergence and morphological differences between Bering Sea and British Columbia isolates (Marshall and Berbee 2013) documented here. As the first saprotrophic species in the Mesomycetozoea, sympatric speciation mediated by resource partitioning away from the symbiotic relationship may have favored the development of a free-living life history strategy, e.g. long-lived motile spores and lipid energy reserves. The geographical distance (~3,000 km) between isolation sites of Bering Sea and British Columbia species is compatible with divergence and speciation under allopatric conditions. In the nearshore environment, varying salinities from freshwater discharge exert strong selection pressure on marine organisms. The Bering Sea isolates we describe here, possess the ability to grow under variable salinities. This halotolerance may be an enhancer of geographical isolation linked to brackish water systems, leading to speciation and divergence from other sphaeroformids.

Conclusions

The newly described species, *Sphaeroforma sirkka* and *S. napiecek* considerably expand the genetic, environmental, and life history diversity of the genus *Sphaeroforma*. They represent the first saprotrophic sphaeroformids and mesomycetozoeans to be isolated from a non-animal host.

Methods

Isolation and culture: A water sample containing the filamentous macroalgae *Ulva* sp. was collected from the estuarine Safety Cove east of Nome, Alaska (64°28'19.55"N, 164°44'47.23"W; salinity 17) on August 30th, 2013. Safety Cove salinity was measured in the lab using a temperature/salinity probe (YSI) from water samples stored at 4 °C. Water samples were baited with *Liquidambar styraciflua* (sweetgum) pollen (Sparrow 1960) and incubated for 3-days at 4 °C. Pollen containing fungal-like organisms was streaked onto PmTG media containing 1-g peptonized milk, 1-g tryptone, 5-g glucose, and 20-g agar liter⁻¹ of Instant Ocean seawater adjusted to a salinity of 20 and amended with streptomycin sulfate and penicillin G antibiotics. Six isolates were harvested, resuspended in Instant Ocean seawater and subcultured from a single cell, grown in axenic culture and maintained on PmTG agar at 4 °C until molecular analysis.

DNA extraction, amplification, and sequencing: Total genomic DNA was isolated from 14-day cell cultures using the DNeasy Plant Mini Kit (Qiagen) following manufacturer's protocols. Segments of the major ribosomal RNA coding region were amplified by polymerase chain reaction (PCR) using the following primer pairs: LR0R/LR5, which targets a ~900 basepair (bp) segment of the 28S rRNA gene (Rehner and Samuels, 1994 and Vilgalys and Hester, 1990), NS1/NS4, which targets a ~1200-bp portion of the 18S rRNA gene (White et al. 1990), and ITS4/ITS5, which targets the entire ITS1-5.8S-ITS2 internal transcribed spacer (White et al. 1990). 28S primers were used to preliminarily screen isolates of interest, but not included in phylogenetic analysis. PCRs were conducted using Platinum Taq (Life Sciences); reagent concentrations were according to manufacturer's protocol with a starting concentration of 10ng/ μ l of genomic DNA. Thermocycling parameters were: 28S LSU: 29 cycles at 95 °C melting for 1-minute, 50 °C annealing for 30-seconds, 72 °C extension for 90-seconds; 18S: 10 cycles- 95 °C melting for 29-seconds, 50 °C annealing for 29-seconds, and an extension step at 72 °C for 90-seconds, 29-cycles- 95 °C melting for 29-seconds, 47 °C annealing for 29-seconds and a final extension for 90-seconds; ITS1-5.8S-ITS2: 95 °C melting for 1-minute, 50 °C annealing for 1-minute, 72 °C extension for 1-minute with a final extension of 5-minutes at 72 °C. Amplification products were purified using the PureLink PCR Purification kit (Life Sciences) and then used as templates in Sanger sequencing reactions using the BigDye Terminator v3.1 chemistry (Applied Biosystems). Purified sequencing reaction products were analyzed on a 3130xl ABI instrument at the Institute of Arctic Biology DNA Core Lab at the University of Alaska Fairbanks. PCR products were sequenced in both directions to maximize confidence on base calls along the length of the amplicon. Chromatographs were examined in MEGA6 (Tamura et al. 2013) for the presence of secondary peaks and conflicting bases. Low quality sequencing reads were discarded and the amplicons resequenced or re-amplified and resequenced. High quality sequences were aligned by gene region with ClustalW. High variability regions with ambiguous alignment were manually edited to minimize homology artifacts introduced by automated alignment. All aligned sites were included in subsequent analyses. The resulting multiple sequence alignments (MSAs) were then expanded with the addition of publicly available sequence data and used in subsequent phylogenetic analysis.

Phylogenetic analysis: MSAs including sequences from the six Nome, Alaska isolates and all other publicly available homologous sequences from species of *Sphaeroforma* were employed in these analyses. Maximum likelihood (ML) and maximum parsimony trees were estimated from each of the three MSAs. The nucleotide substitution model used in ML analyses was selected by application of the model comparison routines implemented in MEGA6. Both Bayesian and Akaike information criteria identified the Tamura-3-parameter model (Tamura 1992) with among site rate variation (T92+G) as the best fitting model for concatenated sequences. ML trees were generated with MEGA6 using the best

fitting model. Bootstrap values were generated through tree estimation from 1000 pseudoreplicates (site resampling with replacement) of the MSAs. Maximum parsimony analysis was conducted in SeaView (Bazin et al. 2014) using 1000 bootstrap replicates.

Morphology and substrate utilization: Life history and growth substrate utilization was assessed for the six Nome isolates. Two isolates representative of *S. sirkka* and *S. napiecek* (B1 and B4) were grown independently in PmTG broth in 96-well plates at room temperature and also at 4 °C for live 48-hour video recording (United Scope, MU500) of growth development on a Zeiss Telaval 31 inverted scope. After 48-hours, growth was observed and photographed every 12-hours. Due to the low concentration of unique cell types, snapshots of the life history were obtained using a Leica DM2000 compound microscope with mounted samples on a standard glass slide with coverslip to supplement monitored growth. Additionally, reproduction of all six isolates was assessed on several media including: tryptone and agar, peptonized milk and agar, and PmTG media. Peptonized milk agar was amended with variable salinities of: 8.75, 17.5, 26.25, and 35, corresponding to roughly 25%, 50%, 75%, and 100% of standard marine salinity and observed for visible growth after 7-days.

Nucleic acid staining was conducted using DAPI (Sigma-Aldrich) DNA light and a Zeiss Axiovert 35 inverted microscope with UV filter set. Colonies with a consistent opaque unraised matrix of cells were harvested from 2-month old cultures and suspended in sterile seawater amended with DAPI staining solution on a glass slide with coverslip and studied live with video recording by a ocular-mounted camera (United Scope, MU500).

TEM: Cells were fixed in Modified Karnovsky's fixative for 1-hour at room temperature and pelleted lightly. Cells were washed and post fixed for 1 hour in 1% Osmium tetroxide in 0.1 M Sodium cacodylate buffer in the dark. After post-fixation cells were washed with 0.1 M sodium cacodylate buffer twice, once with nanopure water, and en-bloc stained with 2% uranyl acetate. The pellets were dehydrated through a graded series of ethanol, followed by 3-changes of acetonitrile and embedded in Eponate. 70-nm cross sections were cut on a Leica UC6 ultramicrotome and post-stained with uranyl acetate and lead citrate. Images were TEM collected on a JEOL (Model: JEM 1200 EXII) with a Tietz TEM high-resolution camera (Model: F224).

Acknowledgements

This material is based upon work supported by the National Science Foundation under the grants “Marine Ecosystem Sustainability in the Arctic and SubArctic (MESAS)” IGERT (Award DGE-0801720) and “The Diversity, Seasonality and Function of Parasitic fungi in Arctic Sea Ice” (Award# 1303901). TEM analysis and ultramicrotomography was conducted by the Pennsylvania State University Microscopy and Cytometry Facility - University Park, PA. We thank Dr. Katrin Iken for her expertise in macroalgae identification, the staff at UAF's Core Facility for Nucleic Acid Analysis for technical assistance in molecular work and Jennifer Questel for assistance with MEGA6. A very special thanks goes to Erin M. Hassett for her sketches of organismal life histories. Isolation, culturing, DNA extraction, sequencing, PCR, TEM, manuscript writing, manuscript formatting was conducted by Brandon T. Hassett. Phylogenetic analysis was assisted by Andres Lopez. Manuscript editing was conducted by Rolf Gradinger.

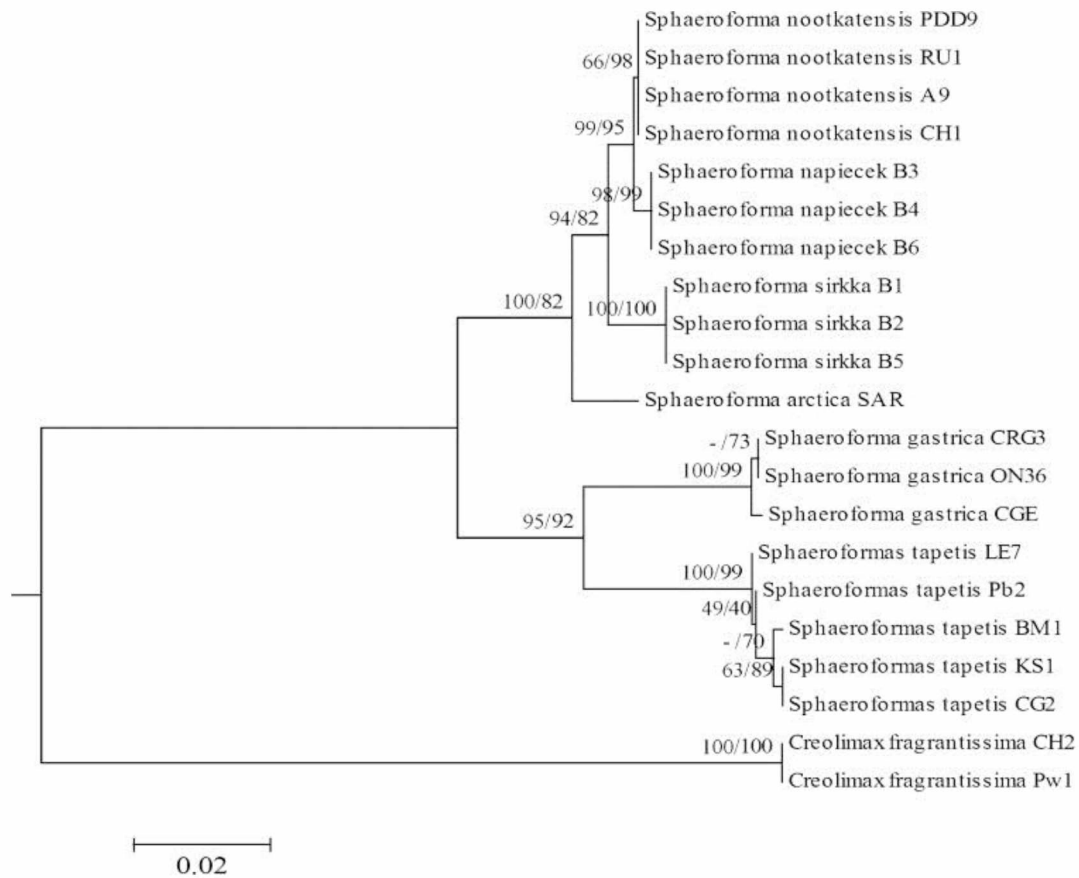


Figure 1.0. Maximum likelihood tree. Maximum likelihood tree with maximum parsimony bootstrap values (MP/ML) of taxa from concatenated ITS/18S sequences showing statistical support of 6 phylotypes. The tree is drawn to scale, with branch lengths measured in the number of substitutions per site. The analysis involved 21 nucleotide sequences. There were a total of 1659 positions in the final dataset.

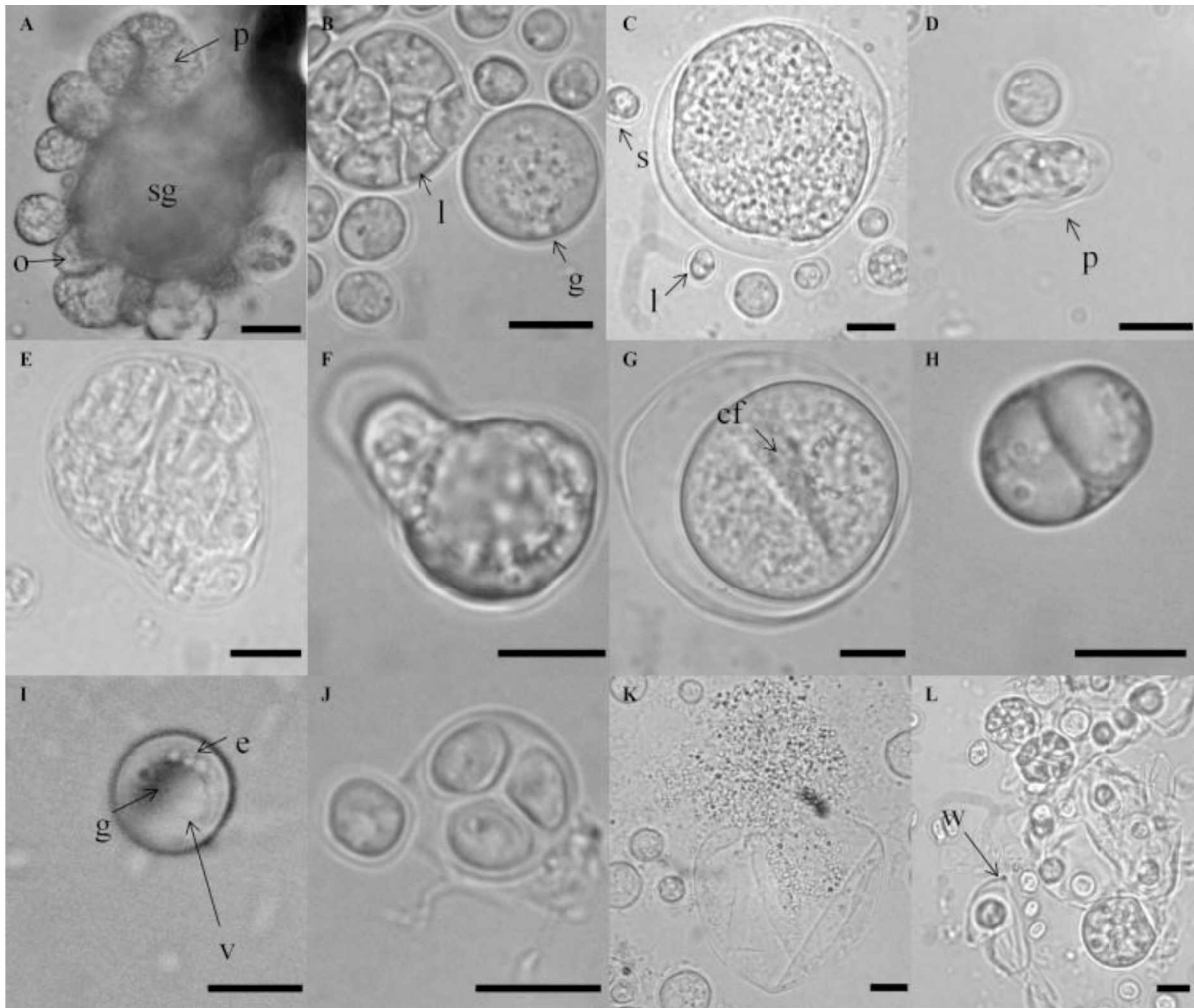


Figure 1.1. Light microscopy-observed morphology of *Sphaeroforma sirkka*. Light microscopy-observed morphology of *Sphaeroforma sirkka* with 100x oil immersion lens. Scale bar represents 10- μ m. A. Sweet gum (sg) pollen colonized by saprotrophic members of *Sphaeroforma* displaying plasmodial (p), oblong (o) and spherical morphology with variable cell size (4-30 μ m). B. Two frequently observed cell types that correspond to mode of asexual reproduction: granular (g) and lobed (l). C. Isolate B1 displaying variable cell size and morphology, including large granular cells up to 50- μ m in diameter, spherical cells (s), and lobed cells (l). D. Plasmodial cell (p) contrasting typical spherical cell. E. Large plasmodial cell. F. Small spherical cell with a pseudopod-like projection. G. Large granular cell with a predominant cleavage furrow (cf), likely differentiating into a lobed cell. H. A differentiating lobed cell. I. Spherical cell with both vacuole (v)-associated endospores (e) and vacuole-localized motile granules (g) (<1 μ m). J. Terminal release of cleaved endospores through the spherical cell wall. K. Granular cell undergoing hemispherical-splitting and subsequent release of endogenous contents and motile propagules. Motile propagules quiescence shortly after release. L. Parent cell wall castings (w) split in even halves following endospore discharge.

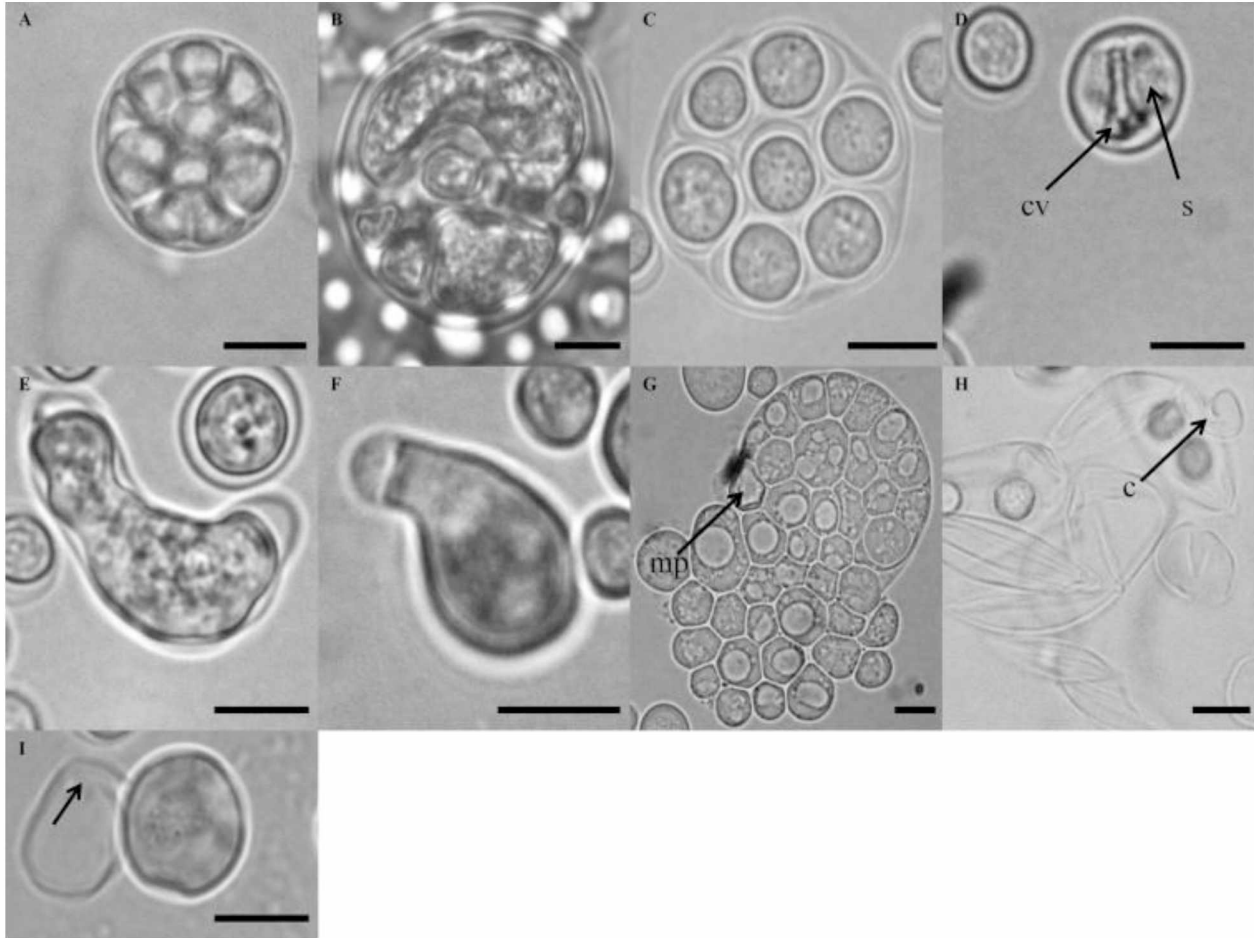


Figure 1.2. Light microscopy-observed morphology of *Sphaeroforma napiecek*. Light microscopy-observed morphology of *Sphaeroforma napiecek* with 100x oil immersion objective. Scale bar represents 10- μ m. A. Typical circular *S. napiecek* cell with multiple cleaving endospores. B. Large multilobed spherical cell. C. Spherical cell with fully cleaved and organized granular endospores of variable size before release. D. Complete-cell swarming motile propagules (s) around the collapsed vacuole (cv). E. Granular plasmodial cell contrasting a typical spherical cell. F. Pseudopod-like projection. G. Terminal release of vacuolated endospores, some containing vacuole-localized motile propagules (mp). H. Cell wall castings displaying equatorial splitting and curled ends (c). I. Operculate-like opening releasing motile propagules terminally in the path denoted by the arrow.

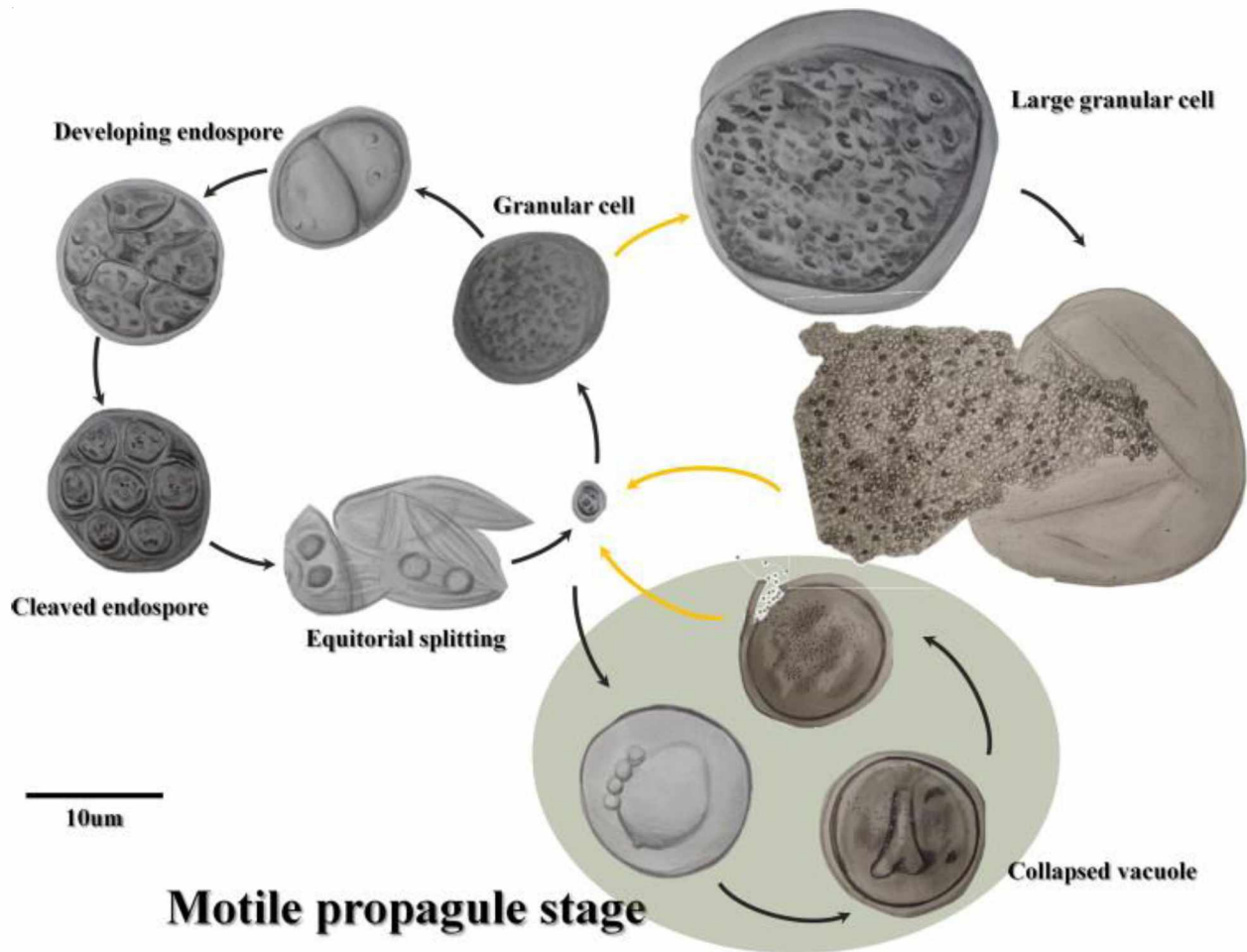


Figure 1.3. Life cycle of *Sphaeroforma sirkka* and *S. napiecek*. Life history of sphaeroformids based on observed (black arrows) and inferred transitions (orange arrows). Three distinct methods of reproduction occur: equatorial splitting and release of cleaved endospores, the development and splitting of large granular cells (not drawn to scale), and the motile propagule stage (green background).

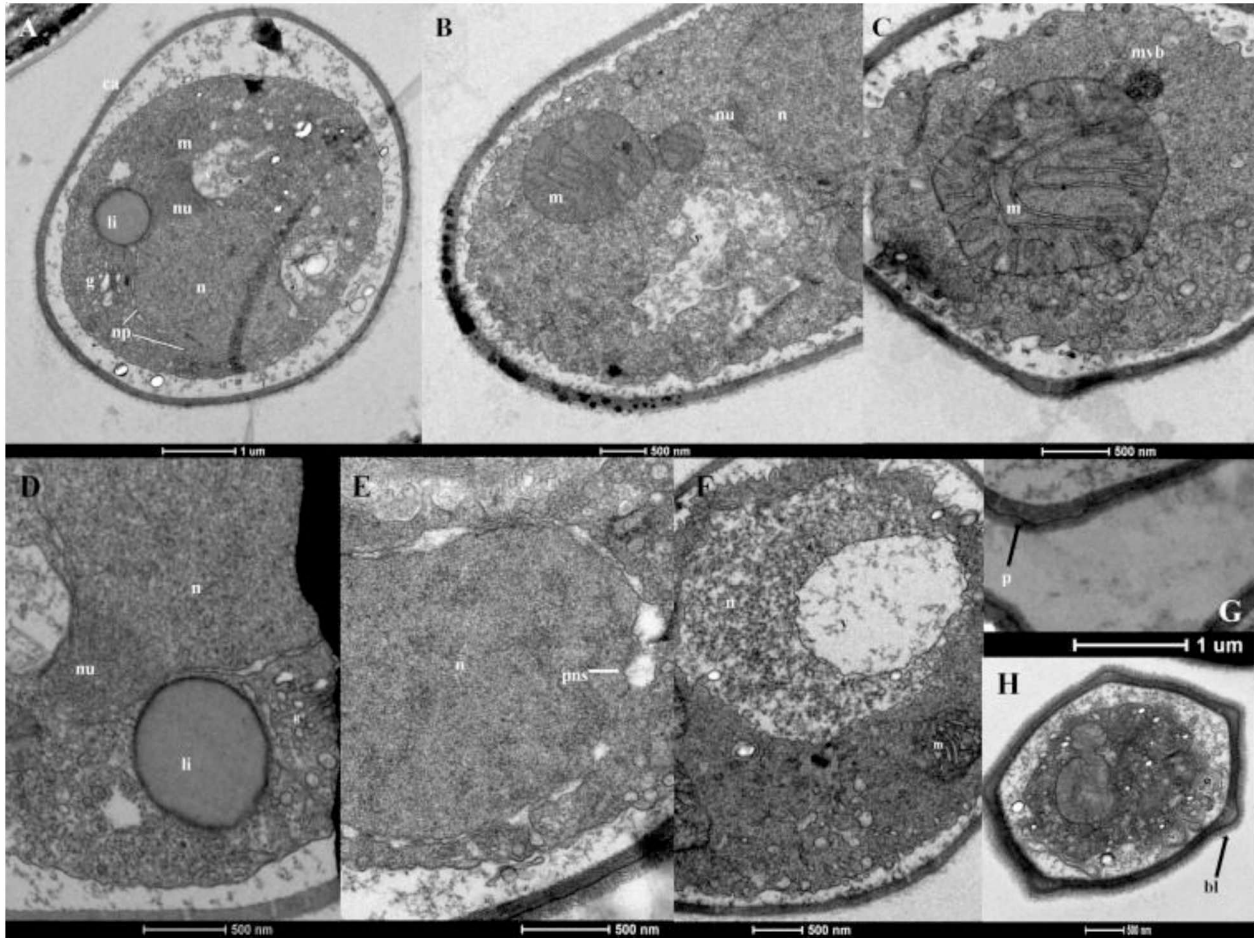


Figure 1.4. Electron micrographs of *S. napiecek* and *S. sirkka*. Electron micrographs of *S. napiecek* and *S. sirkka* displaying typical organelles and cell wall structure. A. *S. napiecek* nucleus (n) with nuclear pores (np) containing a peripheral nucleolus (nu) positioned between a lipid globule (li) and vacuole (v). Golgi body with stacked cisternae associated with nucleus. Cell membrane generally unassociated with the cell wall and mitochondria (m) with plate-like cristae. B. Elongated cell of *S. napiecek* with a central vacuole (v), mitochondria (m) and nucleus (n) with nucleolus (nu). C. Large mitochondria of *S. sirkka* comprising majority of cytoplasmic content with multivesicular body (mvb). D. *S. napiecek* lipid globule (li) in association with Golgi body (g) and nucleus (n). Black markings are an artifact of imaging. E. *S. napiecek* nucleus (n) with swollen perinuclear space (pns). F. *S. napiecek* central vacuole. G. *S. napiecek* cell wall with pores (p). H. *S. sirkka* displaying cell wall blebs (bl) perforated by pores.

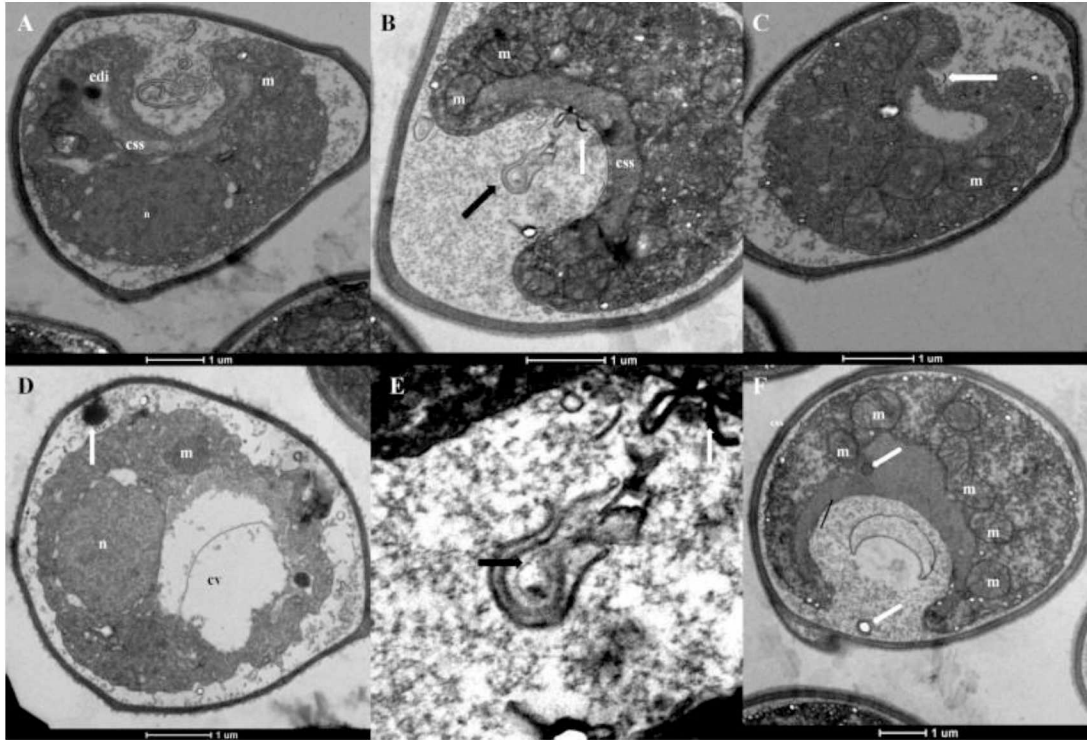


Figure 1.5. *S. napiecek* and *S. sirkka* cells containing crescent shaped structures. A. *S. sirkka* cell with large invagination enclosing a membrane decorated vesicle pinching away from the cell membrane. Invagination is surrounded by a crescent shaped structure (css) that contains an electron-dense inclusion (edi). B. *S. sirkka* cell with invagination giving rise to a membrane-decorated vesicle (black arrow). Invagination contains crescent shaped structure (css) with electron-dense strand at base (white arrow). Note close association of mitochondria (m) with css. C. *S. sirkka* cell with invagination displaying electron-dense strand at base. D. *S. napiecek* cell with large central vacuole (cv) and dark granular vesicle with short flagellum-like strand (white arrow). E. Enlarged view of Figure 6B (above) showing greater resolution of membrane-decorated hyaline vesicle (black arrow). Note short tail. F. *S. sirkka* cell with five mitochondria (m) interacting with crescent-shape structure (css). CSS contains circular vesicle with short flagellum-like tail (white arrow top) and a partially intact mitochondria (black arrow). Membrane-decorate vesicle outside cell membrane (white arrow bottom).

Table 1.0. Sequence database classification with NCBI accession numbers, isolates, and targeted rRNA locus used for phylogenetic analysis and generation of trees.

Species	rRNA Locus	Accession Number
Sphaeroforma nootkatensis PDD9	18S	JX992713.1
Sphaeroforma nootkatensis CH1	18S	JX992714.1
Sphaeroforma nootkatensis A9	18S	JX992712.1
Sphaeroforma nootkatensis RU1	18S	JX992710.1
Pseudoperkinsus tapetis BM1	18S	GU727522.1
Pseudoperkinsus tapetis KS1	18S	GU727524.1
Pseudoperkinsus tapetis CG2	18S	GU727525.1
Pseudoperkinsus tapetis Pb2	18S	GU727526.1
Pseudoperkinsus tapetis LE7	18S	GU727527.1
Sphaeroforma gastrica ON36	18S	JX992717.1
Sphaeroforma gastrica CRG3	18S	JX992715.1
Sphaeroforma gastrica CGE	18S	JX992716.1
Sphaeroforma Arctica	18s	Y16260.2
Sphaeroforma sirkka B1	18S	KJ736745
Sphaeroforma sirkka B2	18S	KJ736746
Sphaeroforma sirkka B5	18S	KJ736747
Sphaeroforma napiecek B3	18S	KJ736748
Sphaeroforma napiecek B4	18S	KJ736749
Sphaeroforma napiecek B6	18S	KJ736750
Creolimax fragrantissima CH2	18S	EU124915.1
Creolimax fragrantissima PW1	18S	EU124914.1
Sphaeroforma nootkatensis PDD9	ITS1-5.8S-ITS2	JX992686.1
Sphaeroforma nootkatensis RU1	ITS1-5.8S-ITS2	JX992693.1
Sphaeroforma nootkatensis A9	ITS1-5.8S-ITS2	JX992684.1
Sphaeroforma nootkatensis CH1	ITS1-5.8S-ITS2	JX992681.1
Sphaeroforma Arctica SAR	ITS1-5.8S-ITS2	JX992683.1
Pseudoperkinsus tapetis Pb2	ITS1-5.8S-ITS2	GU727336.1
Pseudoperkinsus tapetis BM1	ITS1-5.8S-ITS2	GU727345.1
Pseudoperkinsus tapetis KS1	ITS1-5.8S-ITS2	GU727311.1
Pseudoperkinsus tapetis CG2	ITS1-5.8S-ITS2	GU727339.1
Pseudoperkinsus tapetis LE7	ITS1-5.8S-ITS2	GU727338.1
Sphaeroforma gastrica ON36	ITS1-5.8S-ITS2	JX992677.1
Sphaeroforma gastrica CRG3	ITS1-5.8S-ITS2	JX992673.1
Sphaeroforma gastrica CGE	ITS1-5.8S-ITS2	JX992678.1
Sphaeroforma sirkka B1	ITS1-5.8S-ITS2	KJ736752
Sphaeroforma sirkka B2	ITS1-5.8S-ITS2	KJ736751
Sphaeroforma sirkka B5	ITS1-5.8S-ITS2	KJ736753
Sphaeroforma napiecek B3	ITS1-5.8S-ITS2	KJ736754
Sphaeroforma napiecek B4	ITS1-5.8S-ITS2	KJ736755
Sphaeroforma napiecek B6	ITS1-5.8S-ITS2	KJ736756
Creolimax fragrantissima CH2	ITS1-5.8S-ITS2	EU124891.1
Creolimax fragrantissima PW1	ITS1-5.8S-ITS2	EU124895.1

Works Cited

- Bazinet AL, Zwickl DJ, Cummings MP (2014) A gateway for phylogenetic analysis powered by grid computing featuring GARLI 2.0. *Syst Biol* 63: 812-818
- Glockling SL, Marshall WL, Gleason FH (2013) Phylogenetic interpretations and ecological potentials of the Mesomycetozoa (Ichthyosporia). *Fungal Ecol* 6:237–247
- Jostensen JP, Sperstad S, Johansen S, Landfald B (2002) Molecular-phylogenetic, structural and biochemical features of a cold-adapted, marine ichthyosporian near the animal-fungal divergence, described from in vitro cultures. *Eur J Protistol* 38: 93–104
- Lohr JN, Laforsch C, Koerner H, Wolinska J (2010) A *Daphnia* parasite (*Caullelya mesnili*) constitutes a new member of the *Ichthyosporia*, a group of protists near the animal-fungi divergence. *J Eukaryot Microbiol* 57: 328–36
- Marshall WL, Berbee ML (2010) Population-level analyses indirectly reveal cryptic sex and life history traits of *Pseudoperkinsus tapetis* (Ichthyosporia, Opisthokonta): a unicellular relative of the animals. *Mol Biol Evol* 27: 2014-26
- Marshall WL, Berbee ML (2011) Facing unknowns: living cultures (*Pirum gemmata* gen. nov., sp. nov., and *Abeoforma whisleri*, gen. nov., sp. nov.) from invertebrate digestive tracts represent an undescribed clade within the unicellular Opisthokont lineage ichthyosporia (Mesomycetozoa). *Protist* 162:33–57
- Marshall WL, Berbee ML (2013) Comparative morphology and genealogical delimitation of cryptic species of sympatric isolates of *Sphaeroforma* (Ichthyosporia, Opisthokonta). *Protist* 164:287–311
- Paps J, Medina-Chacón LA, Marshall WL, Suga H, Ruiz-Trillo I (2013) Molecular phylogeny of unikonts: new insights into the position of apusomonads and ancyromonads and the internal relationships of opisthokonts. *Protist* 164:2–12
- Raturi A, Simmen T (2013) Where the endoplasmic reticulum and the mitochondrion tie the knot: the mitochondria-associated membrane. *Biochim Biophys Acta* 1833:213-224
- Rehner SA, Samuels GJ (1994) Taxonomy and phylogeny of *Gliocladium* analysed from nuclear large subunit ribosomal DNA sequences. *Mycol Res* 98:625–634

Sparrow FK (1960) Aquatic Phycomycetes. University of Michigan Press, Ann Arbor, 1187 p

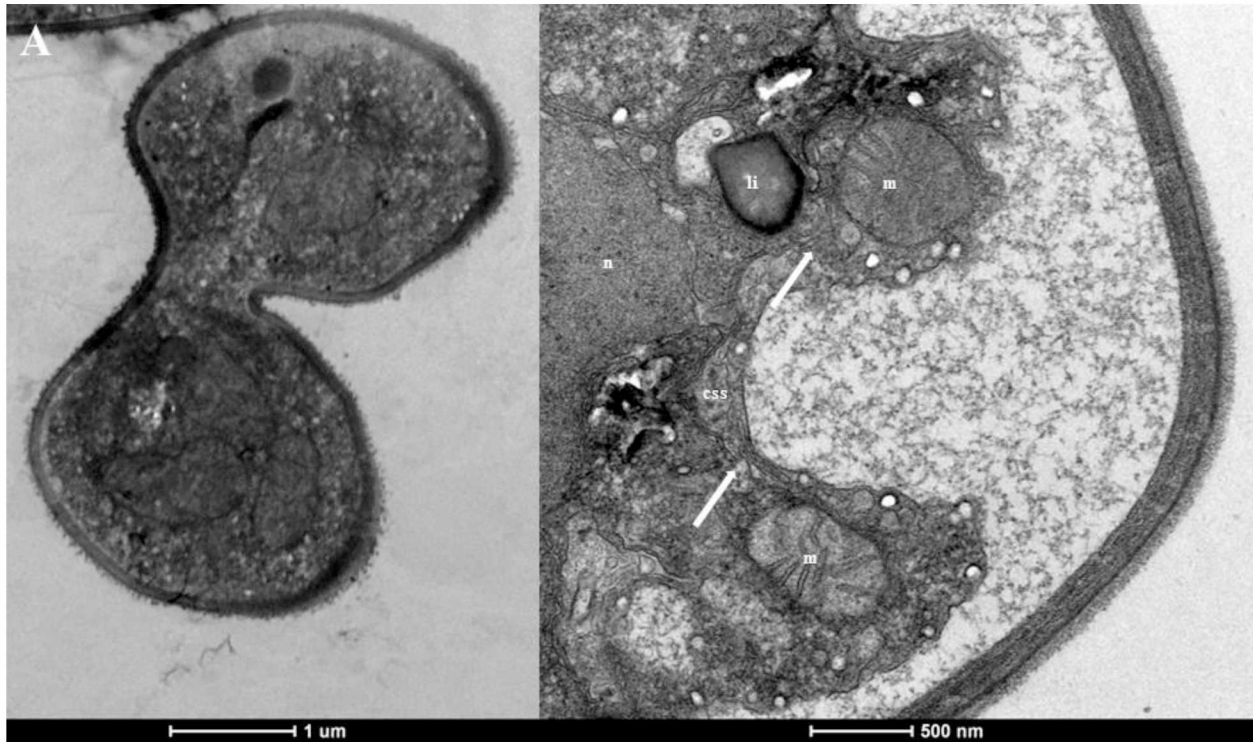
Tamura K (1992) Estimation of the number of nucleotide substitutions when there are strong transition-transversion and G+C-content biases. Mol Biol Evol 9:678–87

Tamura K, Stecher G, Peterson D, Filipski A, Kumar S (2013) MEGA6: Molecular Evolutionary Genetics Analysis version 6.0. Mol Biol Evol 30:2725–2729

Vilgalys R, Hester M (1990) Rapid genetic identification and mapping of several *Cryptococcus* species . J Bacteriol 172: 4238-4246

White T, Lee B, Taylor J (1990) Amplification and direct sequencing of fungal ribosomal RNA genes for phylogenetics. In Innis M, Gelfand D, Sninsky J, White T (eds) PCR protocols: a guide to methods and applications. Academic Press, Orlando, pp 315–322

Supplemental Materials



Supplemental Figure 1.0. Cross section of a plasmodial *S. napiecek* cell. B. *S. sirkka* cell with endoplasmic reticulum (white arrows) contiguous with the nuclear membrane extending and interacting with mitochondria (m). Endoplasmic reticulum fills css at base of invagination. Lipid (li) droplet in close proximity to mitochondria and nucleus (n).

Chapter 2: Draft Genome Sequence of *Sphaeroforma sirkka* B5

Abstract

Until recently, the Mesomycetozoea exclusively comprised organisms isolated from animal symbionts. This paper reports the genome sequences of *Sphaeroforma sirkka*, the first free-living saprotrophic mesomycetozoean.

Genome Announcement

Sphaeroforma sirkka is the first known free-living species in the Mesomycetozoea. It was isolated using pollen grains from a sample collected in the near-shore estuarine environment in the sub-Arctic Bering Sea. The Mesomycetozoea branch near the animal-fungal divergence and are expected to be important to understanding the origins of multicellularity (1, 2). As the first free-living organisms within the diverse mesomycetozoeans, whole genome sequencing could reveal interesting features of sphaeroformids, help guide evolutionary inference and understand the evolution of complex organisms. Novel fatty acid elongase enzymes within the related *Sphaeroforma Arctica* genome have been identified (3) and developed for patent (US 20120233716 A1). To this end, *Sphaeroforma sirkka* is of additional interest, as it is the first sphaeroformid to contain lipid inclusions.

Genomic DNA from *S. sirkka* was generated as previously described (4). A sequencing library was prepared using the Illumina TruSeq Nano DNA Library. The library was loaded on one lane of an Illumina HiSeq 2500 Rapid Run flow cell (v2) and sequenced in a 2 x 100 base pair (bp) paired-end format using HiSeq Rapid SBS reagents (v2). Base calling was performed by Illumina Real Time Analysis (RTA) v1.18.64. Output of RTA was converted to FastQ format with Illumina Bcl2fastq v1.8.4. Final sequence output consisted of 107,591,345 paired-end reads (21.5 Gbp) from a library with an estimated insert size of 750 bps. Assembly was conducted with SOAPdenovo v2.0.4 (5). Maximum read length of 100, average insert size of 750, k-mer size of 66, merge level 2, edge selection of 10X coverage, and a minimum contig length of k+2 were parameterized for assembly. The resulting SOAPdenovo assembly yielded 331,225 contigs assembled into 4,842 scaffolds. Maximum scaffold length was 269,605 bps with an N50/N90 of 45,979/1,535.

Chapter 3: Chytrids Dominate Arctic Marine Fungal Communities¹

Abstract

Climate change is altering Arctic ecosystem structure by changing weather patterns and reducing sea ice coverage. These changes are increasing light penetration into the Arctic Ocean that are forecasted to increase primary production; however, increased light can also induce photoinhibition and cause physiological stress in algae and phytoplankton that can favor disease development. Fungi are voracious parasites in many ecosystems that can modulate the flow of carbon through food webs, yet are poorly characterized in the marine environment. We provide the first data from any marine ecosystem in which fungi in the Chytridiomycota dominate fungal communities and are linked in their occurrence to light intensities and algal stress. Increased light penetration stresses ice algae and elevates disease incidence under reduced snow cover. Our results show that chytrids dominate fungal communities and have the potential to rapidly change primary production patterns with increased light penetration.

¹Hassett BT, Gradinger R (2016) Chytrids dominate Arctic marine fungal communities. *Environmental Microbiology*, doi: 10.1111/1462-2920.13216.

Introduction

The Arctic Ocean remains one of the least studied oceanographic regions in the world (Gradinger, 2009). Its poorly described ecosystem structure and functioning challenge ecologists' abilities to predict food web dynamics and community structures under future climate change scenarios (Boetius *et al.*, 2013; Hollowed *et al.*, 2013; Kortsch *et al.*, 2015). Observed and predicted decreases in sea ice thickness and concomitant increases in light penetration have been linked to changes in the amount and seasonality of primary production on pan Arctic scales (Frey *et al.*, 2014). Such shifts reduce certainty in predicting future food webs even more so, as major components, specifically in the microbial realms have been poorly studied.

The sea ice environment is a dynamic ecosystem that changes its physical structure simultaneously with the strong seasonality of solar radiation at high latitudes and with daily fluctuations of air temperatures. Sea ice is a semi-porous medium that contains a reticulate network of hypersaline brine channels, whose channel size and volume increase with elevated ice temperatures (Cox and Weeks, 1983). In the Arctic winter, air temperatures may be as low as -40°C , resulting in brine channels that are impermeable to fluid and gas exchange. Subsequently, the largest brine channels are frequently located at the ice-water interface adjacent to temperature-stable seawater at its freezing point. Stable temperatures and oceanic fluid exchanges within bottom ice brine channels make this interface a favorable substrate for high concentrations of bacteria, algae and small eukaryotes (Gradinger *et al.*, 2010) (Supplemental Figure 3.0). Within the Arctic sea ice ecosystem, diatoms are often the major contributor of biomass and photosynthate production that drive food webs in Arctic marine ecosystems.

One of the major predicted changes in future Arctic climate scenarios is a shift in precipitation and sea ice coverage duration, leading to a reduced snow cover (Hezel *et al.*, 2013; Webster *et al.*, 2014). Snow cover significantly alters light attenuation (Perovich, 1990, 1998) and regulates photosynthetic ice algal growth (Campbell *et al.*, 2015). Observed snow reductions and increasing sea ice melt pond extent are suggested to cause massive under-ice phytoplankton blooms (Arrigo *et al.*, 2012); however, the increased light intensities can also induce photoinhibition (Cartaxana *et al.*, 2013; Lund-Hansen *et al.*, 2014; Campbell *et al.*, 2015) that exceeds physiological acclimation potentials of the often obligate shade adapted algal species. Consequently, ice ecosystems may approach tipping points, shifting Arctic marine communities and food webs into new equilibrium states (Duarte *et al.*, 2012).

Largely ignored in marine systems (except for commercially relevant fish species), disease is an important structuring component of food webs that can modulate the carbon balance of ecosystems (Olofsson *et al.*, 2011) and facilitate transitions into new equilibrium states (Dakos *et al.*, 2008; Scheffer

et al., 2012). Within aquatic systems, fungi belonging to the Chytridiomycota (chytrids) are important disease-causing organisms of phytoplankton that can delay or terminate algal blooms, rapidly turn over nutrients, and alter microbial successions (Ibelings *et al.*, 2004; Adl and Gupta, 2006; Kagami *et al.*, 2006, 2014; Lepère *et al.*, 2008). Chytrids can also serve as a unique trophic bridge (mycoloop) between phytoplankton and zooplankton/meiofauna by converting carbon acquired from large inedible algae into smaller lipid-rich zoospores used for reproductive dissemination (Kagami *et al.*, 2007). The presence of chytrids have been confirmed from polar sea ice (Horner and Schrader, 1982; Terrado *et al.*, 2011) and detected in zooplankton stomach content in the Bering Sea (Cleary *et al.*, 2015), yet little information is available from any marine ecosystem on the relevance of chytrids, the seasonality and diversity of chytrids, the prevalence of parasitism, and the drivers of this parasitism.

We hypothesized that the sea ice environment could be a prime habitat for parasitic fungi, as it harbors extremely dense blooms of sea ice diatoms in spatially constrained brine channels, making encounter rates between parasites and algae highly probable. Based on a three-year field program in the Alaskan coastal Arctic, our data revealed a dynamic fungal community dominated by the Chytridiomycota actively parasitizing diatoms, whose activity is tightly linked to light-induced algal stress. These data provide the first evidence of a mycoloop in any marine system. We therefore suggest that the mycoloop's relevance to the Arctic marine carbon cycle might increase in the future ocean in regions with less snow and sea ice coverage.

Results

Diatoms typically dominate ice algal diversity and biomass at both poles (Gradinger, 2009), as they did in the Alaskan land-fast ice system we sampled. In May 2013, the ice harbored numerous diatoms infected with chytrid parasites (Fig. 3.0). Parasitized diatoms hosting mature chytrid sporangia visibly possessed less chlorophyll, frequently aggregated around chytrid rhizoids (Fig. 3.0C). Rhizoids extract nutrients from their host for sporangium maturation and the eventual release of free-swimming zoospores to infect new diatoms. Single diatom cells hosted numerous chytrids in different developmental stages (Fig. 3.0D).

In 2014, the seasonality of chytrid parasitism was monitored in Barrow, Alaska from polar night in January to ice melt in August. During the main ice covered period (January to June), chytrids were only observed in April, which typically coincides with the maximum of the ice algal spring bloom, parasitizing 1% of all diatoms. Variability of total disease incidence was low among sample replicates and suggested a high degree of repeatability between sites in close proximity (<1m apart). Observed chytrid parasites showed preference for larger pennate diatoms (>30µm) that frequently localized to an infection court in

close proximity to the diatom girdle band. *Navicula* and *Pleurosigma* species were the most susceptible to chytrid parasitism (Fig. 3.1A).

To further assess the seasonality and occurrence of Arctic Ocean chytrids and the greater fungal community, 18S rRNA barcoding sequences were examined from sea ice and sea floor sediments (<20m depth) in 2014. Based on the analysis of >12 million 18S rRNA gene barcodes, the Chytridiomycota dominated fungal communities in both sea ice (Fig. 3.1A) and sediments (Fig. 3.1B) and constituted up to 10% of all eukaryotic sequences in May sediment. In sea ice, chytrids comprised >70% of all fungal reads in April and over 95% of fungal reads from seafloor samples in May (corresponding to their peak abundances).

BLAST queries and phylogenetic estimates of the five most abundant OTUs from each month in ice and sediment identified the *Mesochytriales*, *Chytridiales*, *Rhizophydiales*, and the *Lobulomycetales* as the closest related taxonomic orders. Additionally, phylogenetic placement of sequence reads grouped two sequences with the *Gromochytriales* (Supplemental Figure 3.1). Additionally, fungal members within the Ascomycota, Basidiomycota, Cryptomycota, Blastocladiomycota, Neocallimastigomycota, and Zygomycota were detected in sea ice and sediment. In January sea ice and in June sediments, members of the Dikarya and the Zygomycota dominated fungal communities, respectively (Fig. 3.1). The Dikarya was comprised of a mixture of ascomycotous yeasts belonging to *Sporobolomyces* and *Kluyveromyces* and conidiating molds, such as *Sporosorium*, *Cladosporium* and *Aureobasidium*. The majority (>99%) of Zygomycota (Entomophthoromycota) sequences belonged to *Basidiobolus*. The taxonomic placement of *Basidiobolus* varies with phylogenetic hypothesis (Gryganskyi *et al.*, 2013) and remains unresolved; subsequently, we placed *Basidiobolus* in their historical context as Zygomycota.

In 2015, we conducted a repeated measures, graded snow cover experiment to assess the effects of reduced snow cover/increased light on chytrid parasitism by removing snow from five random test sites adjacent to a paired control. Snow depth is spatially heterogeneous in the sea ice ecosystem (Perovich, 1990) and ranged from 5-46 cm within our undisturbed control sites in 2015. In snow-cleared sites with elevated under-ice photo flux densities ($43 \text{ uE m}^{-2} \text{ s}^{-1}$), ice algae had significantly (two-tail t-Test, $p=0.001$) reduced photosynthetic yields. Three days into the experiment, parasitism was low and not significantly different between control and experimental plots (ANOVA, $p=0.367$); yet, after seven days, diatoms in the snow-cleared area were nearly 5x more likely (ANOVA, $p<0.001$) to be infected with chytrids relative to the control (Fig. 3.2A). Radiative transfer processes are more exponential than linear with snow depth (Perovich, 1990). To this end, when snow depths from undisturbed control sites were plotted against disease incidence using an exponential curve (due to the exponential relation between light

attenuation and snow depth), snow depth explained 45% of the variability of infection in natural undisturbed plots (Fig. 3.2B). The relationship between light and infection was further explored by plotting normalized 18S rRNA gene barcode sequences against snow depths from the 2014 field data. Snow depth explained 94% of the variability of all Chytridiomycota sequences detected between months (Fig. 3.2C).

Discussion

Fungi are one of the most under-studied microbial groups in the ocean (Singh *et al.*, 2012) and remain largely undescribed in the Arctic marine environment. Based on a three year study in the Alaskan land-fast sea ice ecosystem, we determined that the Arctic marine ecosystem is a prime habitat for a dynamic fungal community. The life histories and abundances of Arctic marine fungi are closely tied to the seasonally varying photon flux that sustains and stresses photosynthetic organisms. These observations from the Alaskan land-fast ecosystem detail the first functional roles for fungi in the Arctic marine environment that may produce a unique trophic bridge to carbon acquisition for smaller metazoans.

We observed a strong seasonality and host specificity of parasitic chytrids on diatoms, as in other aquatic ecosystems (Powell, 1993). Large pennate diatoms were observed to be parasitized in April, near the height of the algal bloom. We did not observe epibiotic chytrids in sediment samples, but rather endogenous chytrid-like cells (Supplemental Figure 3.2) within diatom frustules that could serve as a disease vector, if advected or entrained into ice during ice formation (Eicken *et al.*, 2005). Frequently, single diatom cells were host to multiple chytrids in different developmental stages; subsequently, these observations underline the parasitic nature of diatom-chytrid interactions. Chytrids display a range of diverging morphologies that frequently include endobiotic life histories and life stages without branching rhizoids (Sparrow, 1960); subsequently, our cell counts of only epibiotic chytrids are likely an underrepresentation of true infection rates. We hypothesize that sinking algae may source chytrids to the sediments, resulting in the overwintering of latent inoculum for future disease events.

To supplement cell counts, we sequenced DNA barcodes to assess the seasonal diversity and abundances of fungi. Analysis of these data revealed that members of the Chytridiomycota dominated sea ice and sediment fungal communities. Primer bias can skew organismal abundances during next-gen sequencing; however, in-silico PCR (2 basepair difference) reveals a slight bias against chytrids, amplifying 73% of Dikarya, 83% of Zygomycota, and 67% of the Chytridiomycota (Klindworth *et al.*, 2013). Subsequently, we surmise these data are reflective of a true chytrid dominance of the fungal community.

DNA-detected chytrids were classified into five taxonomic orders by BLAST queries and phylogenetic mapping. Our tree topology does not represent a phylogenetic hypothesis, but is meant to illustrate chytrid diversity within the Arctic marine environment. Each closely related order contains known parasites of algae, capable of infecting diatoms (Simmons *et al.*, 2009), producing endogenous resting spores (Karpov *et al.*, 2014) and existing in marine ecosystems (Lepelletier *et al.*, 2014). Only four species of chytrids have been described from any marine or brackish ecosystem globally (Gleason *et al.*, 2011; Lepelletier *et al.*, 2014). To this end, our data suggest the sea ice ecosystem could be a large reserve of cryptic fungal diversity and provides further evidence that chytrids are integral members throughout the world's cryosphere (Freeman *et al.*, 2009; Naff *et al.*, 2013).

The strong seasonality of chytrid parasitism on algal species (despite the constitutive presence of host species monthly) suggested abiotic variables as a regulating factor for chytrid parasitism. One of the major changes in future Arctic climate scenarios is a shift in precipitation and sea ice coverage duration, leading to a reduced snow cover (Hezel *et al.*, 2013; Webster *et al.*, 2014). As snow cover significantly alters light attenuation (Perovich, 1990, 1998), we hypothesized that reduced snow cover would lead to increased disease susceptibility of diatoms (Harvell *et al.*, 1999) by inducing physiological light stress (Cartaxana *et al.*, 2013; Lund-Hansen *et al.*, 2014). Irradiances exceeding $40 \mu\text{E m}^{-2} \text{s}^{-1}$ saturate photosynthesis in most sea ice algae (Kirst and Wiencke, 1995), with many algae growing best at $10 \mu\text{E m}^{-2} \text{s}^{-1}$ (Karsten *et al.*, 2006). During our graded snow cover experiments, under-ice irradiance exceeded $40 \mu\text{E m}^{-2} \text{s}^{-1}$, resulting in statistically reduced photosynthetic yields, indicative of physiological stress (Manes and Gradinger, 2009). Physiological stress corresponded with significantly elevated disease incidence by chytrids after six days. After nine days, chytrid parasitism dramatically decreased. The mechanism for this reduction is unknown; however, we hypothesize that biological interactions (i.e. induced chytrid mortality from metazoan grazing or another biologic entity) facilitated this attrition.

Fungal community structure is driven by modes of nutrition and environmental selection, yielding major community structural shifts in January and June. During polar night, the sea ice fungal community was dominated by common conidiating members of the Dikarya, likely sourced into the ocean from atmospheric deposition in late summer (Robinson, 2001) and incorporated into sea ice during freeze up. Dikaryotic fungi belonging to *Aureobasidium* and *Cladosporium* are halotolerant/halophilic genera (Kogej *et al.*, 2005; Zalar *et al.*, 2007) that were detected within January sea ice. To this end, we hypothesize that these organisms dominated wintertime fungal communities by tolerating hypersaline conditions within brine channels, during a time when diatom host concentrations are low. In May, an ice melt event expedited transport of algal biomass to the seafloor, resulting in extremely high abundances of chytrids in sediment samples (Supplemental Figure 3.3). Through sedimentation process, sea ice

organisms can settle to the seafloor (Soreide *et al.*, 2013). We hypothesize that sympagic-benthic coupling processes lead to the domination of the fungal community by chytrids in coastal sediment. Following algal sedimentation, the sediment community shifted drastically in June with a dominance of *Basidiobolus sp.* Members of the Zygomycota (Entomophthoromycota) are primarily saprobic (Gryganskyi *et al.*, 2013). This new finding suggests a novel pathway for organic matter in ocean sediments by which organic matter reaching the sea floor may be degraded by saprotrophic Zygomycota (Entomophthoromycota). Specifically in June, saprobic fungal activity may redirect carbon away from higher trophic levels into the microbial loop networks. This process could impact higher trophic levels, as benthic metazoans in Arctic Seas often rely heavily on freshly sinking algal matter for nutrient acquisition (Grebmeier, 2012). This finding is not surprising as fungi are as important in aquatic nutrient cycling as they are in terrestrial environments (Barlocher, 2007).

Our data demonstrate for the first time in a marine environment the seasonality and functionality of parasitic chytrid fungi. Ultimately, the relevance of fungal infection in Arctic ecology remains unknown; however, we suggest that the observed relationship between increasing parasitism with decreasing snow cover may result in the rapid elevation of disease incidence and the restructuring of food webs in the near future by undescribed parasites. Currently, no ecosystem model incorporates the impact of parasitism in the marine environment (Popova *et al.*, 2012), which we believe is a necessity for the future, especially in the Arctic Ocean. Furthermore, the seasonally strong shifts in fungal community structure (on time scales of weeks) suggest a highly dynamic fungal community that is actively metabolizing and facilitating biogeochemical nutrient cycling processes.

Materials and Methods

Ice cores and sea floor sediment samples were collected from the land fast-ice close to Barrow, Alaska (71°21'52.9"; -156°31'26.7"). Sampling sites were located ~3km from the ice edge. Six ice cores were extracted monthly using a 9-cm diameter KOVACs ice corer from the same sampling site monthly (three for DNA analysis and three cores for fungal enumeration). The bottom 10-cm of each core was sectioned using an ethanol sterilized handsaw. Three independent sediment samples were collected monthly through the ice using a Ponar grab and stored in sterile polypropylene tubes.

Ice core sections were melted into 1000 mL of 0.22 µm-filtered seawater. In August, triplicate 1L water samples were collected in a Kemmerer water sampler at 3m depth. Melted ice cores/water were sterilely sieved (64 µm mesh) and vacuum-filtered onto 0.6-µm DTTTP filters (Millipore). Samples were stored at

–80°C until DNA extraction. Samples for cell counts were fixed in formaldehyde (4% final concentration). Fixed samples were stored at room temperature until enumeration.

A 100 m² area of level sea ice was divided into equally spaced grid cells (5 m² each). Five cells were randomly selected from within the grid for repeated sampling. Snow-covered control sites were established 10 m from snow cleared experimental sites. Triplicate random sampling was conducted within both control and experimental sites every other day. To assure the control sites' snow remained undisturbed, a plank was utilized to access the interior of each site for sampling. Experimental sites were cleared of snow every other day. Brine was collected from triplicate ice cores and immediately stored in an insulated chest. Photosynthetic yield of brine was assessed using a Water-PAM (Walz, Germany) from averaged triplicate technical replicates. Under-ice light measurements were assessed using a Li-Cor Li-193 Spherical Quantum Sensor attached to a Li-Cor 1400 data logger.

DNA from sediment was extracted using the PowerMax Soil DNA isolation kit (MO-BIO). Sea ice filter extractions were conducted by bead beating for 1 minute in phosphate buffer, followed by phenol-chloroform extraction. Replicates were pooled before PCR. Target amplicons were generated using the eukaryote-specific primers 18S-82F (5'-GAAACTGCGAATGGCTC-3') and Ek-516R (5'-ACCAGACTTGCCCTCC-3') (López-García *et al.*, 2003). Sequencing libraries were prepared using the TruSeq DNA Library Preparation Kit LT at Michigan State University following the manufacturer's protocol with 6 samples per run. High throughput sequencing was conducted on a MiSeq v2 flow cell using 2x250 paired-end reads. Samples were split according to month and multiplexed in two separate MiSeq runs equally. Base calling was performed by Illumina Real Time Analysis v1.18.54 and was demultiplexed and converted to FastQ files with Illumina Bcl2fastq v1.8.4.

Sequence analysis and processing was conducted using Mothur v1.33.3 (Schloss *et al.*, 2009; Kozich *et al.*, 2013). Sequences were aligned using the SILVA (Quast *et al.*, 2013) reference database (Release 119), screened for chimeras (Edgar *et al.*, 2011) and classified with SILVA, using the K-nearest neighbor algorithm (bootstrap cutoff value of 80% following 1000 iterations). Sequences classified as fungi were parsed from the dataset and grouped into 97% operational taxonomic units using the furthest neighbor clustering. A BLAST query was conducted on representative OTUs with MEGAN v5.10.2 (Huson *et al.*, 2011). Sequences not classified as members of the Chytridiomycota (e.g. Cryptomycota and Neocallimastigomycota) were reclassified manually to determine the relative abundance of chytrids. Datasets were normalized in Mothur (sub.sample) to the lowest number of sequences (979,296).

Fixed ice core samples were gently homogenized, settled in Utermoehl counting chambers and examined with a Zeiss Telaval 31 inverted scope. 1000 diatom cells were initially checked each month for the

presence of chytrid parasitism. If no parasitism was observed after 1000 cells, chytrid parasitism was recorded as absent. From samples with any observable parasitism, one thousand additional algal cells were counted from each replicate to establish total ratios of chytrid infection of diatoms. While counting, algal species observed to be parasitized were identified and counted in each replicate to calculate ratios and standard deviations of parasitism per individual algal species. 1000 diatom cells were counted from each ice core during the repeated measures graded snow cover experiment.

BLAST queries were conducted on the five most abundant OTUs from each month in sea ice and sediment. The five most abundant OTUs were aligned with representative sequences from each taxonomic order (Table S1) of the Chytridiomycota (Karpov *et al.*, 2014) using MUSCLE in MEGA6 (Tamura *et al.*, 2013) and expanded with OTU sequence reads. Unaligned ends were trimmed to generate vetted sequences for neighbor joining tree construction (Tamura-3-parameter model) with 1000 pseudoreplicates for the taxonomic confirmation of BLAST results.

t-test values and regressions were generated using Microsoft Excel. ANOVA data was generated in R with a linear mixed-effects model (package lme4).

Images were acquired using a Zeiss Telaval 31 inverted scope with an ocular-mounted camera (United Scope, MU500).

Acknowledgments:

This material is supported by National Science Foundation Award DGE-0801720, the Marine Ecosystem Sustainability in the Arctic and SubArctic (MESAS) IGERT #1303901 and the Arctic Region Supercomputing Center at the University of Alaska Fairbanks. Sequence data is available at the NCBI SRA under accession SRP059698. The biggest thanks to the Zoosporic Research Institute at the University of Alabama for frequent consultations during this research - their insight is truly invaluable. Many thanks to Anastasia Thayer, Anna Szymanski, Dr. Anne-Lise Ducluzeau, Dr. Eric Collins and Kyle Dilliplaine for help ice coring. Many thanks to Dr. Amy Blanchard for statistical consultations during research design. Research design, research experimentation and analyses, manuscript writing and formatting was conducted by Brandon T. Hassett. Research design and manuscript editing was conducted by Rolf Gradinger.

Conflict of Interest: The authors declare no conflict of interest.

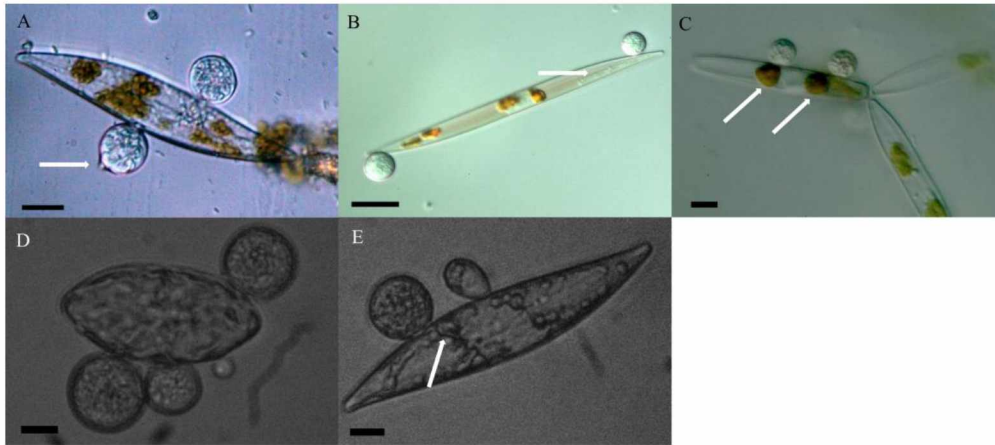


Fig. 3.0. Chytridiomycota from Barrow, AK (May 2013). Light microscopy of the Chytridiomycota from Barrow, AK (May 2013). Scale bar is 10 μ m. (A) *Pleurosigma* sp. with operculated (arrow) chytrids. (B) Epibiotic chytrids encysted with long rhizoids (arrow). (C) Chytrid zoosporangia with chlorophyll aggregates localized at site of infection (arrows). (D) Diatom host to multiple chytrids. (E) Encysted chytrids with branching rhizoids (arrow) in different developmental stages.

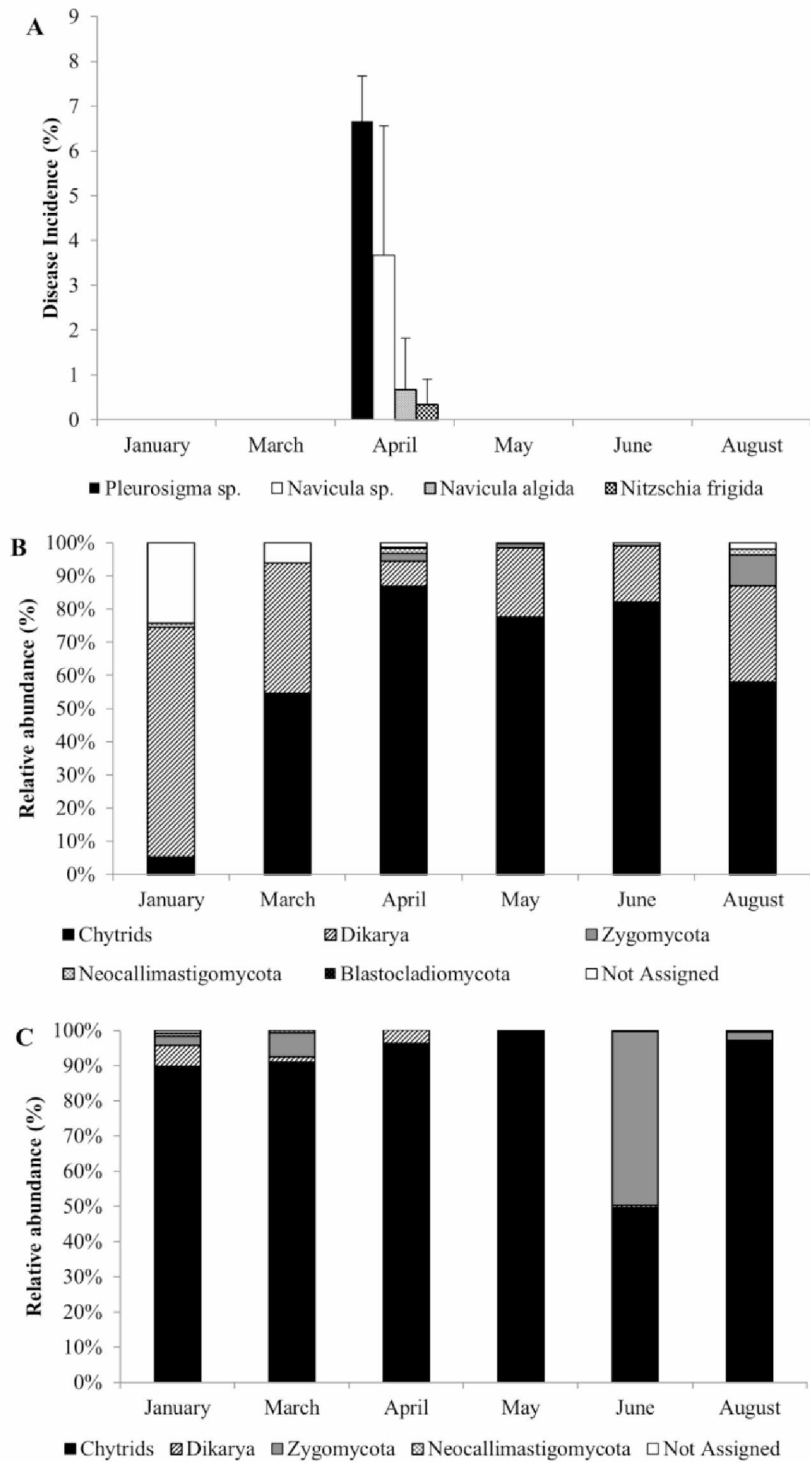


Fig. 3.1. Seasonal patterns of the Chytridiomycota. Note: ice-free water observations in August. (A) Disease incidence by diatom species per month. Error bars show standard deviations. (B) 18S rRNA sequencing-determined fungal community structure per month in sea ice and water (August). (C) 18S rRNA sequencing-determined fungal community structure per month in sea floor sediment.

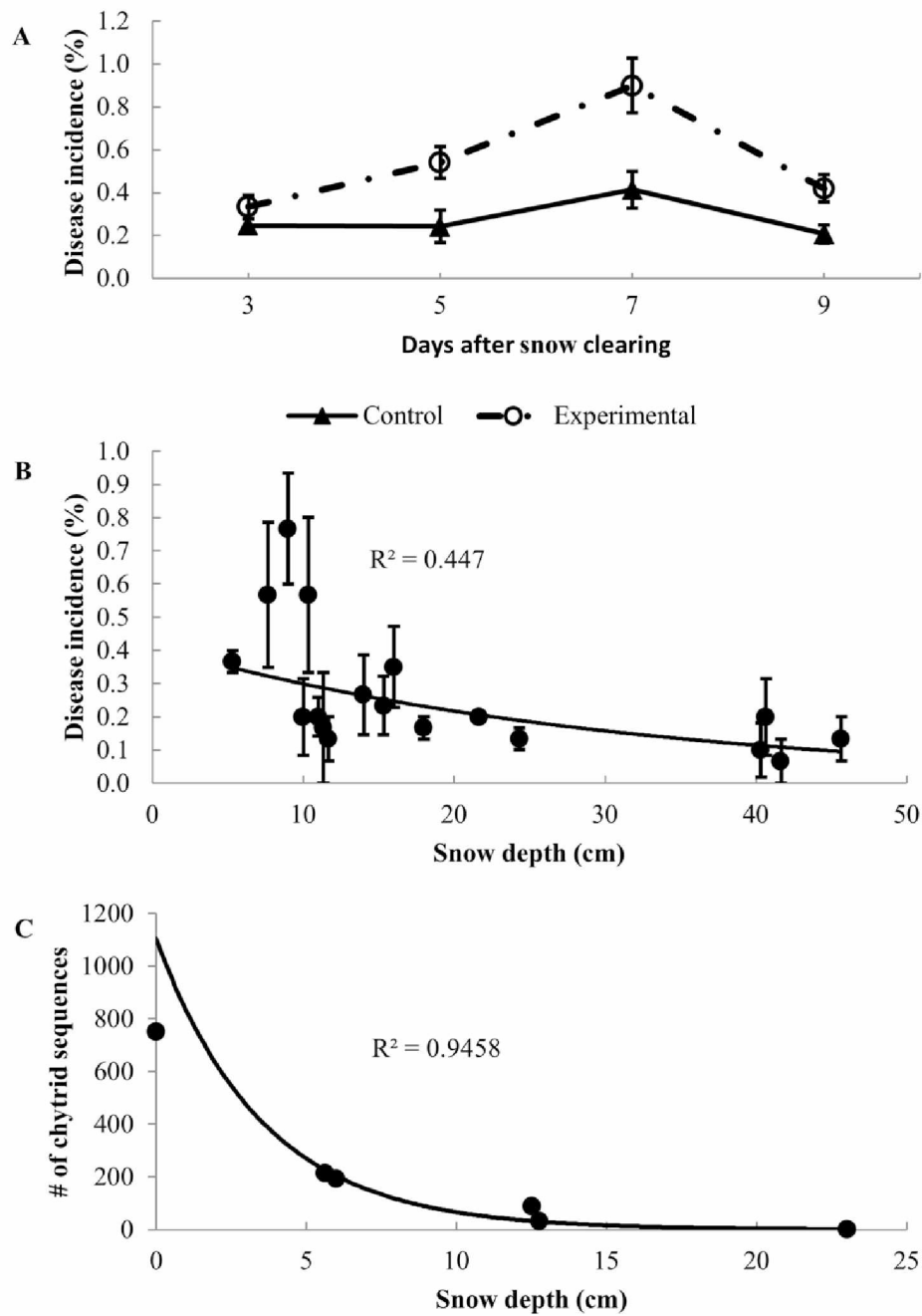


Fig. 3.2. Snow depth helps regulate parasitic activity of the Chytridiomycota. (A) Disease incidence per day after snow clearing. Controls were not statistically different (ANOVA). (B) Number of infected diatom cells as a function of snow depth from randomly selected sites within snow-covered sites modeled as an exponential curve with the formula $y = 0.4124e^{-0.032x}$. Error bars show standard errors. (C) Normalized monthly chytrid abundances (2014) from ice/August water, as a function of snow depth, modeled as an exponential curve with the formula $y = 1103e^{-0.281x}$.

References:

- Adl, M.S. and Gupta, V.S. (2006) Protists in soil ecology and forest nutrient cycling. *Can. J. For. Res.* **36**: 1805–1817.
- Arrigo, K.R., Perovich, D.K., Pickart, R.S., Brown, Z.W., Dijken, G.L. Van, Lowry, K.E., et al. (2012) Massive phytoplankton blooms under Arctic sea ice. *Science*. **336**: 1408.
- Barlocher, F. (2007) Decomposition and fungal community structure in aquatic environments. In, Hurst, C., Crawford, R., Garland, J., Lipson, D., Mills, A., and Stetzenbach, L. (eds), *Manual of Environmental Microbiology*. ASM Press, Washington D.C., pp. 496–478.
- Boetius, A., Albrecht, S., Bakker, K., Bienhold, C., Felden, J., Fernández-Méndez, M., et al. (2013) Export of algal biomass from the melting Arctic sea ice. *Science* **339**: 1430–2.
- Campbell, K., Mundy, C.J., Barber, D.G., and Gosselin, M. (2015) Characterizing the sea ice algae chlorophyll a-snow depth relationship over Arctic spring melt using transmitted irradiance. *J. Mar. Syst.* **147**: 76–84.
- Cartaxana, P., Domingues, N., Cruz, S., Jesus, B., Laviale, M., Serôdio, J., and Da Silva, J.M. (2013) Photoinhibition in benthic diatom assemblages under light stress. *Aquat. Microb. Ecol.* **70**: 87–92.
- Cleary, A.C., Durbin, E.G., Rynearson, T. a, and Bailey, J. (2015) Feeding by Pseudocalanus copepods in the Bering sea: Trophic linkages and a potential mechanism of niche partitioning. *Deep Sea Res. Part II Top. Stud. Oceanogr.*
- Cox, G. and Weeks, W. (1983) Equations for determining the gas and brine volumes in sea-ice samples. *J. Glaciol.* **29**: 306–316.
- Dakos, V., Scheffer, M., van Nes, E.H., Brovkin, V., Petoukhov, V., and Held, H. (2008) Slowing down as an early warning signal for abrupt climate change. *Proc. Natl. Acad. Sci. U. S. A.* **105**: 14308–14312.
- Duarte, C.M., Lenton, T.M., Wadhams, P., and Wassmann, P. (2012) Abrupt climate change in the Arctic. *Nat. Clim. Chang.* **2**: 60–62.
- Edgar, R.C., Haas, B.J., Clemente, J.C., Quince, C., and Knight, R. (2011) UCHIME improves sensitivity and speed of chimera detection. *Bioinformatics* **27**: 2194–2200.

- Eicken, H., Gradinger, R., Gaylord, A., Mahoney, A., Rigor, I., and Melling, H. (2005) Sediment transport by sea ice in the Chukchi and Beaufort Seas: increasing importance due to changing ice conditions? *Deep. Res. Part II Top. Stud. Oceanogr.* **52**: 3281–3302.
- Freeman, K.R., Martin, A. P., Karki, D., Lynch, R.C., Mitter, M.S., Meyer, A. F., et al. (2009) Evidence that chytrids dominate fungal communities in high-elevation soils. *Proc. Natl. Acad. Sci. U. S. A.* **106**: 18315–18320.
- Frey, K., Maslanik, J., Kinney, J., and Maslowski, W. (2014) Recent variability in sea ice cover, age and thickness in the Pacific Arctic region. In, *The Pacific Arctic Region.*, pp. 31–63.
- Gleason, F.H., Küpper, F.C., Amon, J.P., Picard, K., Gachon, C.M.M., Marano, A. V., et al. (2011) Zoosporic true fungi in marine ecosystems: A review. *Mar. Freshw. Res.* **62**: 383–393.
- Gradinger, R. (2009) The changing Arctic sea ice landscape. In, Hempel, G. and Hempel, I. (eds), *The biology of polar seas*. Wirtschaftsverlag, Bonn, pp. 239–246.
- Gradinger, R., Bluhm, B., Hopcroft, R., Gebruk, A., Kosobokova, K., Sirenko, B., and Weslawski, J. (2010) Marine life in the Arctic. In, McIntyre, A. (ed), *Life in the World's Oceans: Diversity, Distribution, and Abundance*. Wiley-Blackwell, pp. 183–202.
- Grebmeier, J.M. (2012) Shifting patterns of life in the Pacific Arctic and sub-Arctic Seas. *Ann. Rev. Mar. Sci.* **4**: 63–78.
- Gryganskyi, A.P., Humber, R.A., Smith, M.E., Hodge, K., Huang, B., Voigt, K., and Vilgalys, R. (2013) Phylogenetic lineages in Entomophthoromycota. *Persoonia* **30**: 94–105.
- Harvell, C.D., Kim, K., Burkholder, J.M., Colwell, R.R., Epstein, P.R., Grimes, D.J., et al. (1999) Emerging marine diseases--climate links and anthropogenic factors. *Science* **285**: 1505–1510.
- Hezel, P.J., Zhang, X., Bitz, C.M., Kelly, B.P., and Massonnet, F. (2013) Projected decline in spring snow depth on Arctic sea ice caused by progressively later autumn open ocean freeze-up this century. *Geophys. Res. Lett.* **39**: 6–11.
- Hollowed, A.B., Planque, B., and Loeng, H. (2013) Potential movement of fish and shellfish stocks from the sub-Arctic to the Arctic Ocean. *Fish. Oceanogr.* **22**: 355–370.

- Horner, R. and Schrader, G.C. (1982) Relative contributions of ice algae, phytoplankton, and benthic microalgae to primary production in nearshore regions of the Beaufort Sea. *Arctic* **35**: 485–503.
- Huson, D., Mitra, S., and Ruscheweyh, H. (2011) Integrative analysis of environmental sequences using MEGAN4. *Genome Res.* **21**: 1552–1560.
- Ibelings, B.W., De Bruin, A., Kagami, M., Rijkeboer, M., Brehm, M., and Donk, E. Van (2004) Host parasite interactions between freshwater phytoplankton and chytrid fungi (Chytridiomycota). *J. Phycol.* **40**: 437–453.
- Kagami, M., De Bruin, A., Ibelings, B.W., and Van Donk, E. (2007) Parasitic chytrids: Their effects on phytoplankton communities and food-web dynamics. *Hydrobiologia* **578**: 113–129.
- Kagami, M., Gurung, T.B., Yoshida, T., and Urabe, J. (2006) To sink or to be lysed? Contrasting fate of two large phytoplankton species in Lake Biwa. *Limnol. Oceanogr.* **51**: 2775–2786.
- Kagami, M., Miki, T., and Takimoto, G. (2014) Mycoloop: chytrids in aquatic food webs. *Front. Microbiol.* **5**: 1–9.
- Karpov, S.A., Kobseva, A.A., Mamkaeva, M.A., Mamkaeva, K.A., Mikhailov, K. V, Mirzaeva, G.S., and Aleoshin, V. V (2014) *Gromochytrium mamkaevae* gen. and sp. nov. and two new orders: Gromochytriales and Mesochytriales (Chytridiomycetes). *Persoonia* **32**: 115–126.
- Karsten, U., Schumann, R., Rothe, S., Jung, I., and Medlin, L. (2006) Temperature and light requirements for growth of two diatom species (Bacillariophyceae) isolated from an Arctic macroalga. *Polar Biol.* **29**: 476–486.
- Kirst, G. and Wiencke, C. (1995) Ecophysiology of polar algae. *J. Phycol.* **Volume 31**: 181–199.
- Klindworth, A., Pruesse, E., Schweer, T., Peplies, J., Quast, C., Horn, M., and Glöckner, F.O. (2013) Evaluation of general 16S ribosomal RNA gene PCR primers for classical and next-generation sequencing-based diversity studies. *Nucleic Acids Res.* **41**: 1–11.
- Kogej, T., Plemenitas, A., and Gunde-cimerman, N. (2005) The halophilic fungus *Hortaea werneckii* and the halotolerant fungus *Aureobasidium pullulans* maintain low intracellular cation concentrations in hypersaline environments. *Appl. Environ. Microbiol.* **71**: 6600–6605.

- Kortsch, S., Primicerio, R., Fossheim, M., Dolgov, A. V, Aschan, M., and Kortsch, S. (2015) Climate change alters the structure of Arctic marine food webs due to poleward shifts of boreal generalists. *Proc. R. Soc. B Biol. Sci.* doi: 10.1098/rspb.2015.1546.
- Kozich, J.J., Westcott, S.L., Baxter, N.T., Highlander, S.K., and Schloss, P.D. (2013) Development of a dual-index sequencing strategy and curation pipeline for analyzing amplicon sequence data on the MiSeq Illumina sequencing platform. *Appl. Environ. Microbiol.* **79**: 5112–5120.
- Lepelletier, F., Karpov, S. a., Alacid, E., Le Panse, S., Bigeard, E., Garcés, E., et al. (2014) *Dinomyces arenysensis* gen. et sp. nov. (Rhizophydiales, Dinomycetaceae fam. nov.), a chytrid infecting marine Dinoflagellates. *Protist* **165**: 230–244.
- Lepère, C., Domaizon, I., and Debroas, D. (2008) Unexpected importance of potential parasites in the composition of the freshwater small-eukaryote community. *Appl. Environ. Microbiol.* **74**: 2940–2949.
- López-García, P., Philippe, H., Gail, F., and Moreira, D. (2003) Autochthonous eukaryotic diversity in hydrothermal sediment and experimental micocolonizers at the Mid-Atlantic Ridge. *PNAS* **100**: 697–702.
- Lund-Hansen, L.C., Hawes, I., Sorrell, B.K., and Nielsen, M.H. (2014) Removal of snow cover inhibits spring growth of Arctic ice algae through physiological and behavioral effects. *Polar Biol.* **37**: 471–481.
- Manes, S.S. and Gradinger, R. (2009) Small scale vertical gradients of Arctic ice algal photophysiological properties. *Photosynth. Res.* 1–14.
- Naff, C.S., Darcy, J.L., and Schmidt, S.K. (2013) Phylogeny and biogeography of an uncultured clade of snow chytrids. *Environ. Microbiol.* **15**: 2672–2680.
- Olofsson, J., Ericson, L., Torp, M., Stark, S., and Baxter, R. (2011) Carbon balance of Arctic tundra under increased snow cover mediated by a plant pathogen. *Nat. Clim. Chang.* **1**: 220–223.
- Perovich, D.K. (1998) Optical properties of sea ice. In, Lepparanta, M. (ed), *Physics of Ice-Covered Seas*. University of Helsinki, Helsinki, pp. 195–230.
- Perovich, D.K. (1990) Theoretical estimates of light reflection and transmission by spatially complex and temporally varying sea ice covers. *J. Geophys. Res.* **95**: 9557.

- Popova, E.E., Yool, A., Coward, A.C., Dupont, F., Deal, C., Elliott, S., et al. (2012) What controls primary production in the Arctic Ocean? Results from an intercomparison of five general circulation models with biogeochemistry. *J. Geophys. Res. Ocean.* **117**: 1–16.
- Powell, M.J. (1993) Looking at mycology with a Janus face: a glimpse at chytridiomycetes active in the environment. *Mycologia* **85**: 1–20.
- Quast, C., Pruesse, E., Yilmaz, P., Gerken, J., Schweer, T., Yarza, P., et al. (2013) The SILVA ribosomal RNA gene database project: improved data processing and web-based tools. *Nucleic Acids Res.* **41**: 590–596.
- Robinson, C.H. (2001) Cold adaptation in Arctic and AntArctic fungi. *New Phytol.* **151**: 341–353.
- Scheffer, M., Carpenter, S.R., Lenton, T.M., Bascompte, J., Brock, W., Dakos, V., et al. (2012) Anticipating Critical Transitions. *Science.* **338**: 344–348.
- Schloss, P.D., Westcott, S.L., Ryabin, T., Hall, J.R., Hartmann, M., Hollister, E.B., et al. (2009) Introducing Mothur: open-source, platform-independent, community-supported software for describing and comparing microbial communities. *Appl. Environ. Microbiol.* **75**: 7537–7541.
- Simmons, D.R., James, T.Y., Meyer, A.F., and Longcore, J.E. (2009) Lobulomycetales, a new order in the Chytridiomycota. *Mycol. Res.* **113**: 450–460.
- Singh, P., Wang, X., Leng, K., and Wang, G. (2012) Diversity and ecology of marine-derived fungi. In, Jones, G. and Pang, K. (eds), *Marine Fungi and fungal-like organisms*. De Gruyter, Berlin, pp. 383–407.
- Søreide, J.E., Carroll, M.L., Hop, H., Ambrose, W.G., Hegseth, E.N., and Falk-Petersen, S. (2013) Sympagic-pelagic-benthic coupling in Arctic and Atlantic waters around Svalbard revealed by stable isotopic and fatty acid tracers. *Mar. Biol. Res.* **9**: 831–850.
- Sparrow, F. (1960) *Aquatic Phycomycetes* University of Michigan Press, Ann Arbor.
- Tamura, K., Stecher, G., Peterson, D., Filipski, A., and Kumar, S. (2013) MEGA6: Molecular evolutionary genetics analysis version 6.0. *Mol. Biol. Evol.* **30**: 2725–2729.
- Terrado, R., Medrinal, E., Dasilva, C., Thaler, M., Vincent, W.F., and Lovejoy, C. (2011) Protist community composition during spring in an Arctic flaw lead polynya. *Polar Biol.* **34**: 1901–1914.

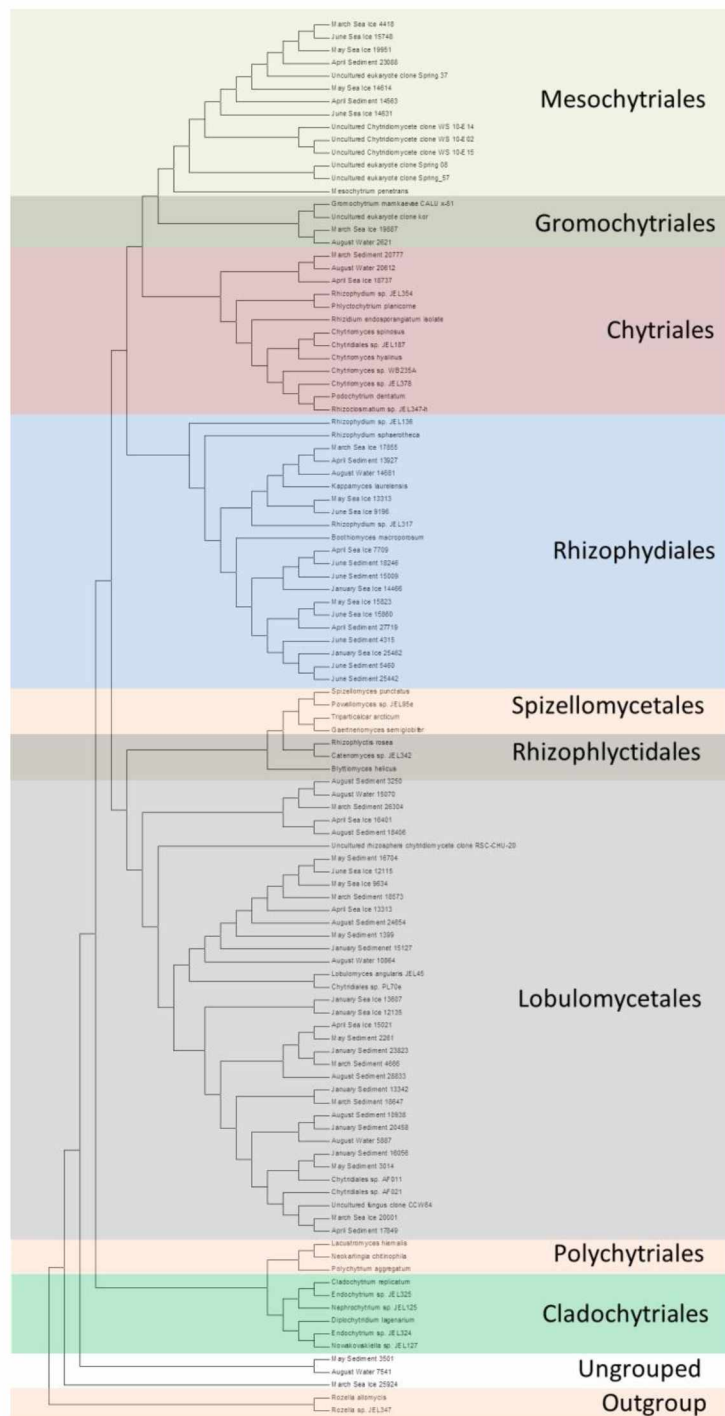
Webster, M.A., Rigor, I.G., Nghiem, S. V., Kurtz, N.T., Farrell, S.L., Perovich, D.K., and Sturm, M. (2014) Interdecadal changes in snow depth on Arctic sea ice. *J. Geophys. Res. Ocean.* **119**: 5395–5406.

Zalar, P., De Hoog, G.S., Schroers, H.J., Crous, P.W., Groenewald, J.Z., and Gunde-Cimerman, N. (2007) Phylogeny and ecology of the ubiquitous saprobe *Cladosporium sphaerospermum*, with descriptions of seven new species from hypersaline environments. *Stud. Mycol.* **58**: 157–183.

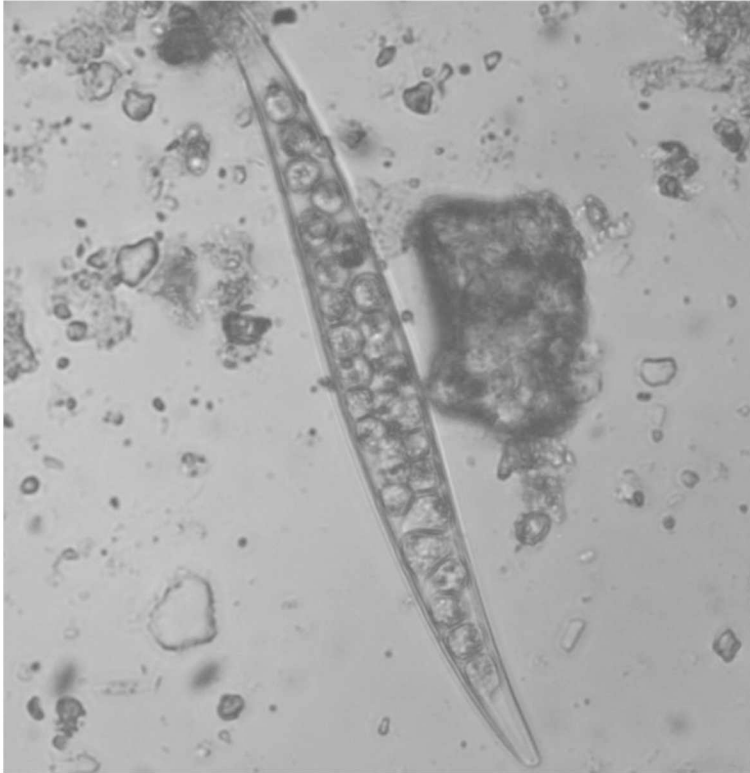
Supplemental Materials



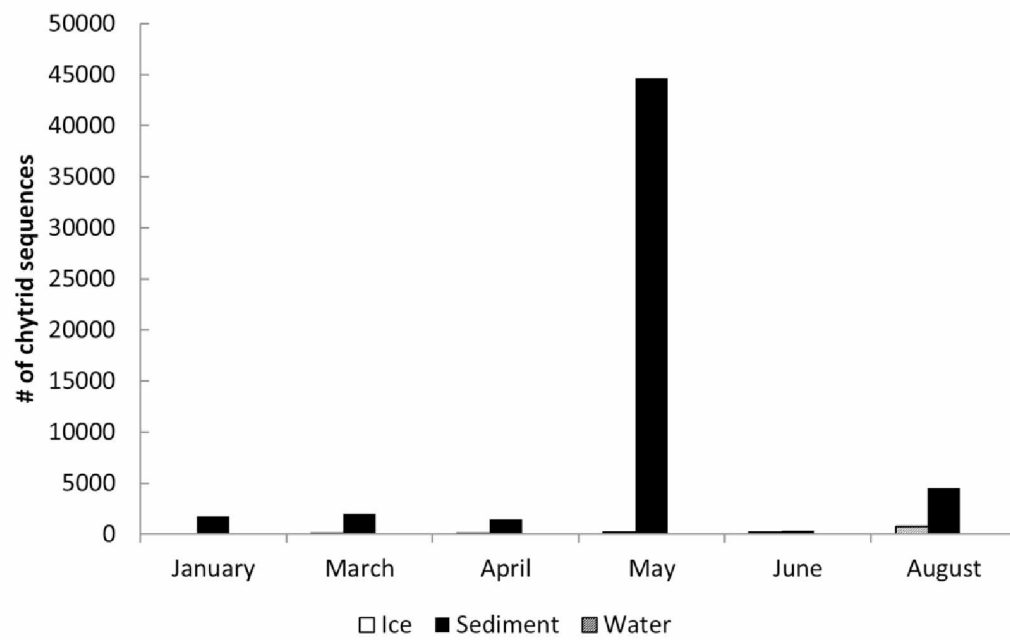
Supplemental Figure 3.0. Dense algal growth at the bottom of ice cores. Ice cores were extracted from Barrow, AK (May 2013). Photo credit: Dr. R. Eric Collins.



Supplemental Figure 3.1. Neighbor joining, bootstrap consensus tree. Tree was constructed from 457 base pair 18S rRNA reads, showing the phylogenetic relationship of the five most abundant OTUs detected in sea ice and sediment.



Supplemental Figure 3.2. *Pleurosigma* sp. filled with chytrid-like organisms from Barrow Sediment.



Supplemental Figure 3.3. Normalized abundance of chytrid sequences.

Supplemental Table 3.0. List of 18S rRNA taxa and accession numbers used in phylogenetic analysis.

Taxonomic Order	Identifier	GenBank Accession Number
Mesochytriales	Uncultured eukaryote clone Spring 37	JX069054.1
Mesochytriales	Uncultured Chytridiomycete clone WS 10-E02	AJ867629.1
Mesochytriales	Uncultured Chytridiomycete clone WS 10-E14	AJ867630.1
Mesochytriales	Uncultured Chytridiomycete clone WS 10-E15	AJ867631.1
Mesochytriales	Uncultured eukaryote clone Spring 08	JX069031.1
Mesochytriales	Uncultured eukaryote clone Spring 57	JX069067.1
Mesochytriales	Mesochytrium penetrans	FJ804149.1
Gromochytriales	Gromochytrium mamkaevae strain CALU x-51	KF586842.1
Gromochytriales	Uncultured eukaryote clone kor	FJ157331.1
Chytridiales	Rhizophyidium sp. JEL354	AY635827.1
Chytridiales	Phlyctochytrium planicorne	DQ536473.1
Chytridiales	Rhizidium endosporangiatum	DQ536484.1
Chytridiales	Chytriomycetes spinosus	AH009063.1
Chytridiales	Chytridiales sp. JEL187	AY635825.1
Chytridiales	Chytriomycetes hyalinus	DQ536487.1
Chytridiales	Chytriomycetes sp. WB235A	DQ536486.1
Chytridiales	Chytriomycetes sp. JEL378	DQ536483.1
Chytridiales	Podochytrium dentatum	AH009055.1
Chytridiales	Rhizoclosmatium sp. JEL347-h	AY601709.1
Rhizophydiales	Rhizophyidium sp. JEL136	AY601710.1
Rhizophydiales	Rhizophyidium sphaerotheca	AY635823.1
Rhizophydiales	Kappamyces laurelensis	DQ536478.1
Rhizophydiales	Rhizophyidium sp. JEL317	AY635821.1
Rhizophydiales	Boothiomycetes macroporum	DQ322622.1
Rhizophlyctidales	Blyttiomycetes helicus	DQ536491.1
Rhizophlyctidales	Rhizophlyctis rosea	AY635829.1
Rhizophlyctidales	Catenomyces sp. JEL342	AY635830.1
Spizellomycetales	Spizellomyces punctatus	AY546684.1
Spizellomycetales	Powellomyces sp. JEL95	AF164245.2
Spizellomycetales	Triparticalcar Arcticum	DQ536480.1
Spizellomycetales	Gaertneriomycetes semiglobifer	AF164247.2
Polychytriales	Polychytrium aggregatum	AY601711.1
Polychytriales	Lacustromyces hiemalis	AH009039.1
Polychytriales	Neokarlingia chitinophila	HQ901766.1
Cladochytriales	Diplochytridium lagenarium	AH009044.1
Cladochytriales	Endochytrium sp. JEL324	AY635844.1
Cladochytriales	Nowakowskiella sp. JEL127	AY635835.1
Cladochytriales	Cladochytrium replicatum	AY546683.1
Cladochytriales	Endochytrium sp. JEL325	AY349046.1

Supplemental Table 1.0
continued....

Cladochytriales	Nephrochytrium sp. JEL125	AH009049.1
Lobulomycetales	Uncultured chytridiomycete clone RSC-CHU-20	AJ506002.1
Lobulomycetales	Chytridiales sp. PL70	EF443138.1
Lobulomycetales	Lobulomyces angularis JEL45	AF164253.2
Lobulomycetales	Chytridiales sp. AF011	EF432819.2
Lobulomycetales	Chytridiales sp. AF021	EF432822.2
Lobulomycetales	Uncultured fungus clone CCW64	AY180029.1
Outgroup	Rozella allomycis	AY635838.1
Outgroup	Rozella sp. JEL347	AY601707.1

Chapter 4: Eukaryotic Microbial Richness Increases with Latitude and Decreasing Temperature in the Pacific Arctic Domain in Late Winter¹

Abstract

The Bering Sea has some of the highest concentrations of inorganic nutrients of any marine system that drives one of the most productive ecosystems globally. We conducted a detailed survey of the eukaryotic microbial community structure across the southeast Bering Sea and surrounding areas from the open sea into ice-covered waters. Deep sequencing of 18S rRNA from the chlorophyll maximum accounted for >96% sample coverage of eukaryotic microbes that corresponded to high estimated Chao1 richness (>6,000). MDS ordination analysis revealed nearly identical community structures for samples acquired south of the Aleutian Islands and samples acquired in proximity to the ice edge. Different diversity indices in conjunction with nearly identical community structure suggests the potential lack of functional redundancy within shelf break regions and underlines the susceptibility of these ecosystems to climate change. Organisms detected in the Gulf of Alaska site were more likely to be detected in the Bering Sea than organisms detected in sea ice, despite the existence of sea ice in the Bering Sea. Ordination with inorganic nutrients and water mass data suggested that temperature was related to microbial community structure during late winter.

¹Hassett BT, Gradinger R (Submitted). eukaryotic microbial richness increases with latitude and decreasing temperature in the Pacific Arctic Domain in late winter. *Applied and Environmental Microbiology*.

Introduction

Microbes are the foundation of all marine food webs and catalyze essential biogeochemical cycling throughout the world's oceans. Microbes comprise 90% of all living oceanic biomass (1), yet are proportionally vastly understudied in the Arctic and sub-Arctic (2). As high latitude seas continue to warm, the metabolic activity and structure of microbial communities are likely to change, favoring organisms genetically capable of coping with elevated temperatures (3), fluxes within the nutrient regime (4), and biological competition due to range extensions of boreal taxa, as established for several trophic levels within sub-Arctic and Arctic seas (5, 6). As microbes differentially respond to environmental perturbations (7), future community equilibriums remain uncertain, owed in part to the lack of contemporary species inventories and the understudied nature of abiotic drivers for large-scale microbial diversity patterns.

In general, organismal diversity gradients within high-latitude seas are known to differ along longitudinal (8) and latitudinal axes (9), driven by a combination of evolutionary history (10) and seasonal physical forcing (11). Physical forcing in the sub-Arctic and Arctic is particularly strong on diversity patterns, governed by the extreme seasonality of light (12), and temporally and spatially changing nutrient concentrations (13) that regulate the phenology of photosynthetic primary production of ice algae and phytoplankton (14). Additionally, the seasonally increasing marine primary productivity in polar regions stimulates and regulates microbial community diversity patterns (15, 16). Subsequently, the winter season is the optimal time window for assessing diversity, as the microbial community structure changes minimally (17) and diversity is the highest (15, 18).

The Bering Sea is a semi-enclosed high latitude sea, consisting of a deep central basin with surrounding continental shelves. Circulation patterns in the Bering Sea are driven by the Alaskan Coastal Current and the eastward flowing Aleutian North Slope current that flows northwestwardly (as the Bering Slope current) and finally southwardly (as the Kamchatka Current) near Russia. This anticyclonic flow of water forms part of the North Pacific sub-Arctic gyre (19). High production on the northern Bering Sea shelf is supported by the continuous advection of nutrient-rich waters, while the southeastern shelf depends on cross-shelf exchanges (20). The continental shelf of the eastern Bering Sea is one of the most productive marine ecosystems in the world (6) that is experiencing significant warming (21). Increased warming on continental shelves should lead to a northward migration of the Arctic-sub-Arctic ecotone (6).

The rapid growth rate of microorganisms (relative to zooplankton or larger metazoans) allows microbial communities to rapidly shift into different equilibrium states, serving as useful indicator organisms for

environmental change (7). We hypothesized that the eukaryotic microbial community structure would differ with hydrography, possibly indicating temperature-induced changes in the microbial population. We also hypothesized that the nutrient-rich waters of the Bering Sea would be a significant driver of microbial community structure, favoring the growth of specific microbial clades.

Materials and Methods

In late winter/early spring of 2015 (14 March to 25 March) seawater sampling was conducted onboard the R/V *Sikuliaq* across the Gulf of Alaska into the Bering Sea (Figure 4.0). Sampling was designed to target microbial communities in the water column along a northern transect from open ocean conditions in the northern North Pacific into the ice-covered areas of the Bering Sea (Table 4.0). Sea ice sampling was conducted at one station to further assess diversity difference and serve as a standard reference for interpreting MDS spatial plotting distance.

Three true replicate samples were collected at all water stations and at a single sea ice station for the assessment of eukaryotic microbial diversity. A single replicate corresponded to a single Niskin bottle or a single 10 cm bottom ice core section. Water samples were collected using a CTD/Rosette sampler holding 24 10-liter Niskin bottles from the chlorophyll *a* maximum. The chlorophyll *a* maximum depth was identified with *in situ* readings of a CTD-mounted fluorometer (Seapoint) and sampled to reduce the variability due to depth and algal biomass (9, 22). All replicates at a sampling site were collected from a single CTD cast. For all water samples, corresponding triplicate nutrient samples (100 mL) were acquired for PO₄, Si(OH)₄, NO₃, NO₂, and NH₃ analysis.

One liter of water was collected per replicate immediately following CTD retrieval for the analysis of community structure. Samples were separately filtered onto 0.6- μ m DTP filters (Millipore) using a vacuum filter. Samples were stored in sterile polypropylene tubes at -80°C until DNA extraction. At the Sea Ice station, three ice cores were extracted using a 9-cm diameter KOVACs ice corer. The bottom 10-cm of each core was sectioned using an ethanol-sterilized handsaw. Ice core sections were melted at room temperature into 1000 mL of 0.22- μ m-filtered seawater. After complete melt of the ice cores, samples were vacuum-filtered onto 0.6- μ m DTP filters (Millipore) and were stored in sterile polypropylene tubes at -80°C until DNA extraction.

DNA extractions from filters were conducted by bead beating for 1 minute in phosphate buffer, followed by phenol-chloroform extraction. Replicates were pooled before PCR. Target amplicons were generated using the Earth Microbiome Project primers: Euk_1391f: (5'- GTACACACCGCCCGTC-3') and EukBr: (5'- TGATCCTTCTGCAGGTTACCTAC-3 ') (23) to generate ~170 base pair reads. Sequencing

libraries were prepared using the TruSeq DNA Library Preparation Kit LT at Michigan State University following the manufacturer's protocol. High throughput sequencing was conducted on a MiSeq v2 flow cell using paired-end reads. Samples were split according to month and multiplexed in a single MiSeq run. Base calling was performed by Illumina Real Time Analysis v1.18.54 and was demultiplexed and converted to FastQ files with Illumina Bcl2fastq v1.8.4.

Sequence analysis and processing was conducted using Mothur v1.33.3 (24, 25). Sequences were aligned using the SILVA (26) reference database (Release 119), screened for chimeras (27) and classified with SILVA, using the K-nearest neighbor algorithm (bootstrap cutoff value of 80% following 1000 iterations). Bacteria, Archaea and metazoans were removed from all data sets. Sequences were then clustered into operational taxonomic units (OTUs) at 97% similarity using the Average Neighbor distance. Datasets were normalized in Mothur (sub.sample) to the lowest number of sequences (62,588) for all downstream analyses.

Rarefaction curves were generated in Mothur (subsampling frequency of 500). To assess the OTU sampling coverage of normalized datasets. Good's nonparametric estimate of richness was used to assess success of sampling coverage. Taxonomic graphs representing eukaryotic supergroups were generated using the SILVA classification and manually grouped to reflect recent eukaryotic taxonomy (28). Based on this classification, the Cryptophytes, Picozoa, Kathablepharidae, Centrohelida, Haptophyta, Centrohelida, and Telonema were grouped as Incertae Sedis. Ordination was conducted in R using the Vegan package. For MDS plots, Bray-Curtis distance was used to assess community dissimilarities (β -diversity) in two dimensions with minimal stress.

Results

Following sequence vetting and processing, 1,695,188 high-quality unique DNA sequence reads from the six stations were used in downstream analysis. After data normalization in Mothur and OTU generation, 11,135 distinct OTUs were observed across all sampling sites (Table 4.1). Sequencing depth from a single MiSeq run was adequate to obtain >96% sample coverage across all sites (Table 4.1). This sequencing depth resulted in near-saturation of rarefaction curves (Supplemental Figure 4.0).

In all water samples, the Alveolates had the highest relative abundance among the eukaryotic supergroups, followed by Stramenopiles and Opisthokonts. In sea ice, the community structure was markedly different and was comprised of mostly the Stramenopiles, followed by Alveolates and Rhizaria (Figure 4.1). Sites sampled in southwestern Alaska (Shelikof Strait and Deep Water Basin) had strikingly similar community structure, despite substantial geographic distance (~800 km). While these sites did

maintain analogous structure, estimated richness was markedly different. Chao1 estimates of species richness across all sites revealed that microbes within Shelikof Strait had the highest estimated richness (6,801) and that the Deep Water Basin had the lowest (2,912). The low estimate of richness in the Deep Water Basin corresponded to the lowest number of observed OTUs (1,863). North of the Aleutian Islands, eukaryotic community structure varied with increasing latitude, even across short geographical distances (e.g. ~160 km between Pribilof Islands/Bering Sea Shelf sites). In the Bering Sea, Chao1 species richness increased with decreasing temperature, with the marginal ice zone (MIZ) (-1.7°C) having the highest species richness of all Bering Sea water samples. Multidimensional scaling of samples illustrated the dissimilarity of community structure (Figure 4.2). β -diversity showed tight grouping between the two locations in southwestern Alaska. A second grouping consisted of the MIZ and Bering Shelf location, while the sea ice sample grouped separately (Figure 4.2A).

Often, the greatest number of observed OTUs did not correspond to the highest richness estimate for a location (e.g. the Sea Ice station), largely explainable, as Chao1 is a measure of singleton abundance. To this end, samples with a higher abundance of singletons have higher Chao1 estimates/extrapolations of species richness (Table 4.1). In order to supplement Chao1 estimates, Simpson diversity indices were also used to assess richness. Overall there was good agreement, with the two highest Chao1 sites (Shelikof Strait and MIZ) also having the highest Simpson diversity recorded among water sites. The Deep Water Basin, with the lowest Simpson diversity, also had the lowest Chao1 richness estimate.

To explore the relationship between inorganic nutrients and water masses in helping shape pelagic eukaryotic microbial community structure, MDS ordination was employed to assess community dissimilarity and fitted with vectored nutrient data and water temperature (Figure 4.2B). R^2 values revealed that the majority of dimensional variability was explained by phosphate ($R^2=0.93$), silicate ($R^2=0.99$) and temperature ($R^2=0.97$) with a stress value of 7.71×10^{-5} , indicating a quality relationship for MDS in two dimensions. The inorganic chemical signatures of structurally similar communities were analogous (Table 4.0) between grouped sites, with the exception of silicate. Silicate concentrations were lowest within the Bering Sea Shelf site and highest at the Pribilof Islands site. Silicate (MDS, $p=0.09$) and phosphate (MDS, $p=0.12$) values were not significant drivers of community structure. Decreasing water temperature across the south-north transect was a significant driver of microbial community structures (MDS, $p=0.03$).

Comparative analysis of terminal sites (i.e. Shelikof Strait and the Sea Ice station) versus all other sites revealed a decreasing number of shared OTUs with increasing distance from terminal sites (Supplemental

Figure 4.1, Table 4.2). Organisms detected in the Shelikof Strait site were more likely to be detected in the Bering Sea than organisms detected in the sea ice, despite the existence of sea ice in the Bering Sea.

Discussion

The objective of this research was to identify the eukaryotic microbial structure across the Alaskan sub-Arctic marine system and to explore the effects of nutrients and water masses in shaping these communities. We detected an extremely diverse microbial community across the shelf ecosystem with Chao1 richness exceeding the estimated microbial richness of deserts (29), coral reefs systems (30) and fungal diversity in rainforests (31). Similarly, these Bering Sea richness estimates exceed Archaeal diversity in the coastal Arctic Ocean (32) and microbial communities in Arctic lakes (33).

We detected all major taxonomic supergroups (STable 4.1), with a high diversity of dinoflagellates, diatoms, and ciliates. Functionally, there was a strong prevalence of fish and invertebrate symbionts (e.g. *Paramoeba branchiphila*, *Paramoeba eilhardi*, *Debaryomyces hansenii*, *Thalassomyces fagei*, *Pseudocollinia oregonensis*, and *Blastodinium navicula*), diatom parasites (e.g. chytrids and *Pirsonia sp.*) and toxin-producing phototrophs (e.g. *Alexandrium sp.*, *Pseudo-nitzschia australis* and *Aureococcus anophagefferens*). A number of terrestrial organisms were detected at sampling stations, including: Agaricomycetes and *Udeniomyces pannonicus*. The eastern Bering Sea receives a disproportionate amount of terrestrial-sourced freshwater runoff along the shelf region (34), likely sourcing these organisms into the Bering Sea with aeolian input (35). Additionally, a number of cryptic clades were detected across our sample sites, including: nine Marine Stramenopile (MAST) clades, Novel Apicomplexa Class 2, DH147-EKD23 ciliate clade, SL163A10 AntArctic clade, SCM28C5, the NOR26, TAGIRI-17, D-52, FV36-2G-8, E222 and a number of clone-detected species.

Assessing the true species richness of eukaryotes using NGS techniques is confounded by the application of multiple species concepts across different eukaryotic clades (36). For instance, diatom taxonomy employs a morphospecies concept that does not correspond with the phylogenetic species concept (37). We therefore suggest that our species number estimate is likely incomplete for organisms defined by morphology. Additionally, divergent paralogous evolution of 18S rRNA genes (38, 39) can lead to overestimation of diversity. In some diatom species, intragenomic variation of 18S rRNA can approach 2% divergence (39). To address these issues, we employed stringent quality filtering of sequence reads and 3% similarity clustering to reduce overestimations of diversity.

When assessing community structure, we phylogenetically classified our sequences using an 80% bootstrap cutoff and conservatively assessed community structure by binning these organisms into

taxonomic supergroups. The Deep Water Basin site and Shelikof Strait had nearly identical community structures (Figure 4.1, 4.2). This finding can be explained by the tight oceanographic coupling between these two sites. Strong advection from the Alaska Coastal Current and the Alaska Stream will produce similar water masses with related temperatures and salinity in regions south of the Aleutian Islands. These similarities are heightened by reduced vertical mixing with increasing depth. The Shelikof Strait and the Deep Water Basin sites had similar temperatures that were the highest among all sites sampled (Table 4.0). Water mass similarities, as depicted by temperature and inorganic nutrients, resulted in structurally similar microbial communities that are likely under comparable environmental selection pressures. Despite similar community structure, eukaryotic microbial community diversity was markedly lower in the Deep Water Basin, relative to Shelikof Strait (Table 4.1). The diversity differences between the southern Alaskan sites were largely driven by the abundance of singleton taxa. This implies that the same community structure is being maintained by fewer taxa in the Deep Water location, suggesting diminished ecological functional redundancy in the Deep Water Basin and increased potential susceptibility of eukaryotic microbial communities along the shelf break region to disturbances. Additional research elucidating functional gene repertoires would help understand redundancy and potential susceptibility of microbial organisms to climate change within shelf break regions.

MDS analysis of normalized OTU abundances augmented community structural similarities between the Deep Water Basin/Shelikof Strait stations and the MIZ/Bering Sea Shelf stations. The MIZ and the Bering Sea Shelf stations had the coldest temperatures from any water column sites. The Pribilof Islands site was spatially ordinated between shallow northern cold water sites and deeper southern warm water sites. The Pribilof Islands receive a mixture of northerly advected Alaskan Coastal Current water and Aleutian North Slope Current (20). We sampled in proximity to the transition zone between the middle and outer shelf domain. Thus, the Pribilof Island eukaryotic microbial community structure likely represents an intermediate wintertime community comprised largely of southerly taxa and some northerly taxa (Table 4.2).

Originally, we hypothesized that the eukaryotic microbial community structure would differ with hydrography. Within the wintertime Bering Sea, we found strong evidence that hydrography shapes large scale spatial diversity patterns of eukaryotic communities resulting in spatially-ordinated Bering Sea communities in sequential order of latitude that reveals a positive relationship between latitude and estimated richness. This relationship resulted in the MIZ having the highest estimated richness in the Bering Sea. The MIZ is a unique community composed of true pelagic organisms and those sourced from the sea ice (40). A number of taxa were only detected within both sea ice and the MIZ: *Eugregarinorida*, *Strombidinopsis sp.*, *Euplotes charon*, *Maullinia ectocarpi*, *Guinardia delicatula*, *Rhizosolenia imbricate*,

and the FV36-2G-8 clade. Subsequently, we hypothesize that dual contributions from the pelagic and sea ice realm resulted in the highest Chao1 richness within the MIZ. By extension, the decreasing richness at the Bering Sea Shelf station and Pribilof Islands was likely influenced by ice cover and organisms seeded from the sea ice environment. Strong northerly winds can advect sea ice into the southeastern Bering Sea, ephemerally covering the Bering Sea Shelf station, as it did in 2015. This advection resulted in a mixture of taxa found only in sea ice, the MIZ and the Bering Sea Shelf site (e.g. SCM28C5 clade, *Eutimninus* sp., *Paulinella chromatophora*, Globothalamea, Rotaliida, D52 clade); however, the shared number of OTUs between sea ice and other sites was minimal, relative to the Shelikof Strait site (Table 4.2).

Subsequently, we surmise that temperature is a larger driver of eukaryotic microbial community structure than proximity to the sea ice. These results support previous observations made in the Arctic Ocean (41).

We hypothesized that the high concentrations of nitrate, silicate, and phosphate (among the highest in any marine system globally) within the Bering Sea (42) would be a driver for microbial community structure. Analysis of nutrient data were within the historical ranges previously reported for nitrate (43) and silicate (44). Overall, we did not find strong evidence for the significant effects of nutrients on structuring microbial communities in wintertime, even by focusing our analysis on the chlorophyll maximum that is often dominated by photosynthetic diatoms that require inorganic silicate. Further research is needed to evaluate the synergism of nutrients (such as phosphate), temperature and seasonality in structuring microbial communities.

We believe that our data delineate the Arctic-subArctic ecotone region (Supplemental Figure 4.1) of eukaryotic microbial communities in wintertime. This ecotone is defined by the spatial-temporal distribution of sea ice coverage that creates a gradient of cold water across the southeastern Bering Sea shelf. As solar irradiance increases in spring and stimulates the phytoplankton bloom, other factors such as light regime, stratification, and biological interactions will largely shape the eukaryotic community; however, in wintertime with overall low or non-existing new primary productivity, large scale diversity patterns appear to be driven by temperatures, irrespective of the unique chemical signatures across large geographical distances. Ultimately, our observations reinforce the coupled nature between physical oceanography and microbial diversity patterns and greatly underline the diversity responses of microbial communities to temperature. We suggest that an increase in microbial diversity studies would greatly benefit the understanding of biological responses to climate change by focusing on the base of food webs and the organisms that are likely to respond the quickest to abiotic perturbations.

Acknowledgements

Research design, experimentation, analyses, manuscript writing, manuscript formatting was conducted by Brandon T. Hassett. Manuscript editing was conducted by Rolf Gradinger.

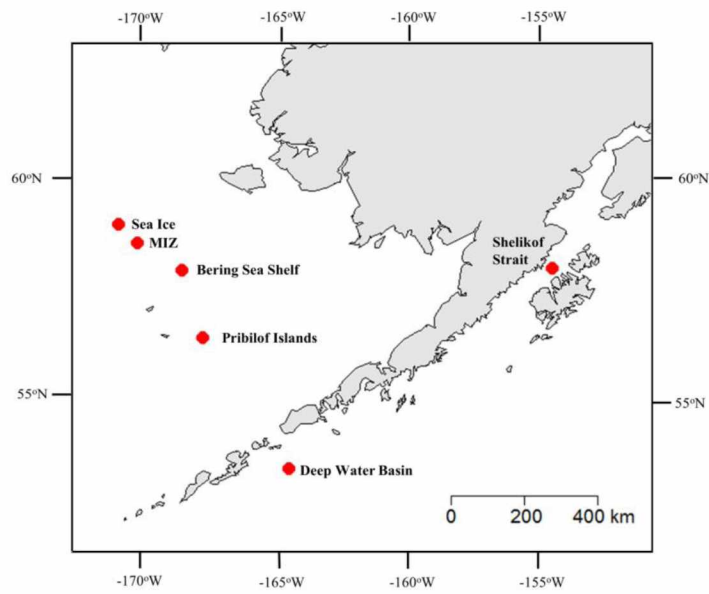


Figure 4.0. Study area in the eastern Bering Sea during an expedition in March 2015.

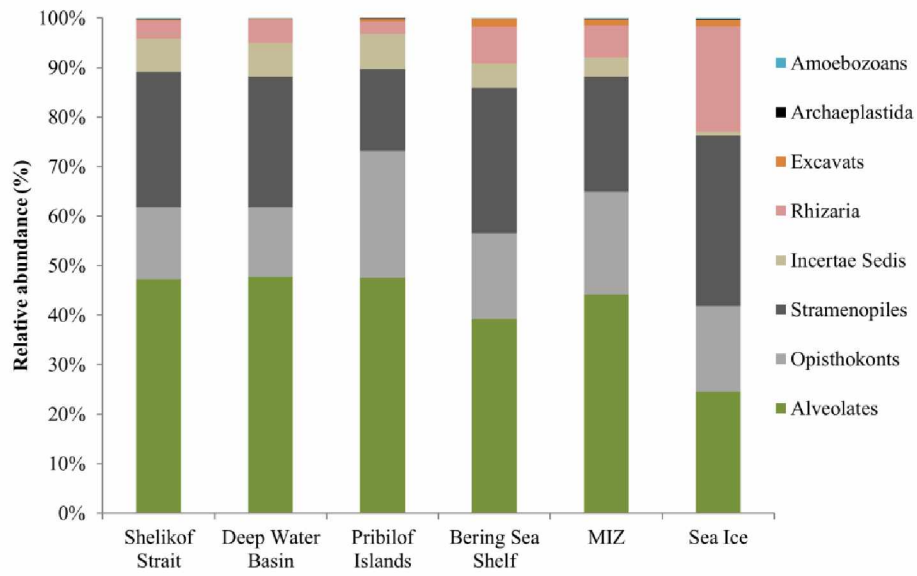


Figure 4.1. Relative abundance of eukaryotic supergroups illustrating general community structure.

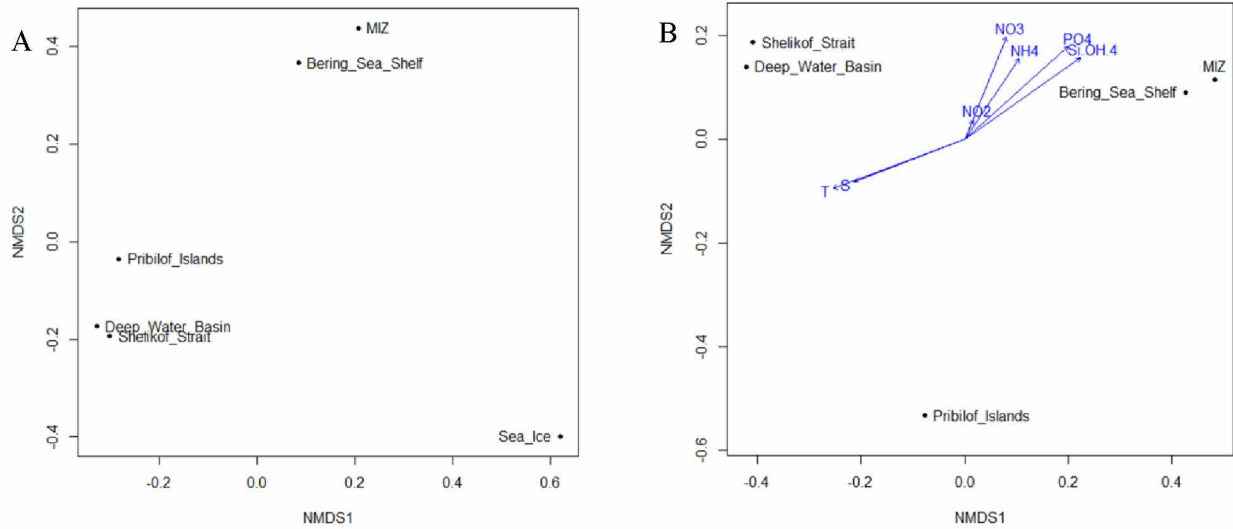


Figure 4.2. MDS plots of eukaryotic microbial community structure. MDS plots of eukaryotic microbial community structure computed by the Bray-Curtis dissimilarity index. A) MDS plot of five water sites along a northern transect. An ice station was included as a positive control to illustrate relative dissimilarity distance. B) MDS plot of water samples only with environmental vectors used to explain inorganic nutrient- and temperature-driven groupings.

Table 4.0. Sampling locations, date, depth of chlorophyll *a* maximum, temperature (T) and salinity (S).
 Brine salinity values are listed for sea ice.

Site name	Location	Date	Chlorophyll <i>a</i> depth (m)	T	S
Shelikof Strait	N58°17'58.6314", W-153°52'41.1954"	14 March	225	6.2	32.5
Deep water basin	N53°36'40.4274", W-164°35'34.2594"	16 March	266	5.6	33.5
Pribilof Islands	N56°32'2.4606", W-167°59'24.4572"	20 March	104	5.3	32.9
Bering Sea Shelf	N57°52'40.7388", W-168°51'22.0782"	21 March	64	0.3	32.2
Marginal Ice Zone	N58°37'6.8988", W-170°43'13.98"	24 March	72	-1.7	31.7
Sea Ice	N58°34'28.5708", -W170°51'50.1654"	25 March	NA	-1.8	35.6

Table 4.1. Site diversity and attributes of vetted datasets.

Site Name	Sample Coverage (%)	# OTUs	# Singletons	Chao1	Simpson
Shelikof Strait	97.1225	3199	1801	6,801.0	0.107
Deep Water Basin	98.6755	1863	829	2,912.5	0.062
Pribilof Islands	97.4404	3123	1602	5,380.7	0.218
Bering Sea Shelf	97.2311	3425	1733	5,874.2	0.107
MIZ	96.8444	3780	1975	6,788.2	0.185
Sea Ice	97.1288	3912	1797	5,982.5	0.121

Table 4.2. Comparative analysis between terminal sites representing the number of shared OTUs.

Sea Ice versus MIZ	436	Shelikof Strait versus Deep Water Basin	744
Sea Ice versus Bering Sea Shelf	432	Shelikof Strait versus Pribilof Islands	778
Sea Ice versus Pribilof Islands	214	Shelikof Strait versus Bering Sea Shelf	685
Sea Ice versus Deep Water Basin	146	Shelikof Strait versus MIZ	624
Sea Ice versus Shelikof Strait	224	Shelikof Strait versus Sea Ice	224

Works Cited

1. **Suttle CA.** 2007. Marine viruses--major players in the global ecosystem. *Nat Rev Microbiol* **5**:801–812.
2. **Gradinger R, Bluhm B, Hopcroft R, Gebruk A, Kosobokova K, Sirenko B, Weslawski J.** 2010. Marine life in the Arctic, p. 183–202. *In* McIntyre, A (ed.), *Life in the World's Oceans: Diversity, Distribution, and Abundance*. Wiley-Blackwell, West Sussex.
3. **Steele M, Ermold W, Zhang J.** 2008. Arctic Ocean surface warming trends over the past 100 years. *Geophys Res Lett* **35**:1–6.
4. **Doney SC, Ruckelshaus M, Emmett Duffy J, Barry J, Chan F, English C, Galindo HM, Grebmeier JM, Hollowed AB, Knowlton N, Polovina J, Rabalais NN, Sydeman WJ, Talley LD.** 2012. Climate change impacts on marine ecosystems. *Ann Rev Mar Sci* **4**:11–37.
5. **Fossheim M, Primicerio R, Johannesen E, Ingvaldsen RB, Aschan MM, Dolgov A V.** 2015. Recent warming leads to a rapid borealization of fish communities in the Arctic. *Nat Clim Chang* **5**:1–6.
6. **Mueter FJ, Litzow M.** 2008. Sea ice retreat alters the biogeography of the Bering Sea continental shelf. *Ecol Appl* **18**:309–320.
7. **Comeau AM, Li WKW, Tremblay JÉ, Carmack EC, Lovejoy C.** 2011. Arctic ocean microbial community structure before and after the 2007 record sea ice minimum. *PLoS One* **6**.
8. **Piepenburg D, Archambault P, Ambrose WG, Blanchard AL, Bluhm B, Carroll ML, Conlan KE, Cusson M, Feder HM, Grebmeier JM, Jewett SC, Lévesque M, Petryashev V V, Sejr MK, Sirenko BI, Wlodarska-Kowalczyk M.** 2011. Towards a pan-Arctic inventory of the species diversity of the macro- and megabenthic fauna of the Arctic shelf seas. *Mar Biodivers* **41**:51–70.
9. **Yasuhara M, Hunt G, van Dijken G, Arrigo KR, Cronin TM, Wollenburg JE.** 2012. Patterns and controlling factors of species diversity in the Arctic Ocean. *J Biogeogr* **39**:2081–2088.
10. **Galand PE, Casamayor EO, Kirchman DL, Lovejoy C.** 2009. Ecology of the rare microbial biosphere of the Arctic Ocean. *Proc Natl Acad Sci U S A* **106**:22427–22432.

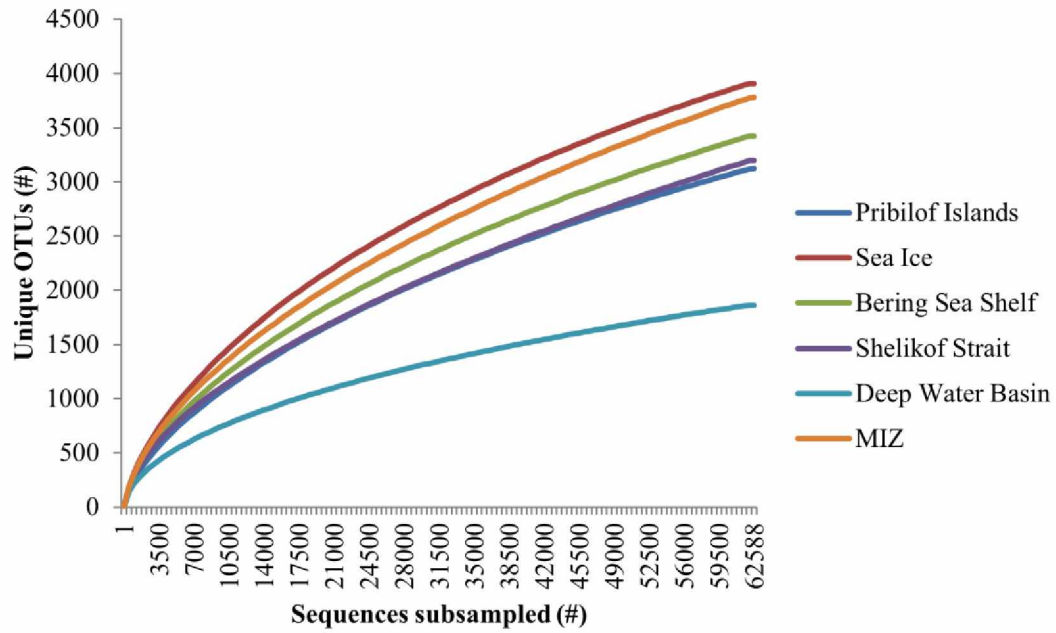
11. **Carmack E, Barber D, Christensen J, Macdonald R, Rudels B, Sakshaug E.** 2006. Climate variability and physical forcing of the food webs and the carbon budget on panArctic shelves. *Prog Oceanogr* **71**:145–181.
12. **Gradinger R.** 2009. Sea-ice algae: Major contributors to primary production and algal biomass in the Chukchi and Beaufort Seas during May/June 2002. *Deep Res Part II Top Stud Oceanogr* **56**:1201–1212.
13. **Holmes RM, McClelland JW, Peterson BJ, Tank SE, Bulygina E, Eglinton TI, Gordeev V V., Gurtovaya TY, Raymond P, Repeta DJ, Staples R, Striegl RG, Zhulidov A, Zimov S.** 2012. Seasonal and annual fluxes of nutrients and organic matter from large rivers to the Arctic Ocean and surrounding seas. *Estuaries and Coasts* **35**:369–382.
14. **Leu E, Mundy C, Assmy P, Campbell K, Gabrielsen T, Gosslin M, Juul-Pedersen T, Gradinger R.** 2015. Arctic spring awakening – steering principles behind the phenology of vernal ice algae blooms. *Prog Oceanogr* 1–31.
15. **Hodges LR, Bano N, Hollibaugh JT, Yager PL.** 2005. Illustrating the importance of particulate organic matter to pelagic microbial abundance and community structure - an Arctic case study. *Aquat Microb Ecol* **40**:217–227.
16. **Roy K, Jablonski D, Valentine JW, Rosenberg G.** 1998. Marine latitudinal diversity gradients: tests of causal hypotheses. *Proc Natl Acad Sci U S A* **95**:3699–3702.
17. **Terrado R, Vincent WF, Lovejoy C.** 2009. Mesopelagic protists: diversity and succession in a coastal Arctic ecosystem. *Aquat Microb Ecol* **56**:25–40.
18. **Gilbert J, Steele J, Caporaso G, Steinbrück L, Reeder J, Temperton B, Huse S, McHardy A, Knight R, Joint I, Somerfield P, Fuhrman J, Field D.** 2012. Defining seasonal marine microbial community dynamics. *ISME J* **6**:298–308.
19. **Stabeno P, Schumacher J, Ohtani K.** 1999. The physical oceanography of the Bering Sea, p. 1–28. *In* Loughlin, T, Ohtani, K (eds.), *Dynamics of the Bering Sea*. University of Alaska Sea Grant, Fairbanks.

20. **Aydin K, Mueter F.** 2007. The Bering Sea-A dynamic food web perspective. *Deep Res Part II Top Stud Oceanogr* **54**:2501–2525.
21. **Stabeno P, Bond N, Kchel N, Salo S, Schumacher J.** 2001. On the temporal variability of the physical environment over the south-eastern Bering Sea. *Fish Oceanogr* **10**:81–98.
22. **Nelson J, Ashjian C, Bluhm B, Conlan K, Gradinger R, Grebmeier J, Hill V, Hopcroft R, Hunt P, Joo H, Kirchman D, Kosobokova K, Lee S, Li K, Lovejoy C, Poulin M, Sherr E, Young K.** 2014. Biodiversity and biogeography of the lower trophic taxa of the Pacific Arctic Region: sensitivities to climate change, p. 269–336. *In* Bregmeier, J, Maslowski, W (eds.), *The Pacific Arctic Region: ecosystem status and trends in a rapidly changing environment*. Springer.
23. **Stoeck T, Bass D, Nebel M, Christen R, Jones MDM, Breiner HW, Richards T.** 2010. Multiple marker parallel tag environmental DNA sequencing reveals a highly complex eukaryotic community in marine anoxic water. *Mol Ecol* **19**:21–31.
24. **Kozich JJ, Westcott SL, Baxter NT, Highlander SK, Schloss PD.** 2013. Development of a dual-index sequencing strategy and curation pipeline for analyzing amplicon sequence data on the MiSeq Illumina sequencing platform. *Appl Environ Microbiol* **79**:5112–5120.
25. **Schloss PD, Westcott SL, Ryabin T, Hall JR, Hartmann M, Hollister EB, Lesniewski R a., Oakley BB, Parks DH, Robinson CJ, Sahl JW, Stres B, Thallinger GG, Van Horn DJ, Weber CF.** 2009. Introducing Mothur: Open-source, platform-independent, community-supported software for describing and comparing microbial communities. *Appl Environ Microbiol* **75**:7537–7541.
26. **Quast C, Pruesse E, Yilmaz P, Gerken J, Schweer T, Yarza P, Peplies J, Glöckner FO.** 2013. The SILVA ribosomal RNA gene database project: improved data processing and web-based tools. *Nucleic Acids Res* **41**:590–596.
27. **Edgar RC, Haas BJ, Clemente JC, Quince C, Knight R.** 2011. UCHIME improves sensitivity and speed of chimera detection. *Bioinformatics* **27**:2194–2200.
28. **Burki F.** 2014. The eukaryotic tree of life from a global phylogenomic perspective. *Cold Spring Harb Perspect Biol* **6**:a016147–a016147.

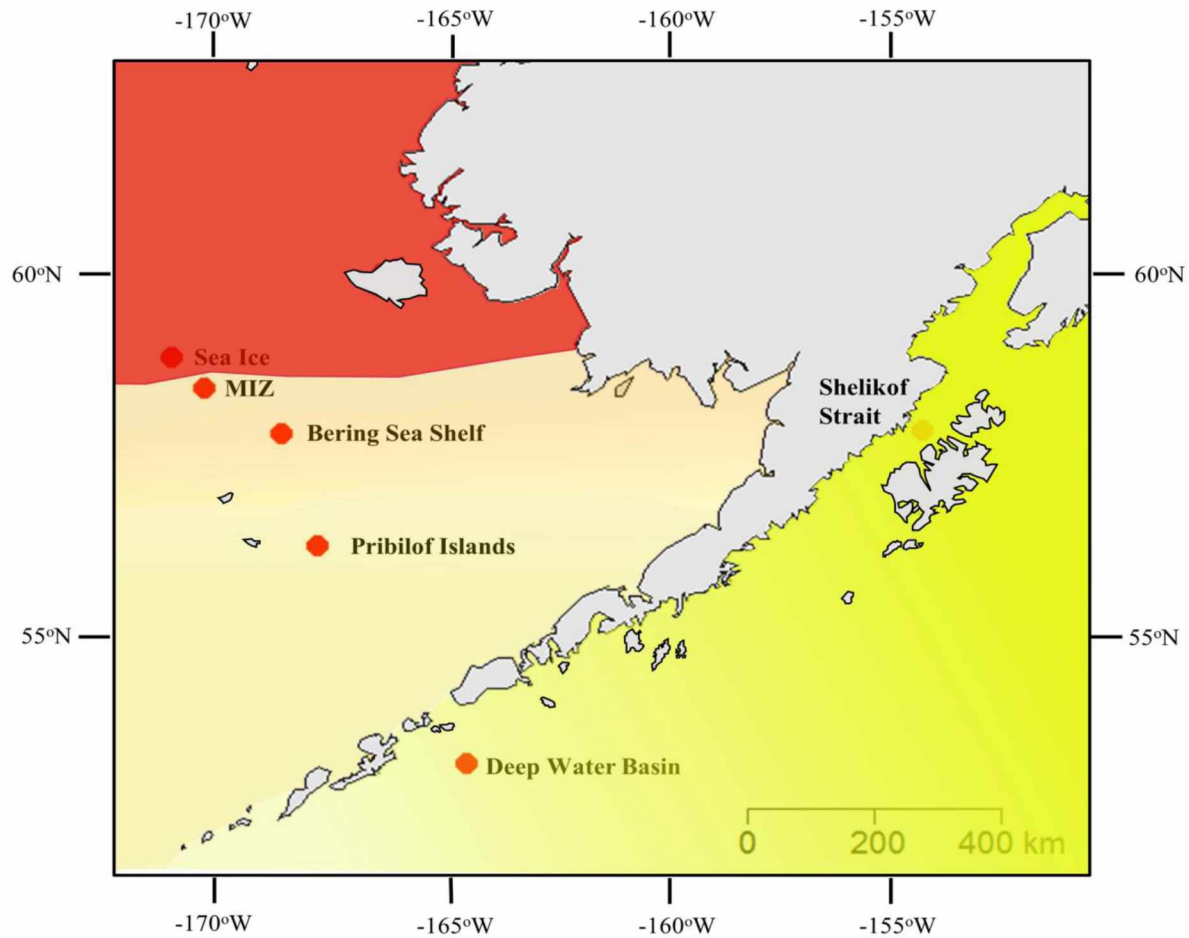
29. **An S, Couteau C, Luo F, Neveu J, DuBow MS.** 2013. Bacterial diversity of surface sand samples from the Gobi and Taklamaken Deserts. *Microb Ecol* **66**:850–860.
30. **Barott KL, Rodriguez-Brito B, Janouškovec J, Marhaver KL, Smith JE, Keeling P, Rohwer FL.** 2011. Microbial diversity associated with four functional groups of benthic reef algae and the reef-building coral *Montastraea annularis*. *Environ Microbiol* **13**:1192–1204.
31. **Paulus BC, Kanowski J, Gadek P, Hyde KD.** 2006. Diversity and distribution of saprobic microfungi in leaf litter of an Australian tropical rainforest. *Mycol Res* **110**:1441–1454.
32. **Galand P, Lovejoy C, Vincent WF.** 2006. Remarkably diverse and contrasting archaeal communities in a large Arctic river and the coastal Arctic Ocean. *Aquat Microb Ecol* **44**:115–126.
33. **Galand P, Lovejoy C, Pouliot J, Garneau M, Vincent WF.** 2008. Microbial community diversity and heterotrophic production in a coastal Arctic ecosystem: a stamukhi lake and its source waters. *Limnol Oceanogr* **53**:813–823.
34. **Hansell D, Kadko D, Bates N.** 2004. Degradation of terrigenous dissolved organic carbon in the western Arctic Ocean. *Science* **304**:858–861.
35. **Serno S, Winckler G, Anderson RF, Hayes CT, McGee D, Machalett B, Ren H, Straub SM, Gersonde R, Haug GH.** 2014. Eolian dust input to the SubArctic North Pacific. *Earth Planet Sci Lett* **387**:252–263.
36. **Grattepanche JD, Santoferrara LF, McManus GB, Katz L a.** 2014. Diversity of diversity: Conceptual and methodological differences in biodiversity estimates of eukaryotic microbes as compared to bacteria. *Trends Microbiol* **22**:432–437.
37. **Moniz MBJ, Kaczmarska I.** 2010. Barcoding of diatoms: nuclear encoded ITS revisited. *Protist* **161**:7–34.
38. **Kondrashov F, Rogozin I, Wolf Y, Koonin EV.** 2002. Selection in the evolution of gene duplications. *Genome Biol* **3**:RESEARCH0008.1–0008.9.
39. **Alverson AJ, Kolnick L.** 2005. Intragenomic nucleotide polymorphism among small subunit (18S) rDNA paralogs in the diatom genus *Skeletonema* (Bacillariophyta). *J Phycol* **41**:1248–1257.

40. **Moran SB, Lomas MW, Kelly RP, Gradinger R, Iken K, Mathis JT.** 2012. Seasonal succession of net primary productivity, particulate organic carbon export, and autotrophic community composition in the eastern Bering Sea. *Deep Sea Res Part II Top Stud Oceanogr* **65-70**:84–97.
41. **Lovejoy C, Massana R, Pedro C.** 2006. Diversity and distribution of marine microbial eukaryotes in the Arctic Ocean and adjacent seas. *Appl Environ Microbiol* **72**:3085–3095.
42. **Whitledge T, Luchin V.** 1999. Summary of chemical distributions and dynamics in the Bering Sea, p. 217–249. *In* Loughlin, T, Ohtani, K (eds.), *Dynamics of the Bering Sea*. University of Alaska Sea Grant, Fairbanks.
43. **Sherr EB, Sherr BF, Ross C.** 2013. Microzooplankton grazing impact in the Bering Sea during spring sea ice conditions. *Deep Res Part II Top Stud Oceanogr* **94**:57–67.
44. **Tsunogai S, Kusakabe M, Iizumi H, Hattori A.** 1979. Hydrographic features of the deep water of the Bering Sea - The Sea of Silica. *Deep Res* **26**:641–659.

Supplemental Materials



Supplemental Figure 4.0. Sampling rarefaction curves. Curves were generated after sequence vetting, subsampling (62,588) and clustering at 97% similarity, generated per site displaying the unique number of OTUs per sampling effort.



Supplemental Figure 4.1. Shared OTU map. Map illustrates the Arctic-sub Arctic ecotone. Map represents the number of shared OTUs between the Sea Ice station (red) versus all other sites and the Shelikof Strait station (yellow) versus all other sites, as a function of percent color opacity. Intermediate sites are more yellow than red, as these sites had a higher proportion of organisms found in the Shelikof Strait site. The MIZ and Bering Sea Shelf site are more orange, as these sites had a higher proportion of organisms found in sea ice.

Supplemental Table 4.0. Inorganic nutrient data (μM). Data was acquired from all water sites. Standard deviations (s.d.) are the result of three independent replicates.

Station Name	PO₄	+/- s.d.	Si(OH)₄	+/- s.d.	NO₃	+/- s.d.	NO₂	+/- s.d.	NH₄	+/- s.d.
Shelikof Strait	1.40	0.31	19.89	4.70	11.81	3.36	0.12	0.05	1.13	1.96
Deep Water										
Basin	1.31	0.16	20.88	4.25	12.18	2.82	0.09	0.02	0.008	0.02
Pribilof Islands	1.77	0.35	29.77	7.43	15.08	4.72	0.14	0.07	1.85	3.21
Bering Sea Shelf	1.23	0.04	18.57	0.79	9.43	0.43	0.10	0.003	4.0x10 ⁻⁵	3.2x10 ⁻⁸
MIZ	1.67	0.17	29.69	3.61	11.76	1.68	0.08	0.02	0.70	1.2

Supplemental Table 4.1. Condensed taxonomy of detected organisms in the Bering Sea region: Shelikof Strait (SS), Deep Water Basin (DWB), Pribilof Islands (PI), Marginal Ice Zone (MIZ) and Sea Ice. Organisms classified to minimally the taxonomic genus level are represented below. Select taxonomic clades in the Phaeophytes and fungi were represented by only sequences classifiable to Order and were included in this table. The majority of our sequences did not classify to the genus level and were not represented in this table. For example, the Prasinophytes were detected at every station, but *Prasinoderma sp.* is represented at only three stations.

	SS	DWB	PI	BSS	MIZ	Sea Ice
Amoebozoa						
Dactylopodids						
<i>Paramoeba sp.</i>	+	+	-	-	+	+
<i>Paramoeba branchiphila</i>	+	-	-	-	-	-
<i>Paramoeba eilhardi</i>	-	+	-	-	-	-
Tubulinds						
<i>Vermamoeba sp.</i>	+	-	-	-	-	-
<i>Vermamoeba vermiformis</i>	+	-	-	-	-	-
<i>Paraflabellula hoguae</i>	-	-	-	+	-	+
Excavata						
Diplonemids						
<i>Diplonema sp.</i>	-	-	+	-	-	-
Euglenids						
<i>Petalomonas cantuscygni</i>	+	-	-	-	-	-
<i>Neobodo sp.</i>	-	-	-	+	+	-
<i>Ichthyobodo sp.</i>	-	-	-	+	+	-
Archaeplastida						
Prasinophytes						
<i>Prasinoderma sp.</i>	-	-	-	+	+	+
Opisthokonta						
Choanoflagellates						
Stephanoecidae	+	+	-	+	+	+
<i>Diaphanoeca grandis</i>	+	-	-	-	+	+
Mesomycetozoea						
<i>Pseudoperkinsus tapetis</i>	-	-	+	+	+	+
Fungi						
Chytrids						
Rhizophlyctidales	-	-	-	+	+	-
Ascomycota						
Capnodiales	-	-	-	-	+	-
Dothideales	+	-	-	-	-	-
Pleosporales	+	-	-	+	+	+

**Supplemental Table 4.1
continued.....**

<i>Penicillium sp.</i>	+	-	+	-	-	-
Helotiales	+	+	+	+	+	-
Xylariales	-	+	+	+	+	-
<i>Debaryomyces hansenii</i>	-	-	+	-	-	-
Basidiomycota						
Agaricomycetes	-	+	+	-	-	-
<i>Udeniomyces pannonicus</i>	-	-	+	-	-	-
SAR						
Alveolates						
<hr/>						
Apicomplexa						
<i>Filipodium sp.</i>	-	-	-	+	-	+
<i>Gregarinidae sp.</i>	-	-	-	-	+	+
Novel Apicomplexa Class 2	-	-	-	-	-	+
Ciliates						
DH147-EKD23	+	+	-	+	+	-
<i>Pseudocollinia oregonensis</i>	+	-	-	-	-	-
<i>Peritrichia sp.</i>	-	-	+	-	-	+
<i>Scuticociliatia sp.</i>	-	-	-	-	-	+
<i>Mesanophrys carcini</i>	-	-	-	-	-	+
<i>Parauronema longum</i>	-	-	-	-	-	+
<i>Acineta sp.</i>	-	-	-	-	-	+
<i>Ephelota sp.</i>	+	-	-	-	-	-
<i>Cryptocaryon sp.</i>	-	-	+	-	-	-
<i>Loxophyllum sp.</i>	-	-	-	-	+	-
<i>Myrionecta</i>	+	+	+	+	+	+
<i>Eutintimus sp.</i>	-	-	-	+	+	+
<i>Favella arcuata</i>	-	-	-	-	-	+
<i>Pelagostrobilidium sp.</i>	+	+	+	-	+	-
<i>Stenosemella sp.</i>	+	+	-	+	+	+
<i>Strombidinopsis sp.</i>	-	-	-	-	+	+
<i>Tintinnidium sp.</i>	-	-	-	-	-	+
<i>Tintinnidium mucicola</i>	-	-	-	-	-	+
<i>Tintinnopsis sp.</i>	+	-	-	+	-	+
<i>Tintinnopsis lohmanni</i>	-	-	-	-	-	+
<i>Tintinnopsis sp. JG-2-11a</i>	+	-	-	+	-	+
<i>Rimostrombidium veniliae</i>	+	-	+	-	+	+
<i>Discocephalus ehrenbergi</i>	-	-	-	-	-	+
<i>Euplotes sp.</i>	+	-	-	-	+	+
<i>Euplotes charon</i>	+	-	-	-	+	+
<i>Hypotrichia sp.</i>	+	-	+	+	+	+
<i>Hypotrichia sp. I-99</i>	+	-	-	-	-	-

**Supplemental Table 4.1
continued....**

<i>Holosticha</i> sp.	-	-	-	+	-	-
Oligotrichia	+	-	+	+	+	+
<i>Laboea</i> sp.	+	-	+	+	+	-
<i>Pseudotontonia</i> sp.	-	+	+	+	+	-
<i>Strombidium</i> sp.	+	+	+	+	+	+
Dinoflagellates						
<i>Amphidinium</i> sp.	+	+	+	+	+	-
<i>Gymnodinium</i> sp. CCMF422	-	-	-	+	-	-
<i>Chytriodinium</i> sp.	+	+	+	+	+	-
<i>Lepidodinium</i> sp.	+	+	-	-	-	-
<i>Nematodinium</i> sp.	-	-	+	-	-	-
<i>Polykrikos</i> sp.	-	-	-	-	-	+
<i>Gyrodinium</i> sp.	+	+	+	+	+	+
<i>Azadinium</i> sp.	+	-	-	-	-	-
<i>Karlodinium veneficum</i>	+	+	+	+	+	-
<i>Pelagodinium beii</i>	+	+	+	+	+	+
<i>Symbiodinium</i> sp.	+	+	+	-	-	-
<i>Halostyloidinium</i> sp.	+	-	-	-	-	-
<i>Alexandrium fundyense</i>	+	+	+	+	-	+
<i>Alexandrium ostenfeldii</i>	+	-	+	+	-	+
<i>Alexandrium tamarense</i>	+	+	+	+	+	+
<i>Ceratium tenue</i>	+	+	+	+	+	+
<i>Protoperidinium</i> sp.	+	+	+	+	+	-
<i>Protoceratium reticulatum</i>	-	-	-	-	-	+
<i>Scrippsiella</i> sp.	-	-	-	+	-	+
<i>Tintinnophagus acutus</i>	-	-	-	-	-	+
<i>Prorocentrum donghaiense</i>	-	-	+	-	-	-
<i>Prorocentrum minimum</i>	+	+	+	+	+	-
SL163A10 (AntArctic)	+	+	+	-	+	-
<i>Blastodinium navicula</i>	+	-	-	+	-	-
<i>Haplozoon</i> sp.	+	+	+	+	+	-
<i>Scrippsiella</i> sp.	+	+	+	+	+	-
<i>Paulsenella vonstoschii</i>	-	-	-	-	-	+
<i>Noctiluca scintillans</i>	-	-	-	-	-	+
SCM28C5	-	-	-	+	+	+
<i>Thalassomyces fagei</i>	+	+	+	+	-	-
<i>Euduboscquella crenulata</i>	+	+	+	+	+	+
<i>Takayama pulchellum</i>	+	+	+	-	-	-
Syndiniales						
<i>Amoebophrya</i> sp.	+	-	+	+	+	+
Syndiniales Group I	-	+	+	+	+	+

**Supplemental Table 4.1
continued....**

Syndiniales Group II	+	+	+	+	+	-
<i>Syndinium sp.</i>	-	+	-	-	-	-
<hr/>						
Rhizaria						
<hr/>						
Cercomonads						
<i>Minchinia sp.</i>	-	-	-	-	+	-
<i>Cercozoa sp. CC-2--9d</i>	-	-	-	+	-	-
<i>Minorisa sp.</i>	-	+	-	+	+	+
NOR26	+	+	+	+	+	-
<i>Pseudopirsonia sp.</i>	-	-	-	+	-	+
<i>Nudifila sp.</i>	-	-	-	-	-	+
<i>Paulinella sp.</i>	+	+	+	+	+	-
<i>Paulinella chromatophora</i>	-	-	-	+	+	+
<i>Cryothecomonas sp.</i>	+	+	+	+	+	+
<i>Protaspa sp.</i>	-	-	+	+	+	+
<i>Ebria sp.</i>	+	+	+	+	+	+
Thaumatomonads						
<i>Thaumatomastix sp.</i>	-	-	-	-	-	+
Phytomyxea						
<i>Maulinia ectocarpi</i>	-	-	-	-	+	+
<i>Spongospora sp.</i>	-	-	-	-	-	+
Paradinium						
<i>Paradinium poucheti</i>	-	-	+	-	-	-
Acantharia						
<i>Acanthometra sp.</i>	-	+	-	-	-	-
Uncultured marine acantharean DH147-EKD17	-	+	-	-	-	-
<i>Chaunocanthida sp.</i>	+	+	-	-	-	-
Foraminifera						
Globothalamea	-	-	-	+	+	+
Rotaliida	-	-	-	+	+	+
Polycystinea						
<i>Lithomelissa setosa</i>	+	+	+	-	-	-
<hr/>						
Stramenopiles						
<hr/>						
Incertae Sedis						
<i>Pirsonia sp.</i>	+	-	+	+	+	+
<i>Pirsonia guinardiae</i>	+	-	+	-	-	+
Labyrinthulids						
D52	-	-	-	+	+	+
TAGIRI-17	-	-	-	-	-	+
<i>Aplanochytrium sp.</i>	-	-	-	+	-	+
MAST-1	-	+	-	+	+	+
MAST-2	+	+	+	+	+	+

**Supplemental Table 4.1
continued....**

MAST-3	+	+	+	+	+	+
MAST-4	+	+	+	+	+	-
MAST-6	+	+	+	-	+	+
MAST-7	+	+	+	+	+	-
MAST-8	+	+	+	+	+	-
MAST-9	+	+	+	+	+	-
MAST-12	+	+	+	+	+	-
Chrysophytes						
<i>Spumella</i> sp.	+	-	-	-	-	+
E222	+	+	+	+	+	+
<i>Ochromonas</i> sp.	+	-	-	-	-	-
<i>Chrysophyceae</i> sp.	+	-	-	-	-	-
Diatoms						
<i>Asterionellopsis glacialis</i>	-	-	-	-	-	+
<i>Asteroplanus karianus</i>	+	+	+	+	+	+
<i>Fragilariopsis</i> sp.	+	+	+	+	+	+
<i>Navicula</i> sp.	-	-	+	-	-	+
<i>Nitzschia</i> sp.	+	+	+	+	+	+
<i>Pleurosigma</i> sp.	+	+	+	+	+	+
<i>Pseudo-nitzschia australis</i>	+	+	+	-	+	-
<i>Attheya longicornis</i>	+	+	+	+	+	+
<i>Brockmanniella brockmannii</i>	-	-	-	+	+	-
<i>Chaetoceros</i> sp.	+	+	+	+	+	+
<i>Chaetoceros rostratus</i>	+	+	+	+	+	+
<i>Chaetoceros</i> sp. CCAP 1-1-/16	-	-	-	+	-	-
<i>Chaetoceros</i> sp. p442	+	+	+	+	-	-
<i>Cyclotella choctawhatcheeana</i>	-	+	-	-	-	+
<i>Cymatosira belgica</i>	-	-	-	+	-	+
<i>Ditylum brightwellii</i>	+	+	+	+	+	-
<i>Hyalosira</i> sp. CCMP469	+	-	+	-	-	+
<i>Minutocellus</i> sp.	+	+	+	+	+	+
<i>Porosira</i> sp.	+	+	+	+	+	+
<i>Skeletonema</i> sp.	+	+	+	+	+	+
<i>Thalassiosira</i> sp.	+	+	+	+	+	+
<i>Thalassiosira concaviuscula</i>	+	-	+	+	+	-
<i>Thalassiosira guillardii</i>	+	-	-	-	-	+
<i>Thalassiosira nordenskiöldii</i>	-	-	-	-	-	+
<i>Thalassiosira oceanica</i>	-	-	-	+	-	-
<i>Thalassiosira punctigera</i>	+	+	+	-	-	-
<i>Actinocyclus curvatulus</i>	+	+	+	+	+	+
<i>Corethron criophilum</i>	+	+	+	+	+	-

**Supplemental Table 4.1
continued...**

<i>Coscinodiscus radiates</i>	+	+	+	-	+	-
<i>Coscinodiscus sp. GGM-2—4</i>	+	-	-	-	-	-
<i>Melosira sp.</i>	+	+	+	-	-	-
<i>Stephanopyxis nipponica</i>	+	+	+	-	-	-
<i>Leptocylindrus minimus</i>	+	-	+	+	+	-
<i>Proboscia alata</i>	+	+	+	+	+	-
<i>Guinardia delicatula</i>	-	-	-	-	+	+
<i>Rhizosolenia imbricate</i>	-	-	-	-	+	+
Dictyochophytes						
<i>Dictyocha speculum</i>	+	+	+	+	+	-
<i>Florenciella sp.</i>	-	-	+	-	-	-
<i>Pseudochattonella verruculosa</i>	+	+	+	+	+	-
<i>Apedinella radians</i>	+	-	+	-	-	-
FV36-2G-8	-	-	-	-	+	+
<i>Pseudopedinella elastica</i>	+	-	+	+	-	-
<i>Pteridomonas sp.</i>	+	-	-	+	-	+
Pelagophytes						
<i>Aureococcus anophagefferens</i>	+	+	+	+	+	-
<i>Pelagococcus subviridis</i>	+	+	+	-	-	-
<i>Pelagomonas calceolata</i>	+	+	+	+	+	-
Phaeophytes						
Ectocarpales	-	-	-	-	-	+
Laminariales	-	-	-	-	-	+
<i>Costaria costata</i>	-	-	-	-	-	+
Peronosporomycetes						
Halocrusticida	-	-	-	-	-	+
Bolidomonas						
<i>Bolidomonas pacifica</i>	+	+	+	+	+	-
Incertae Sedis						
Cryptophytes						
<i>Rhodomonas sp.</i>	-	-	+	+	+	+
<i>Teleaulax sp.</i>	+	+	+	+	+	+
Kathablepharidae						
<i>Katablepharis sp.</i>	-	-	+	+	+	+
<i>Leucocryptos sp.</i>	-	-	-	+	-	-
Picozoa						
<i>Picomonas sp.</i>	+	+	+	+	+	-
Centrohelida						
<i>Chlamydaster sterni</i>	-	-	-	+	-	-
Haptophyta						
<i>Emiliana huxleyi</i>	+	+	-	-	+	-

**Supplemental Table 4.1
continued**

<i>Isochrysis galbana</i>	+	-	-	-	-	-
<i>Phaeocystis antArctica</i>	+	+	+	+	+	-
<i>Phaeocystis cordata</i>	-	+	-	-	-	-
<i>Chrysochromulina sp.</i>	+	+	+	+	+	-
<i>Chrysochromulina campanulifera</i>	+	+	+	-	-	-
<i>Chrysochromulina parva</i>	+	+	+	-	-	-
Haptophytes						
<i>Haptolina sp.</i>	+	-	+	+	+	-
Telonema						
<i>Telonema antArcticum</i>	+	-	+	+	+	-

General Conclusions

The Arctic Ocean still remains one of the least studied oceanographic regions in the world. During the time of this research, sea ice reached the 6th lowest extent on record in both 2013 and 2014 and the lowest maximum extent ever in 2015. With these changes are coming continued perturbations to the Arctic marine environment, with concomitant shifts in ecology. Although substantial progress has been made towards characterizing marine biodiversity, numerous species remain undescribed, especially in the microbial realm. The uncharacterized nature of Arctic marine microbes is a challenge for assessing species richness and predicting shifts in microbial ecological patterns, even when equipped with high-throughput sequencing technologies.

Using the contemporary paradigm for the description of new species, this research expands the known diversity of organisms by describing two new marine eukaryotes. By describing these organisms, the life history of the sphaeroformids was expanded to include a free-living saprotrophic stage and lipid inclusions, attributes previously unassociated with the taxonomic class and genus, respectively. Genetic characterization of these new species expanded public sequencing databases with 18S rRNA and ITS barcodes. The addition of these barcodes is the first step to filling in the blanks of unknown diversity encountered during high throughput sequencing analysis. My success in culturing unknown organisms underscores the merit in conducting culturing-based assessments of diversity in the future, especially in high latitude seas. Though only 1% or fewer microbes are thought to be culturable, the introduction of non-standard culturing techniques (such as the use of complex organic baits) could substantially augment culturing success for eukaryotes.

Culturing-based studies of microbes can expand known biodiversity; however, established culture libraries can serve as an important source for genomic DNA for full genome assembly. As of November 30th, 2015, 186 protist genomes have been sequenced and deposited in GenBank from across the globe. By comparison, over 700 species of diatoms are found in Arctic sea ice, underscoring the vast potential for breakthroughs in understanding the genetic composition of Arctic eukaryotic microbes, including easily grown, cosmopolitan species. The present research included genome assembly and annotation of a newly cultured species, *Sphaeroforma sirkka*. Annotated genes within the assembled *S. sirkka* genome were found to have closest identity to *Oncorhynchus mykiss* (Rainbow Trout), underscoring the vast potential for understanding the evolution of multicellular organisms from these and future genome data. Genomic data can be extensively analyzed to explore the potential presence of useful gene products (Figure 5.0) that could be beneficial to humans. My research identified diverging fatty-acid related catalytic enzymes that are functionally similar to gene products incorporated into patent products (e.g. US

20120233716 A1). The application of genetic resources has substantial academic potential to explain and guide organism-specific ecological hypotheses. The presence or absence of genes details the genetic potential that dictates functionality in an ecosystem (Figure 5.0). From these data, gene products can be organized into known metabolic pathways to map theoretical biochemical pathways (Figure 5.1). This metabolic mapping from encoded genes can guide sound scientific hypotheses about the life history and response of specific organisms to changes in the environment, such as organismal response to an influx of sourced terrestrial matter (Hilton *et al.*, 2015; Blair and Aller, 2012) or identifying organisms for potential use in bioremediation (Kües, 2015) or bioreactors (Farinas, 2015). Alternatively, genomic data provide substantial resources for multigene phylogenies that can circumscribe taxonomic clades and refine species definitions (Kim *et al.*, 2015; Cavalier-Smith *et al.*, 2015) that are essential for guiding estimates of microbial richness. My research increases the known genetic diversity within eukaryotic microbes and highlights some immediate applications for its use, such as metabolic mapping and classifying functional gene repertoires.

Genetic data generated during the description of novel organisms and genome assembly can be used as biological markers for the assessment of environmental microbial diversity. Short regions of taxonomically informative DNA loci (gene barcodes) (e.g. ITS, 18S, 28S rRNA) can be sequenced to determine the relative abundance of microbial species within a local community. High throughput sequencing results can exceed millions of taxonomic data points that can be analyzed for diversity patterns across time and space to guide inductive and deductive research. My research used 18S rRNA barcodes to assess fungal diversity patterns within sea ice and seafloor communities in Barrow, Alaska. Analysis of fungal community sequence data revealed a dynamic community fluctuating with season, in which saprotrophic Zygomycota fungi dominate sediment fungal communities during algal decay, parasitic Chytridiomycota dominate in the presence of photosynthesizing algae, and the Dikarya dominate during polar night. These sequence data led to further experimental and observational results that delineated a cryptic carbon cycle in a marine environments, the mycoloop. More importantly, this research highlighted the strong interactions between the physical environment and biological interactions by employing a classic disease paradigm, the disease triangle. Specifically, strong influxes of light can physiologically stress photosynthetic organisms, rendering them susceptible to fungal infection. To date, marine mycology has been largely anecdotal and comprised of temporal/spatial snapshots e.g. (Pernice *et al.*, 2015). This research is the first analysis in any marine environment that details the seasonal composition, functionality and genetic diversity of marine fungi. Most importantly, this research places marine fungi within a functional paradigm that is predictable and expected. The ultimate ecological outcome of marine fungal activity remains unknown; however, my research establishes the conceptual

framework in which marine fungi can be further explored. Fungal sequences generated in this time-series analysis comprised <5% of the total eukaryotic sequence data generated. Future research should analyze the remaining data to assess the total eukaryotic community structure in sea ice and sediment as a function of time and environmental drivers.

Assessing the abiotic drivers of microbial community structure is essential for explaining the current spatial diversity patterns of microbes. This research mapped eukaryotic microbial community structure in the Bering Sea by using 18S rRNA gene barcodes to establish baseline diversity estimates and the physical drivers behind large-scale diversity patterns. Data from this study was determined to have successfully mapped >96% of the eukaryotic microbial diversity and revealed an extremely diverse population whose structure is shaped by decreasing temperature with increasing latitude. By analyzing community structure in conjunction with diversity, different regions of the Bering Sea were determined to be structurally similar, yet less diverse. These data suggested that the same ecosystem processes were being maintained by fewer individuals and that these microbial communities were structured by temperature. These results suggest that the eukaryotic microbial population is sensitive to temperature changes and underlines the potential impacts of climate perturbations to the base of marine food webs.

Ultimately, this research advances the field of marine science by expanding the known diversity of microorganisms, genes, food webs, and spatial biological patterns in high-latitude seas. Future researchers are now better equipped to interpret findings within an established context, as this research has defined the fundamental physical parameters that constrain microbial communities and identified major players in the Arctic and sub-Arctic seas.

References

- Blair NE, Aller RC. (2012). The fate of terrestrial organic carbon in the marine environment. *Ann Rev Mar Sci* **4**:401–423.
- Cavalier-Smith T, Fiore-Donno AM, Chao E, Kudryavtsev A, Berney C, Snell E a., *et al.* (2015). Multigene phylogeny resolves deep branching of Amoebozoa. *Mol Phylogenet Evol* **83**:293–304.
- Farinas CS. (2015). Developments in solid-state fermentation for the production of biomass-degrading enzymes for the bioenergy sector. *Renew Sustain Energy Rev* **52**:179–188.
- Hilton RG, Galy V, Gaillardet J, Dellinger M, Bryant C, O'Regan M, *et al.* (2015). Erosion of organic carbon in the Arctic as a geological carbon dioxide sink. *Nature* **524**:84–87.
- Kim JI, Linton EW, Shin W. (2015). Taxon-rich multigene phylogeny of the photosynthetic euglenoids (Euglenophyceae). *Front Ecol Evol* **3**:1–11.
- Kües U. (2015). Fungal enzymes for environmental management. *Curr Opin Biotechnol* **33**:268–278.
- Pernice MC, Giner CR, Logares R, Perera-Bel J, Acinas SG, Duarte CM, *et al.* (2015). Large variability of bathypelagic microbial eukaryotic communities across the world's oceans. *ISME J* 1–14.

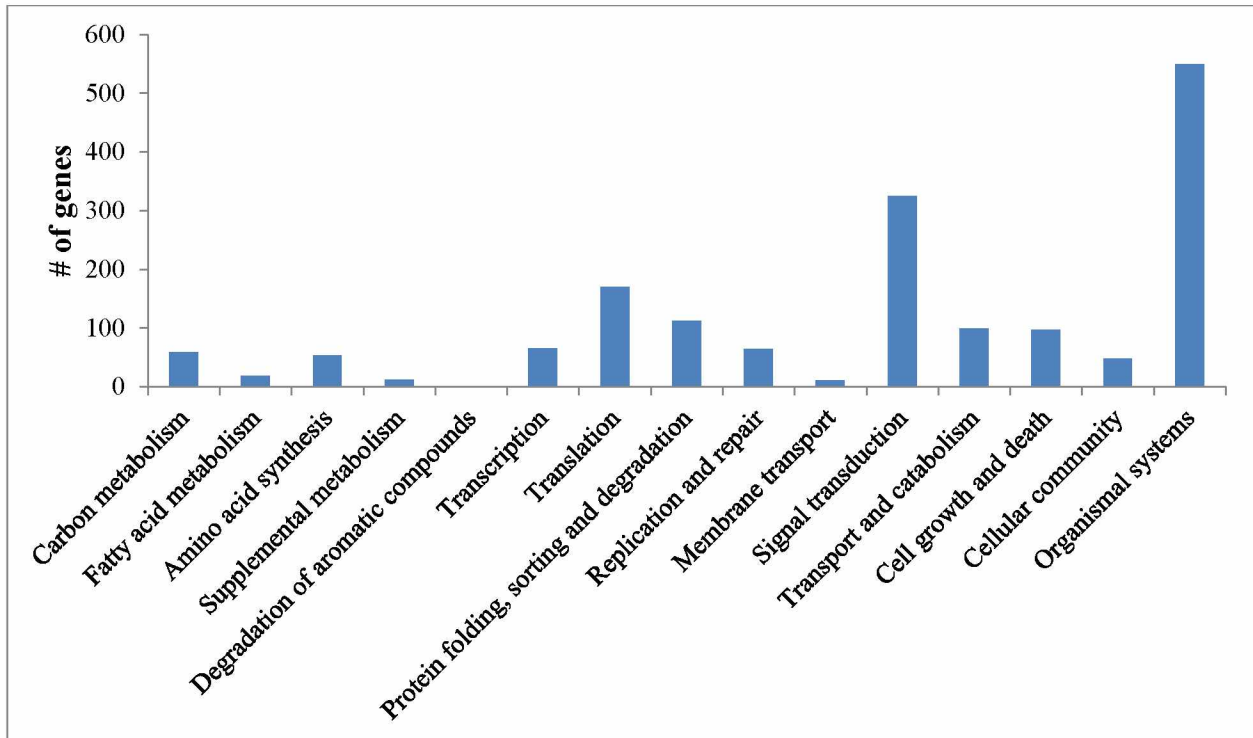


Figure 5.0. KEGG-classified gene products. Annotated genes from the genome of *Sphaeroforma sirkka* were classified into functional pathways. Graph shows the number of genes belonging to major cellular functions.

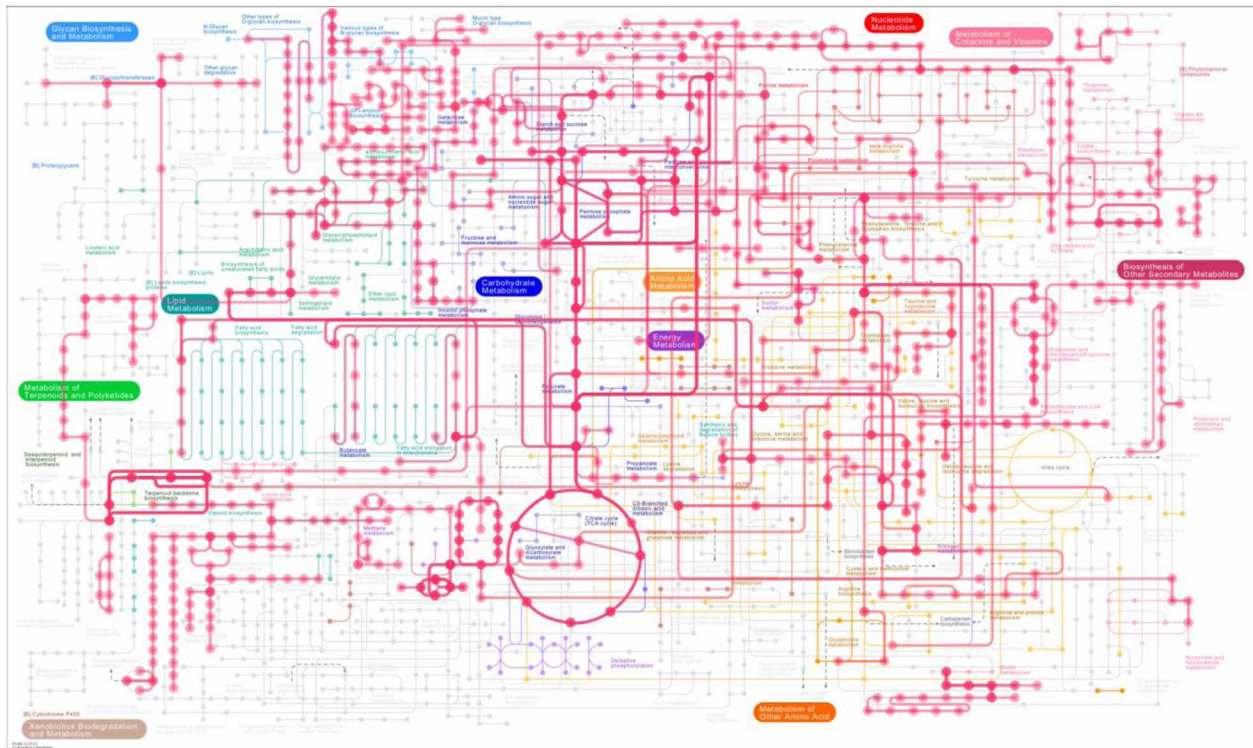


Figure 5.1. KEGG-classified metabolic pathways. Annotated genes (dots) from the genome of *Sphaeroforma sirkka* superimposed onto known pathways. Highlighted red pathways are theoretical paths through known genes.